Bulletin of Romanian Chemical Engineering Society

2 2014

ISSN 2360-4697

Edited by SICR and Matrix Rom

ISSN 2360-4697

Bulletin of Romanian Chemical Engineering Society

Volume 1 2014 Number 2

Contents

CHEMICAL ENGINEERING, QUO VADIS?

Ilie SIMINICEANU *

Department of Chemical Engineering, Faculty of Chemical Engineering and Environmental Protection, "Gheorghe Asachi" Technical University of Iasi, 73 prof. dr. docent Dimitrie Mangeron street, Iasi, 700050, Romania

Abstract

This paper is dedicated to the memory of Dirk Willem Van Krevelen (1914- 2001), the founder of Chemical Reaction Engineering (CRE). According to Hans Kramer, Van Krevelen coined the term CRE, organized the first European Symposium of CRE (ESCRE-1) at Amsterdam in 1957, defined the object of the new discipline in his article"Micro- and Macrokinetics", co- edited the journal Chemical Engineering Science, served as the first head of the Chemical Reaction Engineering Working Party of EFCE in 1953, and made 6 major discoveries with his name, such as "Van Krevelen diagram", "Van Krevelen method" etc. This paper also presents a short history of Chemical Engineering evolution since 1887 to the currently mature state, including 3 main disciplines: Transport Phenomena and Physical Unit Operations, Chemical Reaction and Reactor Engineering, Chemical Process and Plant Engineering (analysis and synthesis, simulation and optimization). Finally, to answer the question in title, the 7 new frontiers previewed by the "Amundson's Report" are shortly reviewed.

Keywords: Unit Operations, Macro- kinetics, Chemical Reaction Engineering, Hatta number, Thiele Modulus, Enhancement factor

1. Introduction

Under the *British Alkali Act* of 1863, **George E. Davis** (1850- 1907) was appointed Alkali inspector to curb the discharge of hydrochloric gas into the air from the Le Blanc soda ash plants. During his long career, he inspected many of the Lead Chambers, Le Blanc and Solvay plants in the Midland area of England. What he learned convinced him of the necessity for a new branch of engineering that combined applied chemistry and traditional mechanical engineering. In 1880, June 4, George E. Davis wrote an article in *Chemical News*, where he proposed the formation of a *Society of Chemical Engineers.* This failed to become a reality, because the "chemical engineer" did not exist yet. Therefore, Davis decided to form such specialists. In 1887 he gave a series of 12 lectures of chemical engineering at the Manchester Technical School (today, UMIST). In 1901 he published these lectures under the title **Handbook of Chemical Engineering** (2^{nd} edition, 1904, in two volumes). Therefore, George E. Davis is considered the conceptual father of the **Chemical Engineering,** the 4^{th} main branch of

Corresponding author: E-mail address: isiminic@ch.tuiasi.ro

engineering, with civil, mechanical, and electrical engineering [1]. To define the **chemical engineer,** Davis took as model the profile of **Ernest Solvay** (1838-1922) who, from laboratory experiments, designed and operated the commercial process for soda ash production, much efficient than Le Blanc. His appeal for a chemical engineer had also a "patriotic reason": the new formed BASF Company in Germany became a danger for the powerful British industry! The table of content of the Davis' handbook reveals his scientific spirit. He did not describe encyclopedically different technologies, like *Georg Lunge* for instance. He observed that different process industries have a number of physical operations in common: transport of liquids, solids, gases; extraction; absorption, crystallization, evaporation etc. In other words, we must teach students how to do distillation or extraction rather than teach how to make sulfuric acid or other hundreds products. We may say that Davis had in mind the concept of **"unit operation"** coined much later by **Arthur Dehon Little (1863- 1935)**, in 1915 at MIT, USA.

The real academic chemical engineering emerged in USA, at the MIT, Department of Chemistry, where Professor *Lewis M. Norton (1855- 1893)* introduced in 1888 **the first curriculum of chemical engineering**, on four years, named *Course X*(ten). The first 7 students graduated in 1891; among them **William Page Bryant –** considered the first "diplomat"/BS in chemical engineering of the world. After the death of Norton, came Professor *Frank H. Thorpe* (1864- 1932) who had BC from MIT, and PhD at Heidelberg - 1893. In 1898 he published the book **"Outlines of Industrial Chemistry".** Here he coined the English term *industrial chemistry.* Georg Lunge (1839- 1923) has taught at ETH Zürich "Technische Chemie" since 1876 till 1907. The same discipline, a branch of chemistry, was taught in France (*Chimie Industrielle).* In fact, in most of European countries, the chemical engineering reduced to industrial chemistry until the post World War II period, and even after 1990. With one exception: The Netherlands [2].

A further step at MIT was made by the couple **William H. Walker** (1861-1934) and **Warren K. Lewis** (1882-1975), both with PhD in Germany. They published in 1923, together with McAdams, the book **Chemical Engineering Principles,** where unit operations were explicitly exposed. In the mean time, in 1920, the first Department of Chemical Engineering, separated from Chemistry, appeared at MIT, headed by Professor **Warren K. Lewis.** In addition, this department granted the first PhD title in Chemical Engineering of the world, in 1924 to **Charles H. Herty (1896-1953)**. Therefore, the real chemical engineering education, based on unit operations, started after 1924, even in USA. Till than, was predominantly industrial chemistry. In 1923, **Walter G. Whitman** (1895-1974) has had published *"The two film theory of gas absorption"* – may be the first fundamental contribution of the new discipline. Another progress was the founding of **American Institution of Chemical Engineers (AIChE)** in 1908

with its journal: AIChE Journal. In 1925 AIChE begins accreditation of chemical engineering programs, and the first 14 schools gain accreditation on their programs. Another great scientific success of the new discipline took place the same year: McCabe and Thiele published the method for the design of distillation column.

The years 1930- 1940 were dominated by great industrial achievements (polyethylene - ICI, Nylon - Du Pont, thermal and catalytic cracking, synthetic rubber). Chemical operations become more and more important. Their macroscopic mechanisms, the interactions between chemical reactions and transport phenomena take a priority in chemical engineering research.

2. Pioneers of a new branch of chemical engineering

Olaf Andreas Hougen (1893- 1986) is the first pioneer of the new branch of chemical engineering: **Chemical Reaction Engineering.** He was Professor at University of Wisconsin - Madison for over 40 years. Many of his colleagues named him "a founding father of modern chemical engineering". He authored 7 books, 156 papers, directed many PhD theses and other research projects. He was the first who elaborated a real strategy to study the chemical processes, starting with stoichiometry, then thermodynamics, kinetics, and reactor design. He exposed this strategy in four main books: *(1) Industrial Chemical Calculations*, Wiley, 1931(1936, 1938) with Watson K.M., on material and energy balances; (2) *Chemical Process Principles.* Part I: *Material and Energy Balances*, Wiley, N.Y., 1943 (1952, 1954, 1956); (3).*Chemical Process Principles.* Part II: *Thermodynamics*, Wiley, N.Y., 1947 (1959 cu Ragatz); (4) *Chemical Process Principles.* Part III: *Kinetics and Catalysis*, Wiley, N.Y., 1947. These are highly cited even today. In Part III was firstly exposed **the method LHHW (Langmuir-Hinshelwood- Haugen- Watson)** to establish kinetic equation in heterogeneous catalytic processes. As a professor, Hougen was much respected. He educated the responsibility of future engineers. In 1974 he was elected at National Academy of Engineering. The three authors of "Transport Phenomena" (BSL), written at Wisconsin University, expressed their respect to Professor Hougen in a codified mode. The first letters of each sentence in the Preface give "This book is dedicated to O.A. Haugen". Nice!

Another important pioneer was **Gerhard Damkoehler (1908-1944),** Professor at the Institute of Physical Chemistry, University of Goettingen. He introduced in 1939 the Damkoehler criterion (Da) as a measure of the external transport influence on the reaction rate. The German school of *Verfahrenstechnik* considers him as a founder of *Chemische Reaktionstechnik.* In the same year, 1939, **Ernest W. Thiele** (1895-1993), scientist at Standard Oil (1925-1960) and

Professor at the Univ. of Indiana, Notre Dame, published the article “Relation between catalytic activity and size of particles” in the journal *Industrial & Engineering Chemistry*, 31, 816-820, 1939.Here, he defined the **Thiele modulus** as ratio between diffusion time and reaction time. **Ahlborn Wheeler (1911-1992),** pioneer of the industrial catalysis (Wheeler A., Adv. Catal., 3, **1951**, 250.), further developed the equation of the effectiveness factor as a function of Thiele modulus under isothermal conditions. This relation was crucial for the rational design of catalytic reactors with porous catalysts. A similar relation will be established by Van Krevelen in 1948 for the reactive absorption, giving enhancement factor (E) as a function of Hatta number [4, 5]. This will be detailed in a next section. Here we must mention two important English contributors: **Kenneth G. Denbigh** (1911-2004), and **Peter V. Danckwerts** (1916-1984). The first introduced the concept of *space time* (see “Velocity and yield in continuous reaction systems”, in Trans. Faraday Soc., 40, **1944**), then published the book *Chemical Reactor Theory*, 1956, where the *ideal reactors* have been defined. As for Peter V. Danckwerts, Shell Professor of Chemical Engineering at Cambridge (UK), he published the famous paper “Continuous Flow Systems-Distribution of Residence Times” in *Chem. Eng. Sci.,* **1953**, which generated an explosion of similar research in the next years.

3. Foundation of Chemical Reaction Engineering: Symposium of Amsterdam-1957

Fig. 1. Dirk Willem Van Krevelen (1914- 2001).

Hans Kramers (1917-2006), Professor and Head of Department of Physical Technology (1947- 1963) at the TU Delft wrote [2]: "Van Krevelen coined this broad field of investigation *Chemical Reaction Engineering (CRE).* With the support of EFCE working group, two related national associations decided to organize one or more international meetings on the subject. Thus, three symposia on CRE were held in Amsterdam (ESCRE 1-1957, ESCRE 2-1960, ESCRE 3-1964). Particularly the first can be regarded as a historical event". The 17 papers presented are all included in the volume 8 of *Chemical Engineering Science* [3]. The paper presented by Van Krevelen, *Micro- and macro-kinetics,* was a general introduction of the symposium, defining the new discipline. The other 16 were presented by experts from Germany (Hofmann H., Schoenemann K., Klinkenberg A., Broetz W., Wicke E.), France (Letort M, Introduction a la cinetique chimique I, II, III), Great Britain (Denbigh K.G., Optimum temperature sequences in reactors; Danckwerts P.V., The effect of incomplete mixing on homogeneous reactions), Norway (Oele A.P., Catalytic combustion of ammonia on platinum gauze), and Netherlands (Kramers H., Van de Vusse J.G., Nysing R.A.T.O., Rietema K., Van Krevelen C.).With 6 articles from 17, The Netherlans had the major contribution of 35.3%. After ESCRE 4 in Brussels, followed the first ISCRE in Washington D.C. in 1970. These biennial symposia are alternatively held in Europe, North America, and since 2002 in Asia, too. The next event, ISCRE 24, will take place in Minneapolis (USA) in 2016. Besides symposia, a new discipline needs good research journals to be consolidated. In October 1951, Pergamon Press published number 1 of volume 1 of *Chemical Engineering Science.* The first Editorial Board included: D.W. Van Krevelen (Geleen), M.B. Donald (London), J.Cathala (Toulouse), A.Guyer (Zürich), F. Giordani (Naples), S.G. Terjesen (Trondheim), and W.L. de Keyser (Brussels). The first number contained 5 articles (3 from Netherlans). D.W. Van Krevelen published "Studies on fluidization: the critical mass velocity". After 1957, **Neal R. Amundson** became the American editor. An important role also played **Peter V. Danckwerts**, co-editor for a long period. The other great journal, edited by ACS in USA since 1909, was split in 1962 into 3 quarterlies. One of them, *I. & E.C. Fundamentals* was edited by Professor **Robert L. Pigford** (1917-1988) during 25 years (1962-1987) and attained a very high standard. Professor Pigford, surnamed "a prince among men", left many other legacies to the profession of chemical engineer. He used computers for process analysis since 1954 at UC Berkeley. In 1987, the three quarterlies collapsed into a single monthly publication: *I. & E.C. Research* (editor, Donald R. Paul).

Table 1.

Selected books of Chemical Reaction Engineering

1947. *Hougen O.A., Watson K.M.*, Chemical Process Principles.Part I: Material and Energy Balances, Wiley, New York (4th ed.1964).
1947. *Hougen O.A., Watson K.M.*, Chemical Process Principles.Part II: Thermodynamics, Wiley, New York (3rd ed. With Ragatz)
1947. *Hougen O.A., Watson K.M.*, Chemical Process Principles.Part III: Kinetics and Catalysis, Wiley, New York
1949. *Walas S.M*. Introduction to Chemical Engineering Thermodynamics (6 eds).
1956. *Denbigh K.G.*, Chemical Reactor Theory, Cambridge Univ. Press, N.Y.
1956. *Walas S.M*., Chemical Engineering Kinetics, McGraw-Hill, New York (4 eds).
1958. *Broetz W*., Grundriss der chemischen Reaktionstechnik, Verlag Chemie, Berlin.
1960. *Levenspiel O*., Chemical Reaction Engineering, Wiley, New York, (3rd 1999).
1963. *Kramers H., Westerterp K.R*., Elements of Chemical Reactor Design and Operation, Academic Press, New York.
1963. *Mihail R.,Carloganu C.*, Reactoare in industria chimica, Editura Tehnică, București.
1963. Perry's Handbook,4th ed., Section 4: "Reaction Kinetics**,** Reactor Design, and Thermodynamics" (8th Edition, 2007, 2640 p.).
1965. *Aris R*., Introduction to the Analysis of Chemical Reactors, Prentice- Hall, N.J.
1967. *Astarita G.*, Mass Transfer with Chemical Reaction, Elsevier, Amsterdam.
1971.*Calistru C,* Ingineria proceselor chimice, in: Tehnologia substanțelor anorganice-Partea I, Edit. Did. și Pedag., București.
1979. *Froment G.F. ,Bischoff K.B*., Chemical Reactor Analysis and Design (2nd ed. 1990).
1979. *Shah Y.T*., Gas- Liquid- Solid Reactor Design, McGraw Hill, New York.
1984.*Trambouze P*. et al, Les reacteurs chimiques: conception, calcul, mise en oeuvre, Edition Tecnip, Paris.(2nd ed, in English, 1988).
1999. *Fogler S.H.*, Elements of Chemical Reaction Engineering, Prentice Hall, (4th ed., 2005).
1998. *Schmidt L.D.*, The Engineering of Chemical Reactions, Oxford Univ. Press, *(2nd ed, 2005)*
2001. *Bozga G., Muntean O.*, Reactoare chimice, Ed.Tehn., București, vol 1, 2.
2009. *Roberts G.W.*, Chemical Reactions and Chemical Reactors, Wiley, New York.
2011. *Salmi T.O., et al*, Chemical Reaction Engineering and Reactor Technology, CRC Press.
2014. *Fogler S.H., Leblanc S.E.*, Strategies for Creative Problem Solving, 3rd ed., Prentice- Hall, N.J.

A third contribution to the advancement of an academic discipline like CRE had the **good books** on the subject. Table 1 present the most important of them. Only the 4th edition of Perry's Handbook included a section 4 with elements of CRE: "Reaction Kinetics, Reactor Design". During the last decades, Fogler's books with "creative problem solving" replaced in popularity the books of Levenspiel – longtime considered "the Seuss of chemical engineering" in USA.

4. Basic contributions of Dirk Van Krevelen to the consolidation of CRE

Professor Van Krevelen has been not only the inventor of the name of CRE, and the organizer of ESCRE 1 in Amsterdam, as well as the first head of the CRE Working Party of the EFCE in 1953. He also discovered/invented 5 new methods/ equations/mechanisms/diagrams: 1. “Van Krevelen diagram” on chemical gas absorption [4, 5]; 2. ”Van Krevelen – Chermin method” for the estimation of the free energy of organic compounds [6]; 3. “Mars – Van Krevelen mechanisms” on catalytic oxidation [7]; 4. “Van Krevelen method” on additive properties of polymers [8]; 5. “Van Krevelen graphical statistical method for the study of structure and reaction processes of coal” [9, 10]. These are also included in the volume [11], and are highly cited, even today [12].

4.1. The “Van Krevelen diagram” on chemical gas absorption [4, 5] based on the “Van Krevelen assumption”

Let’s consider the absorption of gas A accompanied by the reaction (4.1):

$$A + \upsilon_B B \rightarrow \upsilon_C C \tag{4.1}$$

$$D_A \frac{d^2 C_A}{dx^2} + k_2 C_A C_B = 0 \tag{4.2}$$

$$D_B \frac{d^2 C_B}{dx^2} + \upsilon_B k_2 C_A C_B = 0 \tag{4.3}$$

Van Krevelen used the assumption (4.4), i.e. the decrease of B concentration is very small at the interface.

$$\left(\frac{dC_B}{dx} \right)_{x=0} = 0 \tag{4.4}$$

With this hypothesis, he obtained the equation (4.5), and the diagram of Fig.2 based on it.

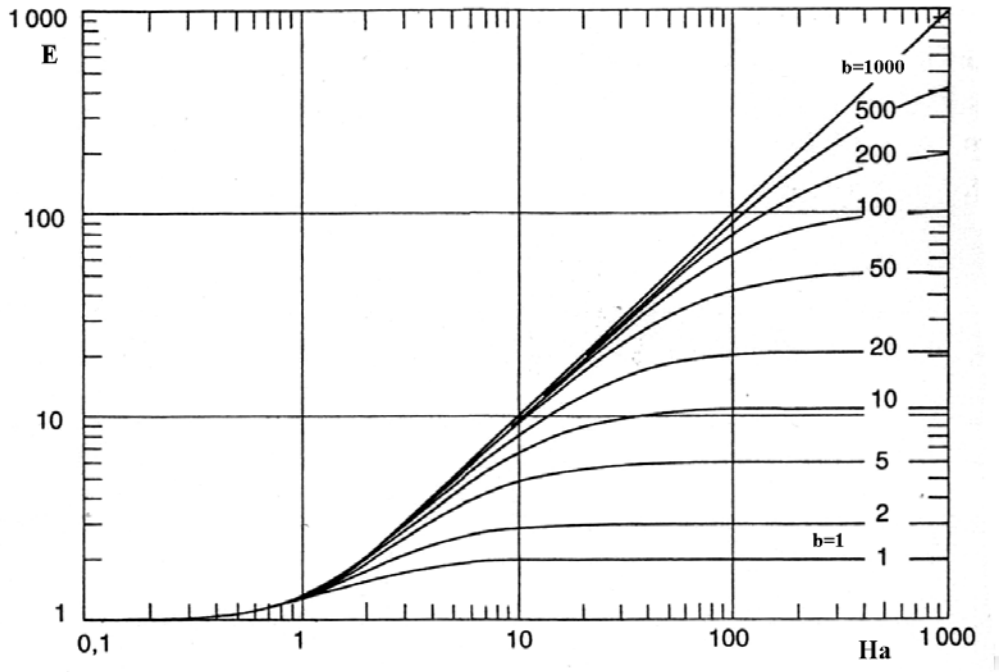

Fig. 2. The "Van Krevelen diagram" on chemical gas absorption [4, 5] based on the "Van Krevelen assumption" (4.4).

$$E = \left(\frac{N_A^{'}}{N_A}\right)_{x=0} = \frac{Ha\left[1-\frac{(E-1)(1-a)}{b}\right]^{1/2}}{th\left[Ha\sqrt{1-\frac{(E-1)(1-a)}{b}}\right]} \frac{1-\frac{a}{ch\left[Ha\sqrt{1-\frac{(E-1)(1-a)}{b}}\right]}}{1-a} \quad (4.5.)$$

$$a = \frac{C_A^0}{C_A^i} \; ; \qquad b = \frac{D_B}{\upsilon_B D_A}\frac{C_B^0}{C_A^i} \quad (4.6)$$

$$\text{Hatta} = \text{Ha} = (k_2\, D_A C^0{}_B)^{1/2} / \, k^0{}_L \quad (4.7)$$

For carbon capture and other applications, the domain Ha> 5, fast reaction, and E= Ha, is very interesting becouse the absorption is highly accelerated by the rapid reaction [5].

4.2."Van Krevelen – Chermin method" for the estimation of the free energy of organic compounds [6]

The article "The estimation of the free enthalpy (Gibbs Free Energy) of formation of organic compounds from group contributions" was published in the number 2 of Chem*ical Engineering Science* (1, 2, 66- 80, 1951) and has a strong impact. The method is cited by all thermodynamic books.

4.3. "Mars – Van Krevelen mechanisms" on catalytic oxidation [7]

There are three kinetic mechanisms/models for catalytic reactions on solid catalysts: LHHW, Eley – Rideal, and Mars – Van Krevelen. The later is presented in the figure 3. Mars and Van Krevelen discovered that oxidation on RuO_2 takes place in two steps: I. the adsorbed reactant is oxidized by the Oxygen from the crystal lattice of the catalyst. Then, II the reduced catalyst is oxidized by oxygen from the gas phase. This was the subject of Mars' PhD thesis, directed by both Van Krevelen and Jan de Boer at TU Delft (1954- 58).

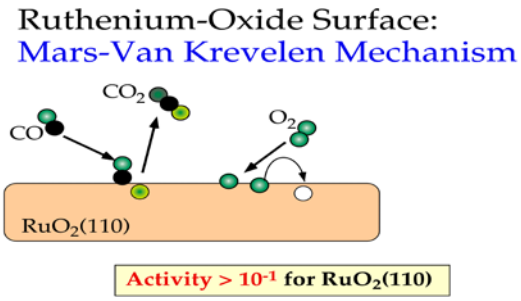

Fig. 3. Mars – Van Krevelen mechanism.

4.4. Life and Work of Dirk Van Krevelen

Dirk Van Krevelen was born in Rotterdam on 8 November 1914, the son of a bookkeeper. His option for the study of the applied chemistry was inspired by

the example of Jacobus van't Hoff (Nobel Chemistry, 1901) and also by his father who argued that there were good employment opportunities in that field, even in times of economic crisis (it was in 1933). After his *kandidaats exam* (BS) in 1935, he continued *physical chemistry* with Prof van Arkel. In parallel, with an industrial carrier in mind, he started in 1937 a minor in *chemical technology* at the laboratory of the Prof Hein Waterman at TU Delft. During 1937-39 Van Krevelen worked at Shell as assistant of Waterman. Meanwhile, in March 1938 he did the *doctoraal exam (MS*) at Leiden, after only 4.5 years (instead of 6-7 years overage). In December 1939 he received his doctorate in chemical engineering with Waterman, at the age of 25! In 1940, January 1 he started working at DSM. In 1943 he became director of the Chemical Engineering Laboratory of DSM newly created. In August 1948 he was promoted research director of the Central Research Laboratory of DSM (Geleen). In September 1959 he accepted the direction of AKU - a much larger company than DSM. Since 1952 till 1980 (retirement) he was invited as Professor of chemical engineering at TU Delft, with a part time of 2 hours per month. He taught CRE, fuel technology, and polymers. He also supervised 23 PhD students (4 in CRE, 10 in polymers, 9 in coal). He was succeed by **Hans Kramers (1917- 2006)** as Professor of chemical engineering at TU Delft. Van Krevelen continued as research advisor at Shell, AKZO, and NORIT. In his spare times he studied history of antique Egypt. As a Professor at TU Delft, he was the first in Europe who adopted «the American style» of chemical engineering. After a visit in USA in 1920' his advisor Waterman introduced the method of "unit operations" at TU Delft. In 1956, R.B. Bird worked as Fulbright lector at the Laboratory of Physical technology of Hans Kramers who taught transport phenomena before "unit operations". Returned to USA, Bird – Steward – Lightfoot have written rapidly in 1958 the "best seller" *Transport Phenomena.* Once again, like in 1887/88, the chemical engineering ideas "emigrated" overseas. The ideas must circulate, it is allowed.

5. Chemical Engineering: *Quo Vadis* ?;New Frontiers

In Fig. 4, Saint Peter met Christ while fleeing Rome, on the Via Appia. Christ was walking toward the burning city (Nero's Fire in AD 64). Peter asked him: "Domine, Quo Vadis?"/Lord, where are you going?". Lord replied: "Eo Romam iterum cricifigi"/"I am going to Rome to be crucified again". So, Peter understood that he must return to Rome to face martyrdom.

Such questions raised in Eastern Europe Countries after 1990, when many chemical factories were destroyed. Many other countries were under the "chemiophoby" terror. Therefore, the chemical engineer had a "Peter Syndrome". He met Lord, transmigrated under the form of "Amundson Report" that depicted the "new frontiers" of chemical engineering research.

Fig.4. Domine, quo vadis ? (Anibale Carraci, 1603)

The current main six directions of development are summarized in the table 2.

Table 2.

New frontiers of Chemical Engineering

Nr.	Direction/Objectives	Inventors
1	Generating energy: from petroleum to renewable resources.	Vladimir Hansel, Eger Murphree
2	Saving the Environment	Kam Sirkar, Ralph Yang
3	Biomedical Engineering	Margaret H. Rousseau
4	Electronics	Andrew Grove, Farhang Shadman
5	New Materials	**Robert Langer**, Nicholas Peppas
6	Enhancing Food Production	Ted Labuza

Robert Langer, born in 1948, is David H. Koch Institute Professor at the MIT laboratory of Chemical and Biomedical Engineering. He published over 1500 articles and 1050 patents, received 220 awards. With over 160 000 citations and a Hirsh index h= 209 he is the most cited chemical engineer of the history.

Table 3.

Scientific production in chemical engineering during the period 1996- 2013

Country	Documents	Citations/Doc	Country	Documents	Citations/Doc
1. USA	7 846 972	22.02	10. Spain	857 158	15.08
2. China	3 129 917	6.81	11. Australia	782 149	18.24
3. Great Britain	2 141 375	19.82	12. South Korea	658 602	11.49
4. Germany	1 983 270	17.39	13. Russian Fed.	639 598	6.00
5. Japan	1 923 402	13.01	14. Netherlans	613 552	**23.03**
6. France	1 421 190	16.85	15. Brazil	529 841	10.98
7. Canada	1 110 886	20.05	**41. Romania**	109 831	6.84
8. Italy	1 083 546	16.45	50. Bulgaria	50 312	8.49
9. India	869718	8.83	239. Takelau	1	36.00

Table 3 presents the contribution of several countries to the scientific production of chemical engineering in the period 1996-2013. The quantity is given in number of documents while the quality through the ratio citations/document. The first in quality are Netherlands, USA and Canada. Romania has a honorable position in quantity: the 41st from 239. China replaced URSS on the 2nd.

6. Conclusions

The Chemical engineering profession evolved from the society's need for products and energy. Today and into the future, chemical and bioengineers will continue to meet society's needs using their process knowledge, their knowledge of fundamental science, and their problem-solving skills.

This paper documents that Dirk Van Krevelen, born one hundred years ago, founded Chemical Reaction Engineering at the Symposium of Amsterdam in 1957 (ESCRE-1).

REFERENCES

[1] De Bernardez Clarc E., The changing face of chemical engineering, *Education*, 79(23), (2001) 63- 66.

[2] Peppas N.A. (editor), *One Hundred Years of Chemical Engineering (1888-1989)*, Kluiver Acad. Publ., Boston, 1989.

[3] Van Krevelen D.W., Micro-and macro-kinetics: General Introduction to the symposium, *Chemical Engineering Science*, 8 (1-2), (1958), 5-17.

[4] Van Krevelen D.W., Hoftyzer P.J., Kinetics of Gas-Liquid Reactions. Part I: General Theory, *Recueil des traveaux chimiques des Pays-Bas*, 67, (1948), 563-568.

[5] Siminiceanu I., *Reactive Absorption*, Technopress, Iasi, 2005.
[6] Van Krevelen D.W., Chermin H.A.G., Estimation of the free enthalpy (Gibbs Free Energy) of formation of organic compounds from group contributions, *Chemical Engineering Science*, 1(2), (1951), 66-80.
[7] Mars P., Van Krevelen D.K., Oxidations carried out by means of vanadium, *Proceedings of the Conference on Oxidation Processes*, Amsterdam, 6- 8 May, pp. 41- 57, 1954.
[8] Van Krevelen D.W., *Properties of Polymers. Their Correlation with Chemical Structure, Their Numerical Estimation and Prediction from Additive Group Contributions*, Elsevier, Amsterdam, Fourth Edition (1st ed., 1972; 2nd ed., 1976; 3rd ed., 1990), pp. 1030, 2009.
[9] Van Krevelen D.W., Graphical- statistical method for the study of structure and reaction processes of coal, *Fuel*, 29, (1950), 269-284.
[10] Van Krevelen D.W., *Coal: Typology, Chemistry, Physics and Constitution*, 3rd ed (1st ed, 1961; 2nd ed 1981), Elsevier, Amsterdam, pp.1020, 1993.
[11] Van Krevelen D.W., *Selected Papers on Chemical Engineering Science*, Elsevier, Amsterdam, pp. 398, 1976.
[12] Albahri A.T., Accurate prediction of standard net heat of combustion from molecular structure, *Journal of Loss Prevention in the Process Industries*, 32, (2014), 377-386.

APPLICATION OF NATURAL SORBENTS IN OIL SPILL CLEANUP

Alina-Georgiana CIUFU[1], Timur Vasile CHIS[2]*

[1]Departament of Chemical and Biochemical Engineering, Faculty of Applied Chemistry and Materials Science, University Politehnica of Bucharest
[2] Technology and Chemical Engineering Department, University "Ovidius", Constanța

Abstract

Oil spill became a significant problem of concern due to its serious impact on the natural marine ecosystem. Therefore, the control of oil spill pollution in the marine environment in a sustainable manner is the main focus of this study. The use of natural sorbents is promising and deserves attention, because they are very efficient, available, eco-friendly and low cost. Sorbents are insoluble materials used to recover liquids through the mechanism of absorption or adsorption or both. In this study, peat moss, sunflower seed cake, polypropylene and clay were used for crude oil sorption. Also, in this study four specific pollutants (most persistent organic pollutants in accidental oil spills) were used: C Marine oil, Russian Export Blend Crude Oil, diesel and gasoline. The results presented and discussed in this work point out that the tested sunflower seed cake may be considered an excellent potential sorbent for oil. This sorbent is a by-product of oil refining (provided by squeezing oil from them), a biodegradable sorbent, with average sorption properties and good buoyancy. Also the results indicate that peat moss has a higher oil sorption capacity compared to the others.

Key words: Oil retention, Natural Sorbent, Oil Spills, Buoyancy, Adsorption

1. Introduction

In his studies Chiş [1, 2] has identified a series of types of pollution that occurred between 1973 (the first ecological accident in Constanța) and 2014. These studies showed that in Constanța County there are on average 15 annually incidents at the oil transportation pipes. Other causes of oil spills are: accidents involving tankers, barges, refineries (toxic chemicals), and storage facilities. Usually these accidents happen while the oil is being transported to us, its users, via rivers, lakes, bays and the ocean.

The National Academy of Sciences estimate that 1.7 to 8.8 million tons of oil are released into worlds water every year, of which more than 70% is directly related to human activities [3]. Oil spills affect ecology, sea life, economy, and the whole coast areas. Most important oil spill, the intentional Gulf War spill in 1990,

*Corresponding author: E-mail address: timur.chis@gmail.com

is ranked as the largest oil spill ever. On April 2010 the attention of the world was drawn to the accidental oil spill in the Gulf of Mexico. An explosion on an operating drilling rig from the coast of Louisiana initiated the release of a huge amount of crude oil into the sea water. Researchers reported that this oil spill was one of the largest accident in the history, after Gulf War spill, and is ranked as the second highest oil spill in the world. The latest and the most awful oil spill in the history is the Exxon Valdez oil spill [4]. Exxon Valdez ship spilled approximately 260,000 barrels of oil in Prince William Sound in Alaska and was ranked the fourth largest in the United States and the 36th largest in the world. This huge damage caused the death of 35,000 birds, 1000 sea otters, 300 seals, 250 eagles, 25 whales and 25 million fish (salmon, herring and other species) [5].

The effects of oil pollution are felt over a large area due to their dispersion on surface water, groundwater and soil. This process is also magnified by climatic element. Most commonly used methods in clean-up operations are burning, flushing, chemical dispersants, skimming, sorbents, bioremediation and joint techniques.

The recovery of crude oils, petroleum products, mineral oils and their waste accidentally spilled into surface waters, when they are in the form of a very thin layer, is achieved by using sorbents, in the final stages of clean-up. The sorbent (adsorbent), represents a solid substance, endowed with the property of absorbing other substances (vapours and solutes) and particles without any covalent bonding. The important factors of a successful sorbent are: hydrophobicity, oleophilicity, retention of oil over time, recovery of oil from sorbents, amount of oil adsorbed per unit weight of sorbent, reusability and biodegradability.

Oil sorbents can be classified into three major classes: organic vegetable products (such as peat moss, cotton fibre, wood fibre, cellulosic kapok fibre, kenaf and other readily available carbon-based products etc.), inorganic mineral products (sorbent clay, vermiculites, volcanic ash, perlite etc.) and organic synthetic products (including materials such as polypropylene, polyethylene and polyurethane) [6].

In this study we compared the oil sorption performance of four sorbents: peat moss, sunflower seed cake, polypropylene and clay.

Although many articles [7-9], practically demonstrated that, synthetic adsorbents (non-biodegradable) are undeniably more recommended in the marine environment remediation/interventions of petroleum products spilled by accident, in our country (due to lower cost and the use of petrochemical-polyethylene waste and polypropylene grinded), some specialized units use specifically adsorbent materials 100% organic and natural biodegradable. Polluters receive clear indications from Romanian experts specifying to use only 100% natural biodegradable adsorbents for large or small pollution. Peat-based sorbents (spill-

sorb, Ecosorb, Enviropeat, Cansorb, peat, nature sip) are imported from countries like Canada, New Zealand, South Africa and are used in a proportion of 85-90%. Synthetic sorbents on the basis of polypropylene and polyethylene are used in a lesser extent, approximately 10-15% of the cases. Synthetic sorbents, based on polypropylene and polyethylene, are used in a lesser extent, approximately 10-15% of the cases [10]. The role of peat as an absorbent material in the remediation process is: encapsulation of spilled petroleum products (preventing their migration), transport medium for petroleum hydrocarbons incorporated into the treatment area, role as support for the process of biodegradation [11,12].

Wood fibre is an organic adsorbent, 100% natural and biodegradable, and can be comparable with peat-based sorbents. According to some environmental studies [13], researchers concluded that piles collected wood fibre and placed in polluted waters may create a threat to the ecosystem. Other scientists have a different view, saying "the solution to pollution is dilution", argument that is not accepted in science. Also, corn cobs are used as an organic natural sorbent to collect spilled oil products in surface waters.

The use of cellulose-based sorbents, as a primary response tool in a major oil spill response at-sea, is not encouraged [14]. In addition to the problems of control of the materials on the water surface and increased volumes of oil waste, the application of cellulose based sorbents does not ease the problems inherent in at-sea containment and recovery operations.

Natural sorbents, inorganic mineral such as: clay, vermiculite, perlite etc. are both 100% biodegradable, oleophilic and are able to absorb larger amounts of oil, from 4 to 20 times their own weight. In addition, these sorbents are relatively inexpensive and readily available in large quantities. Organic and inorganic sorbents can be attractive because they are abundant in nature or in the waste resulting from an industrial process [14]. Also, they can be easily bought at a low cost or even free.

A new sorbent introduced into this study, the sunflower seed cake, is a by-product of oil refining that can be used in the methods of remediation of polluted waters in our country, due to its low price and good adsorption.

Natural sorbents are proposed for an ecological removal of petroleum products from surface waters.

2. Experimental

Materials and methods

To ensure an adequate scientific support for the study, both general and specific research methods were used, such as analysis, synthesis method, observation method and the comparative method. Tests were carried out on several groups of poly-dispersed sorbents such as peat moss, polypropylene, clay

and sunflower seed cake. The peat moss used was taken from Săpânţa, Maramureș Country and was dried at 100°C. Polypropylene extrudates with average size of 0.5 mm were bought from Rompetrol, Midia. Clay was taken from Mircea Vodă village. The physico-chemical properties of the four tested pollutants are presented in Table 1. Table 2 presents the apparent density of the sorbents used.

Table 1.

The properties of the pollutants studied

Propertie/ Pollutant type	**Diesel**	**Gasoline**	**Ţiţei C marin**	**REBCO**
Density of 20°C SR EN ISO 12185:2003	0,820	0,732	0,8336	0,860
Viscosity, cSt SR EN ISO 3104:2002	2,4 of 40 °C	-	21,20 of 20 °C	20,53 of 20 °C
Pour point °C STAS 39-80:1980	-20	-20	+3	-4

Table 2.

The density of the sorbents used

	Polypropylene	**Clay**	**Peat moss**	**Sunflower seed cake**
Density Kg/m^3	0,672	0,673	0,1536	0,24

Adsorption experiments

To determine the sorption capacity of sorbents to/until current date, two standard procedures were elaborated by ASTM (American Society for Testing and Materials), namely:

a. F716-09 – Standard Test Methods for Sorbent Performance of Absorbents;

b. ASTM F726-12 – Standard Test Method for Sorbent Performance of Adsorbents;

To be mentioned that the two standards are the basis of standards developed by IFM (French Institute of Metrology), BSI (British Standards Institution), CANS (American National Standards Institute).

To observe the sorption qualities of the used sorbents, three sets of experiments were performed as follows:

A. Determination of adsorption capacity on the basis of the standard F716-09;

B. The behaviour of sorbents in the water-oil;

C. Determination of the adsorption rate.

The first experiment was conducted mixing petroleum products and sorbents. The F716-09 standard indicates the following working steps:

a. addition of the used sorbents in oil products,

b. measurement of the adsorption capacity after 15 minutes and 24 hours.

Working temperature must be constant (20ºC easily reached in the laboratory). Since testing is done in the laboratory, it could not simulate external parameters that could influence the evolution and evaporation of pollutants in nature (heat transfer processes at the interface oil-air, sea currents, wind etc.). An image of a mixture of diesel fuel and sorbent is presented in Fig. 1. Physico-chemical properties of the tested sorbents are presented in Table 3.

Fig. 1. Images of the mixtures between sunflower seed cake, polypropylene and peat moss and diesel fuel

For the first experiment, 150 mL of crude oil was poured into three 250 mL beakers and then 20 grams of sorbent was added to the crude oil. These tests were performed in a static system, without stirring. After 15 minutes, the content of the beakers was drained for 20 seconds. After this, the sorbents were removed from the beakers and their weight was measured. The images of the tested adsorbents after oil contact are presented in Fig. 2 - 4. The sorption capacity was calculated using the following equation:

$$oil\ sorption\ capacity = \frac{weight\ of\ adsorbed\ oil\ (grams)}{weight\ of\ sorbent\ (grams)} \quad (1)$$

Fig. 2. Sunflower seed cake soaked by diesel

Fig. 3. Crude oil absorbed by sunflower seed cake

Table 3.

Physico – chemical properties of the tested sorbents

No.	Physico-chemical propertie	*Sunflower* seed cake	*Peat moss*	*Clay*	*Polypropylene*
1.	Type sorbent	natural;	100 % natural organic;	100% natural inorganic;	synthetic;
2.	Biodegradability	high;	high;	reduced;	very low;
3.	Chemical formula	65% linoleic acid; and 20% oleic acid;	-	-	$(C_3H_6)n$;
4.	Composition	minimum 34% protein;	peat moss – 90% water – 10%	silicates; quartz;	polyolefins;
5.	Water solubility	insoluble in water;	insoluble in water;	insoluble in water;	insoluble in water;
6.	Aggregation state	solid;	solid;	solid;	solid;
7.	Material	Sunflower seed meal is the by-product of the oil extraction process. This product is rich in protein;	-	-	plastic;
8.	Water sorption capacity	saltwater – good; lakes, rivers, lakes, ponds – good;	saltwater: medium; other categories of water (lakes, rivers, ponds, lakes): average;	medium;	saltwater - average; lakes, rivers, lakes, ponds - good;
9.	Density	240 kg/m3	low;	high;	900 -910 kg / m3
10.	Hardness	high;	-	-	high;
11.	Flexibility	increased;	-	-	-
12.	Buoyancy	float (floating on water);	average; sinks and settles on the bottom;	sinks and settles on the bottom;	float (floating on water);
13.	Toxicity	non-toxic;	non-toxic;	non-toxic;	non-toxic;
14.	Corozivity	noncorrosive;	noncorrosive;	noncorrosive;	noncorrosive;
15.	Iritability	nonirritating;	nonirritating;	nonirritating;	nonirritating;
16.	Made from recycled materials	great;	no;	unrecycled;	medium;
17.	Fire resistance	medium;	good;	high;	medium;
18.	Safety for plants and animals	very good;	very good;	very good;	very good;
19.	Coal ash (%)	0.1 %	-	0%	0,3%
20.	The petroleum products obtained in fractional distillation	90 %	-	-	79%
21.	Color	greyish brown;	in a dry state: reddish brown; in a wet state: brown to black;	brown;	white;
22.	Appearance	with smooth surface and grey stripes;	fiber, with large cells;	fine granules;	fiber;
23.	Porosity	good;	high, about 80%;	medium, 45-50%	good;

a) b) c)

Fig. 4. Images of by peat moss (a), polypropylene (b), clay (c) after the adsorption of crude oil**.**

The second experiment was conducted between water, oil and sorbents. Similar to the first experiment Russian Export Blend Crude Oil (150 mL) and water (400 mL) were introduced in four beakers (Fig. 5). After that, 20 grams of sorbent were added. The experiment was monitored for 15 minutes. The same experiment was repeated for C Marine Crude Oil, Gasoline and Diesel.

Fig. 5. Mixture of REBCO, water and peat moss.

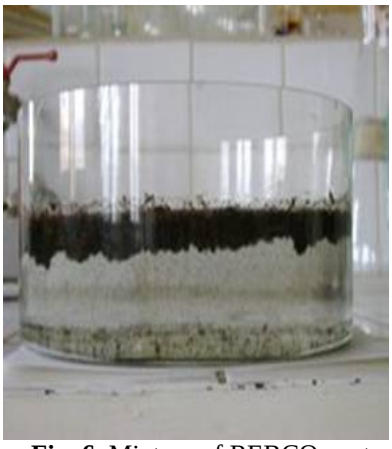

Fig. 6. Mixture of REBCO, water and peat moss after 24 hours.

Fig. 7. Mixture of diesel, water and peat moss after 24 hours.

Fig. 8. The behavior of polypropylene in water and REBCO.

Fig. 9. The behavior of peat moss in water and REBCO.

In this second experiment (some images during the experiment are presented in Fig. 6, 7), we have studied if the adsorbent settles on the bottom of the vessel or not. The observations carried out on the analyzed samples showed very good behavior of polypropylene sorbents, sunflower seed cake and peat moss (images presented in Fig. 8 and 9).

In the third experiment we studied the adsorption rate of the pollutant by capillary ascension sorbent columns. The column used has a diameter of 1.5 cm and a length of 12 cm. REBCO was introduced (75 mL) in a Berzelius beaker and then it was placed the column packed with the sorbents: the first which was tested was the peat moss and then the experiment was repeated with sunflower seed cake (up to 4 cm). During the experiment we have monitored the volume of adsorbed oil by the adsorbent.

3. Results and discussions

A first objective of the research was to study the issue of petroleum hydrocarbons retention and estimate the oil retention of these adsorbents. The adsorption tests were performed to determine the amount of liquid adsorbed by the adsorbent and the results are given in Table 4 and Fig. 10. As it can be seen, the best adsorbent was the peat moss.

Table 4.

Specific retention of oil products on various adsorbents after 15 minutes, at a working temperature of 20°C

Adsorbent	Oil sorption capacity REBCO weight of adsorbed oil (grams)/weight of adsorbent (grams)	Oil sorption capacity C MARINE weight of adsorbed oil (grams)/weight of adsorbent (grams)	Oil sorption capacity DIESEL weight of adsorbed oil (grams)/weight of adsorbent (grams)	Oil sorption capacity GAZOLINE weight of adsorbed oil (grams)/weight of adsorbent (grams)
Sunflower seed cake	2.89	2.56	2.36	2.75
Polypropylene	2.21	2.27	2.11	2.22
Clay	2.26	2.36	1.24	0.83
Peat moss	4.09	4.71	2.42	2.79

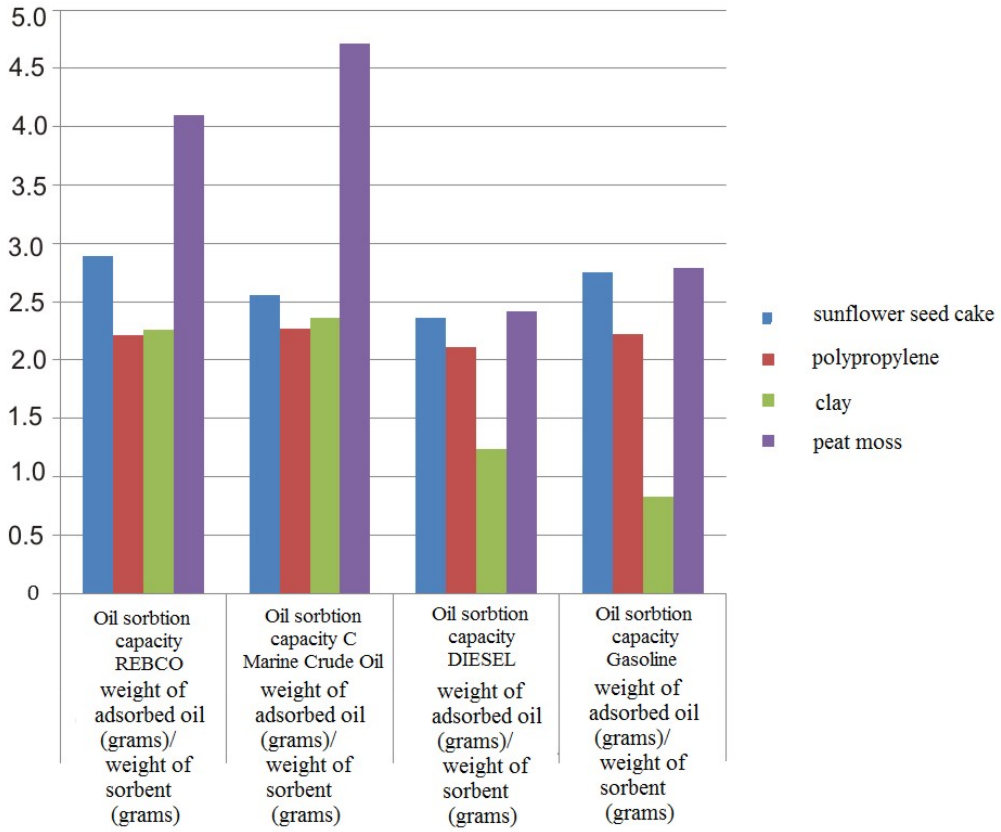

Fig. 10. The oil adsorption capacity of the tested sorbents.

Capillary ascension tests

The phenomenon of adsorption is closely associated with those of absorption, surface tension and capillary action. This test reveals that the phenomenon of adsorption by capillary action occurs on removal of petroleum products from the affected environment.

We have tested the kinetics of the capillary action of liquid in the pores of different sorbents. The column used had a diameter of 1.5 cm, and 12 cm in length.

REBCO, diesel oil and gasoline (75 mL) were poured in Berzelius beakers and then introduced in the column packed with natural sorbents, peat moss and sunflower seed cake (up to 4 cm). Adsorbent suction power was monitored by measuring the time necessary to fill the column with oil. The results are shown in Fig. 11.

As one can see in Fig. 11, gasoline and diesel fuel were retained instantly by the peat moss, and retention time to saturation is $t < 10^{-1}$ min (6 seconds). In the case of crude oil, the retention time is comprised within the range t = 1-10 min. Due to increase of the intrinsic capillary action, peat moss encapsulates the petroleum products into direct contact with them. Fig. 12 presents the results of oil retention by sunflower seed cake.

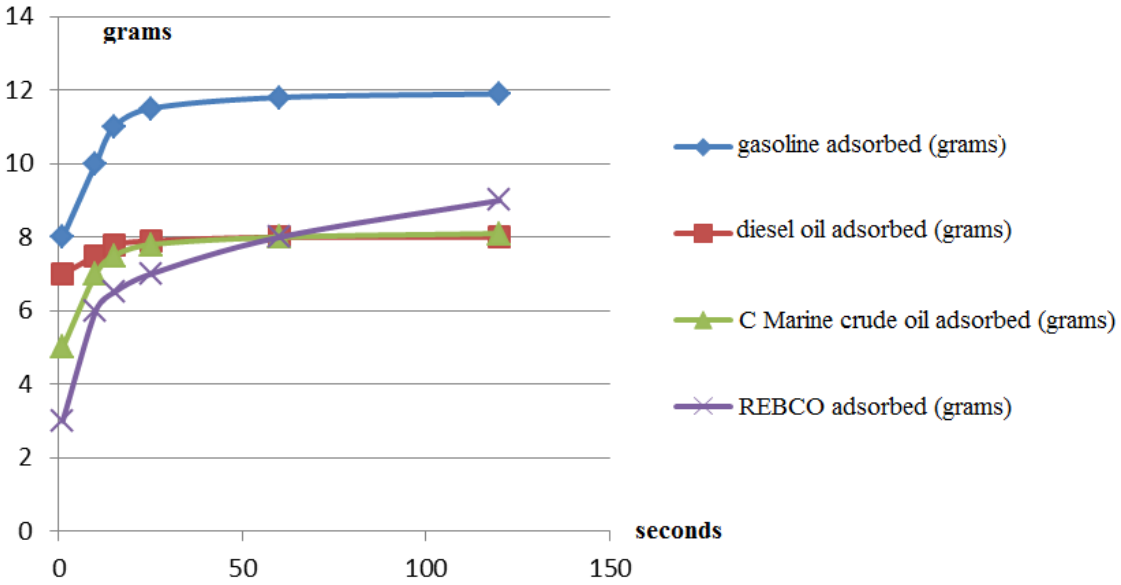

Fig. 11. Curves of oil sorption kinetics on peat moss.

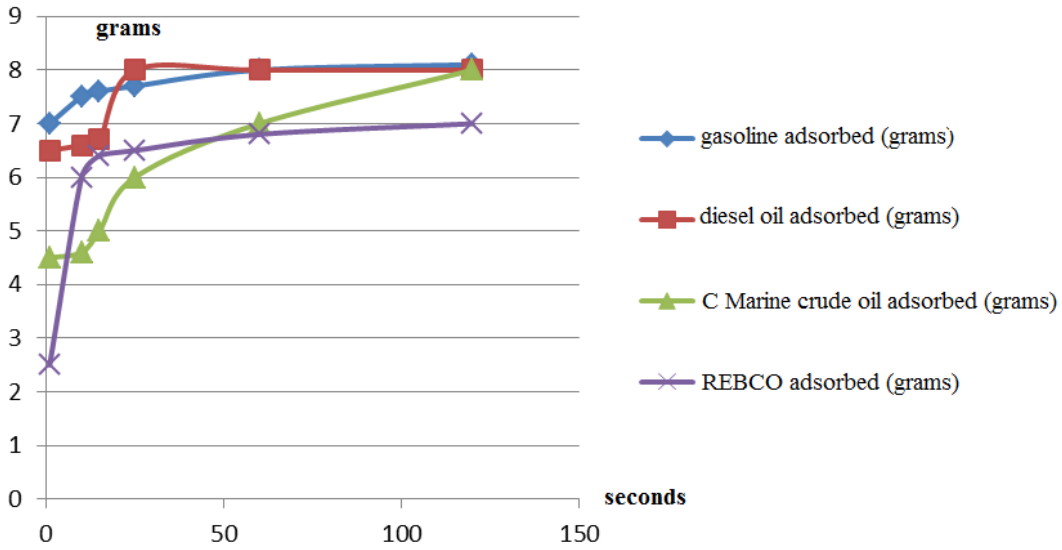

Fig. 12. Curves of oil sorption kinetics on the sunflower seed cake.

Table 5.

The kinetics of retention in the pores of peat moss

times, s	gasoline adsorbed (grams)	diesel oil adsorbed (grams)	C marine crude oil adsorbed (grams)	REBCO adsorbed (grams)
1	8	7	5	3
10	10	7.5	7	6
15	11	7.8	7.5	6.5
25	11,5	7.9	7.8	7
60	11,8	8	8	8
120	11,9	8	8.1	9

Table 6.

The kinetics of retention in the pores of sunflower seed cake

times, s	gasoline adsorbed (grams)	diesel oil adsorbed (grams)	C marine crude oil adsorbed (grams)	REBCO adsorbed (grams)
1	7.0	6.5	4.5	2.5
10	7.5	6.6	4.6	6.0
15	7.6	6.7	5.0	6.4
25	7.7	8.0	6.0	6.5
60	8.0	8.0	7.0	6.8
120	8.1	8.0	8.0	7.0

When a liquid is brought into contact with a dry porous medium such as adsorbents, fluid is drawn into the porous medium. Absorption and retention of liquid is based on the shape and size of pores, the surface tension of the liquid, and the wet surface of the solid. The use of several capillary columns with

different diameters, filled with adsorbent material and immersed in an oil product can simulate the removal of the pollutants through adsorption.

Determination of retention after compression

The four adsorbents resulting from adsorption experiments were subject to final compression test, for one minute, at a pressure of 2 N/m².

Before evaluating retention capacity, each adsorbent was weighted before and after pressure compression. The results are given in Table 7.

Table 7.

Petroleum product lost after compression

Natural adsorbent	**Diesel**	**Gasoline**	**C Marine crude oil**	**REBCO**
Peat moss	2.0 %	1.4 %	3.0 %	3.5 %
Sunflower seed cake	2.2 %	1.6 %	3.2 %	3.6 %
Polypropylene	0.8 %	0.6 %	1.2 %	1.6 %
Clay	0.4 %	0.5 %	1.1 %	1.2 %

Based on the experiments of this work we can sum up the following conclusions:

- Peat moss adsorption capacity of oil products is 2-4 times his weight, depending on the nature of the hydrocarbon oil on the best type of natural sorbent polydispersed;
- Petroleum products are retained within the peat pores by adsorption, peat acting as a sponge that collects the product by capillary phenomena;
- The sunflower seed cake tested is a new biodegradable sorbent, with average sorbtion properties that can be used in the methods of remediation of polluted waters in our country due to its low price. However, sunflower seed cake showed good buoyancy compared to the other three sorbents;
- The four sorbents tested showed similar behavior: initial adsorption rate is high, then the intermediate phase adsorption rate decreases until reaching the stationary phase when no longer does any adsorption;
- The use of peat moss as an sorbent showed high potential to remove petroleum products from marine environments with the advantage of being a natural sorbent and eco-friendly;

- These results were obtained under static conditions; in these conditions the rate of adsorption is slightly higher as opposed to natural processes;

4. Conclusions

This study has confirmed the following conclusions:

- Industrial exploitation of peat moss and its use as an sorbent for the collection of surface oil products is promising, because this type of material has high sorption capacity of oil products;
- Use of sunflower seed cake in aquatic pollution phenomena is achieved due to low unit cost and medium efficiency in the collection of petroleum hydrocarbons;
- The results of experiments showed that clay presents poor performance on retention capacity;
- Natural sorbents are categorized as renewable resources and can be reused several times and recycled during the life cycle;
- These biodegradable materials are easily applied, removing pollutants in contaminated environment, without causing problems in the aquatic ecosystem;
- Natural sorbents don’t eliminate toxic emissions into the environment and don’t have a negative impact on living creatures;
- The time of the adsorption process of hydrocarbons is relatively low;
- Sorbents polydispersity shows high efficiency in collecting oil products;
- External parameters from nature (heat transfer processes at the water-air, water stratification rest masses, sea currents, wind, etc.) influence the absorption of pollutants by the sorbents;
- Bioremediation of natural sorbents collected on the surface of the water may be achieved by increasing the rate of biodegradation by the addition of fertilizer and micro-organisms;

The study shows that natural organic sorbents adsorb oil layer on the water surface in high yields, while being deposited on the bottom of the vessel, so environmental legislation in force require collection sorbents undergo a process of decontamination.

REFERENCES

[1] Chiş, T.-V., The incidental costs of oil pollution, *Review of Scientific Works, Agronomy Series Year*, Publisher Ion Ionescu de la Brad, Iasi, ISSN 1454-7414, 2014.
[2] Chiş, T.-V., The effects of oil pollution on Dobrogea soil, the 48-th Scientific Symposium "*Agriculture and environment-present and perspectives*", University of Agricultural Sciences and Veterinary Medicine, Faculty of Agriculture, 2005.
[3] Fingas M., Oil spill Science and Tehnology, Prevention, Response and Cleanup, Gulf Professional Publishing is an imprint of Elsevier, 2011;
[4] Abdul Aziz Al-Majed, R. Adebayo Abdulrauf, M. Enamul, A novel sustainable oil spill control technology, *Environmental Engineering and Management Journal*, 13 (2), (2013), 265-274.
[5]. Milan I., Gomoiu M. T., Causes and consequences of marine pollution by oil, GEO-ECO-MARINA 14/2008 - SUPPLEMENT NO. 1147, *Earth Science, Knowledge and Environment*, 147-154;
[6] Ladd R. W., Smith D. D., System study of oil spill cleanup procedure, *Society of Petroleum Engineers*, SPE 3047-MS, (1970), 1-30;
[7] Flaherty L. M., Jordan J. M., Sorbent performance study for crude and refined petroleum products, *Oil Spill Conference, Processing*, (1989), 155-160,
[8] Welch J., Stolls A. M. And Etkin D. S., Worldwide oil spill trends, *Oil Spill Conference Processing*, 1991, 720-722;
[9] Etkin D. S., Estimating cleanup costs for oil spills, *Oil Spill Conference, Processing*, (1999), 35-39;
[10] Michel J., Malcolm L. Spaulding, Michel K., MacKinnon M., J. O'Brien, and Stephen Palmer, Spills of nonfloating oils: findings, conclusions, and recommendations to improve preparedness and response, *Oil Spill Conference*, Processing, March 2001, 1301-1305;
[11] Pecheanu, I., Pecheanu, R., Using biodegradable natural adsorbents an controversial issue in Romania, (26-27 June 2008), National symposium with international participation, ACVADEPOL ", Mamaia, XV edition, 1-16.
[12] Li H., Boufadel M.C., Long-term persistence of oil from the Exxon Valdez spill in two-layer beaches, *Nature Geoscience*, 3, (2010), 96–99.
[13] Suni S., Kosunen A. L., Hautala M., Pasila A., Romantschunkl M., Use of a by-product from peat excavation, cotton grass fibre, as a sorbent for oil-spills, *Marine Pollution Bulletin*, 49, (2004), 916-921.
[14] ITOPF: Impact PR and Design Limited, *Use of a sorbent materials in oil spill response*, Canterbury, United Kingdom, 2012, 1-12;

RESPONSE SURFACE MODELING AND MULTI-OBJECTIVE OPTIMIZATION OF A GAS SEPARATION PROCESS BY DYNAMIC ADSORPTION IN FIXED BED

Marius S. SECULA[*1], Benoît CAGNON[2], Maria SPIRIDON[1], Ioan MĂMĂLIGĂ[1]

1 Department of Chemical Engineering, Faculty of Chemical Engineering and Environmental Protection, Gheorghe Asachi Technical University of Iasi, 73 Prof. dr. docent Dimitrie Mangeron Street, Iasi, 700050, Romania
[2] ICMN (Interfaces, Confinement, Matériaux et Nanostructures) UMR 7374-CNRS-University of Orléans, 1B, rue de la Férollerie 45071 Orléans cedex 2, France

Abstract

The paper presents a study on the mathematical modeling and optimization of a pilot plant for gas separation by adsorption in fixed bed, operated under non-isothermal and non-adiabatic conditions. By means of an orthogonal central composite design, considering the gas flow rate, adsorbent bed height and adsorbate concentration in gas as independent variables, respectively, breakthrough time, breakthrough volume and pressure drop as adsorption process responses, three quadratic polynomial models are suggested and statistically validated. The obtained results show that the breakthrough time, breakthrough volume and pressure drop can be predicted in the experimental region with average relative errors of 11.74, 10.78 and 1.64 % respectively. Further, a thorough analysis of the obtained response surface is performed through canonic analysis. A multi-objective method based on the Normal Boundary Intersection algorithm and Lagrange multipliers method are used in order to determine the optimal operating parameters of the pilot-plant as well as to provide an intimate insight on its functionality within the technical ranges of the operating parameters.

Keywords: Central Composite Design, Dynamic adsorption, Fixed bed, Impregnated alumina, Multi-objective optimization, Normal Boundary Intersection algorithm

1. Introduction

Adsorption processes are commonly used in the separation of gas mixtures as an alternative to conventional separation processes such as distillation and absorption. They have attracted great interest due to their reduced energetic consumption and to the achievements in adsorption-based technologies [1].

[*] Corresponding author: E-mail address: mariussecula@ch.tuiasi.ro (Marius Sebastian Secula).

Operations such as air separation, hydrogen purification and dehumidification of gas streams are only a few examples of common applications of adsorption processes [2]. Recently, a new family of sorbent composites "salt in porous matrix" has been developed [3]. These materials have enhanced water selectivity, which is developed by impregnating common matrices, such as activated carbon, alumina or silica gel, with hygroscopic salts such as $CaCl_2$ or LiBr [4,5].

Petrescu and Secula reported an extensive review on the analytical mathematical modeling of gas-solid adsorption in fixed bed under various operating conditions [6]. These mathematical models allow one to design packed-bad adsorbers and optimize their operating regimes. As we have shown in our prior works, statistical modeling based on artificial neural networks [7] or Response Surface Methodology [8, 9] can also be successfully applied to model and optimize gas adsorption processes.

This work reports a study on the Response Surface modeling and optimization of a pilot plant for water vapor separation from air by adsorption in fixed bed of $CaCl_2$-impregnated alumina grains, operated under non-isothermal and non-adiabatic conditions. Air flow rate (Q), adsorbent bed height (H) and inlet relative humidity (φ) are considered as independent variables, whereas the breakthrough time, breakthrough volume and pressure drop are considered as adsorption process responses. Three quadratic polynomial models are suggested and statistically validated for each adsorption process response. After the canonic analysis of the obtained response surfaces is performed, two optimization methods, classic Lagrange multipliers method and an advance multi-objective method based on the NBI algorithm, are used to determine the optimal operating parameters of the pilot-plant, and to provide a thorough insight on its functionality within the technical ranges of the operating parameters.

2. Experimental

Impregnated alumina characterization

Cylindrical alumina having a diameter of $3.2 \cdot 10^{-3}$ m and a length of $3.2 \cdot 10^{-3}$ m was used as adsorbent matrix. Proper amounts of alumina were dried in an oven at 160°C for 4 h and then cooled to room temperature in a desiccator. Solution of 15 wt% $CaCl_2$ was prepared dissolving calcium chloride (Merck analytical reagent) previously dried in oven for 2 h, at 120 °C, and distilled water. Then, 50 g of raw alumina were immersed in 250 mL of 15 wt% $CaCl_2$ solution. After 24 h of impregnation, the composite was separated by filtration under vacuum, at room temperature. The obtained composite was dried for 4 h in the oven at 160°C, and then cooled in a desiccator. The concentration of salt in solid of 7.92 wt% $CaCl_2$

was determined by weighting composite samples before and after impregnation and drying

Textural characteristics of the raw and impregnated alumina were determined by N_2 adsorption-desorption isotherm at -196 °C using a Micromeritics ASAP 2020 as described in reference [9]. The nitrogen adsorption isotherms were analyzed according to the Dubinin theory [10]. Both the specific microporous volume (W_0 in $cm^3\ g^{-1}$) and the mean pore size (L_0 in nm) were estimated from the linear part of the Dubinin-Radushkevich (D-R) plot [10, 11]. Besides, the Sing α_S plots [12] were used to determine the external specific surface (S_{ext} in $m^2\ g^{-1}$) and assuming that for slit-shaped micropores (assumption) the specific surface of micropores (S_{micro} in $m^2\ g^{-1}$) could be estimated using the specific microporous volume and the mean pore size [10]. Figure 1 shows the N_2 adsorption-desorption isotherms of the two materials and the pore size distribution of the impregnated material obtained by DFT method. Table 1 presents the main characteristics of the raw and synthesized impregnated material.

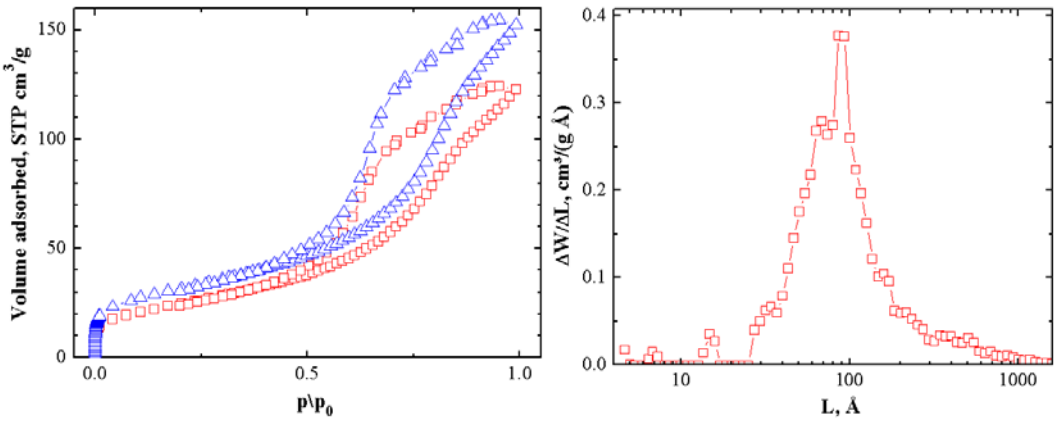

(a) (b)

Fig. 1. Nitrogen adsorption-desorption isotherm of (△) raw alumina and (□) impregnated alumina sorbents (a) and pore size distribution of impregnated alumina sorbent (b).

Table 1

Raw and $CaCl_2$-impregnated alumina porous properties

Materials	W_t (cm^3g^{-1})	W_o (cm^3g^{-1})	L_o (Å)	S_{ext} ($m^2\ g^{-1}$)	S_{micro} ($m^2\ g^{-1}$)	S_{total} ($m^2\ g^{-1}$)
Raw alumina	0.24	-	-	108		
$CaCl_2$-impregnated alumina	0.19	0.03	17.6	97	34	131

Description of the adsorption pilot-plant used in experimental design

The breakthrough curves were obtained using a dynamic adsorption experimental set-up shown in Fig. 2. This consists in a vertical cylindrical column (6), heat exchanger (5), mixing chamber (4), air wetting chamber (3), thermostat (2), ventilating fan (1), valves for controlling air and water flow rates, and measuring and control systems for temperature, pressure and relative humidity.

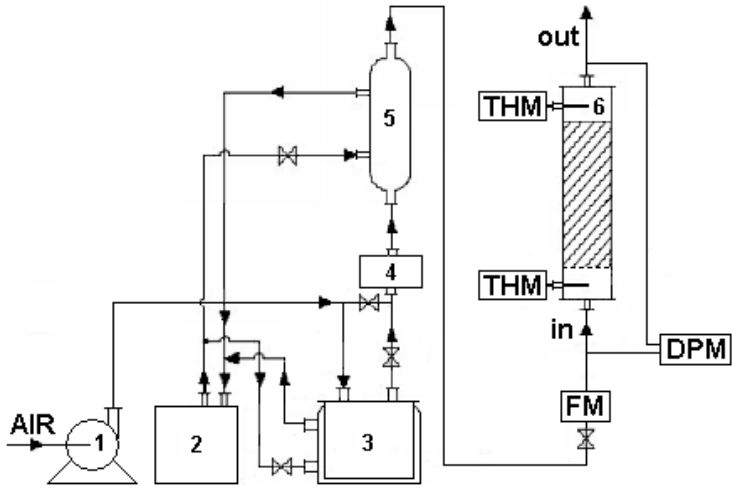

Fig. 2. Dynamic adsorption experimental set-up: 1 – ventilating fan; 2 – thermostat; 3 – wetting chamber; 4 – mixing chamber; 5 – heat exchanger; 6- adsorption column (THM – thermohygrometer, FM – flowmeter, DPM – differential pressure meter).

Experimental investigations were performed under atmospheric pressure and at an initial air temperature value of 27±0.5°C. Wet air having different relative humidity values ranged between 39.5 and 85.5 % was fed into the packed-bed column at flow rate values ranged between 0.61 and 2.19 $m^3 \cdot h^{-1}$.

The adsorption process was achieved in fixed bed operated under dynamic regime and non-isothermal and non-adiabatic conditions. The geometrical parameters of the fixed adsorbent bed were $2.95 \cdot 10^{-2}$ m in diameter while the height was ranged between 0.1228 and 0.2452 m, which correspond to a volume of adsorbent bed of 125 and 250 cm^3 respectively.

In the experiments, the temperature and relative humidity were measured by using two high accuracy and multi-function digital Testo 625 termopsihrometers. The precision of the two sensors for temperature is ± 0.5 ºC, and for air relative humidity is ± 2.5 % RH. The measuring points are located at the inlet and outlet of the adsorbent bed. The pressure drop was measured by means of a PCE P01 differential manometer having an accuracy of ± 0.3 %.

Error analysis

The error analysis of the experimental results on the basis of the uncertainties in the primary measurements was carried out using the Kline and McClintock relationship [13]:

$$\Delta e = \left[\left(\frac{\partial f}{\partial a_1} \right)^2 (\Delta a_1)^2 + \left(\frac{\partial f}{\partial a_2} \right) (\Delta a_2)^2 + \ldots + \left(\frac{\partial f}{\partial a_3} \right) (\Delta a_3)^2 \right]^{1/2} \quad (1)$$

where f is the given function of the independent variables, a_i is one of the variables of the function and Δa_i is the absolute error associated with the variable. Further is described the expression of the relative error:

$$\frac{\Delta e}{e} = \left[\left(\frac{\partial f}{\partial a_1} \right)^2 \left(\frac{\Delta a_1}{e} \right)^2 + \left(\frac{\partial f}{\partial a_2} \right) \left(\frac{\Delta a_2}{e} \right)^2 + \ldots + \left(\frac{\partial f}{\partial a_n} \right) \left(\frac{\Delta a_n}{e} \right)^2 \right]^{1/2} \quad (2)$$

The breakthrough curves determined experimentally represent graphical plots of C/C_0 versus time, where C_0 (kg m^{-3}) is the initial concentration of water vapors in air, C (kg m^{-3}) is the concentration of water vapors in air at the column output. C is defined as follows:

$$C = \rho \cdot w = 0.62198 \cdot \rho \cdot \frac{\varphi \cdot p_{vs}}{P - \varphi \cdot p_{vs}} \quad (3)$$

where ρ is wet air density, kg·m^{-3}, w – weight concentration of adsorbate in gas, kg·kg^{-1}, φ - air relative humidity, %, P – barometric pressure, mmHg, and p_{vs} – saturated vapor pressure, mmHg.

The saturated water vapor partial pressure is expressed. [14]:

$$\ln(p_{vs}) = 5800.22/T - 5.5162 - 4.8640 \cdot 10^{-2} \cdot T + 4.1765 \cdot 10^{-5} \cdot T^2 - \\ -1.4452 \cdot 10^{-8} \cdot T^3 + 6.5460 \cdot \ln(T) \quad (4)$$

A detailed error analysis for water vapor concentration in air indicated an overall accuracy within ± 4.3%.

Experimental statistical design

The statistical design of experiments is a structured and systematized experimentation method in which all independent variables are varied simultaneously over a set of experimental runs in order to determine the relationship between factors influencing the output responses of a process. The statistical experimental design employed to obtain the response surface modeling of a gas separation pilot plant was performed for water vapor adsorption on calcium chloride impregnated alumina. Three factors (independent variables),

namely, the wet air flow rate (Q), adsorbent bed height (H) and initial air relative humidity (φ) were considered.

In Table 2 are listed the controllable variables (factors) and their levels in coded and actual values. The output responses were the breakthrough time (Y_{t_b}), breakthrough volume (Y_{V_b}) and pressure drop ($Y_{\Delta p}$). In order to describe the factors effects on the responses, an orthogonal Central Composite Design (CCD) with star points was employed with 3 factors and 5 levels.

Table 2

Design variables and their coded levels and actual values used in the experimental design

Source of variation	**Actual values of coded levels**				
	$-\alpha$	**-1**	**0**	**1**	**$+\alpha$**
Flow rate, $m^3 \cdot h^{-1}$	0.61	0.80	1.40	2.00	2.19
Bed height, m	0.1228	0.1375	0.1840	0.2305	0.2452
Air relative humidity, %	39.5	45.0	62.5	80.0	85.5

The central composite experimental design (CCD) consists of 16 experiments with 8 orthogonal design points (factorial points), 6 star points to form a central composite design with $\alpha = 1.316$ and 2 center points for replication. The experimental design matrix and the obtained output responses are listed in Table 3.

The first response considered was breakthrough time (t_b), which is the time when mass transfer zone reaches the adsorbent bed outlet. Though an increment in t_b implies that the mass transfer zone advances more slowly, it does not necessarily result in an improved efficiency of the separation process. For this reason, it is useful to calculate the volume of influent adsorbed by gram of adsorbent up to t_b, V_b. The breakthrough time, t_b, was considered at $C/C_0 = 0.15$ [15], and the breakthrough volume was determined by means of the following relationship:

$$V_b = \frac{Q \cdot t_b}{m} \tag{5}$$

In the present work, the calculations were performed by means of MathCAD and Matlab softwares.

3. Results and discussions

Breakthrough curves

Fig. 3 shows several breakthrough curves obtained at room temperature for water vapor adsorption on $CaCl_2$-impregnated alumina.

The normalized concentration of water vapors in air at the output of the packed bed column as determined from psychometric measurements is plotted as

a function of the adsorption time. Thus, the influence of the considered operating parameters (air flow rate, adsorbent bed height and inlet relative humidity) on the breakthrough curves is emphasized.

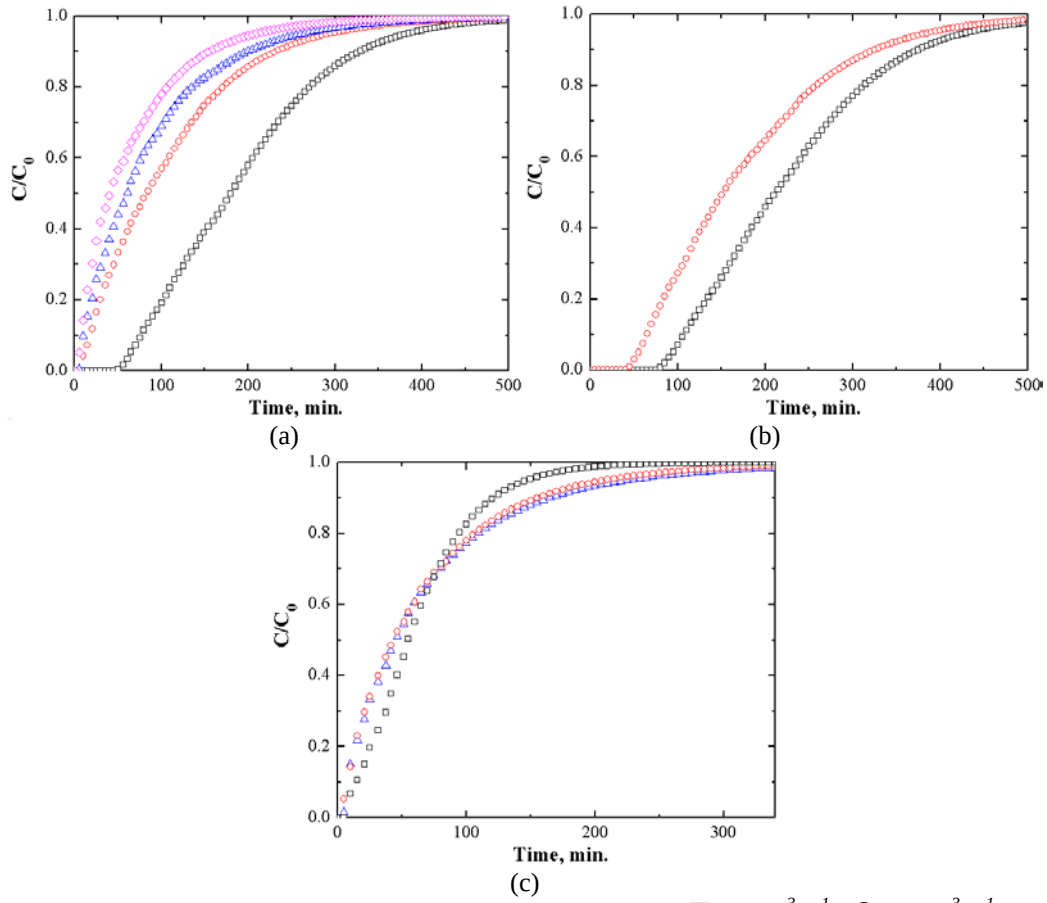

Fig. 3. Breakthrough curves at (a) different values of flow rate: (□) *0.6* $m^3 \cdot h^{-1}$, (○) *1.2* $m^3 \cdot h^{-1}$, (△) *1.7* $m^3 \cdot h^{-1}$, (◇) *1.7* $m^3 \cdot h^{-1}$, and φ *= 62.5%, H = 0.2452 m*; (b) two values of bed height: (○) *0.1840 m*, (□) *0.2452 m*, and φ *= 39.5%, Q = 0.61* $m^3 \cdot h^{-1}$; (c) different values of inlet relative humidity: (△) *39.5%*, (○) *62.5 %*, (□) *85.5 %*, and *H = 0.2452 m, Q = 2.19* $m^3 \cdot h^{-1}$.

Fig. 3a describes the influence of air flow rate on the breakthrough curves, which lies in an important decrease of breakthrough time and a faster passing of the mass transfer zone throughout the height of the adsorbent bed. This is in agreement with the results reported in literature [16]. Fig. 3b shows the results obtained at different values of adsorbent bed height, at constant air flow rate and inlet relative humidity. As can be noticed, with higher heights of adsorbent bed, an important augmentation of the breakthrough time occurs, while the mass transfer zone (the steep region of the curve) remains approximately unchanged.

This is valid also for the breakthrough curves plotted in Fig. 3a due to the driving force in the gas flowing through the adsorbent bed is constant (inlet relative humidity is constant). Fig. 3c depicts the influence of inlet relative humidity on the shapes of breakthrough curves when flow rate and bed height are kept constant. Thus, a lower driving force of the adsorption process respectively a lower initial relative humidity results in a wider mass transfer zone (a gentler slope of the breakthrough curve). In order to emphasize the move of mass transfer area throughout the fixed bed as a function of the air flow rate, adsorbent bed height and inlet relative humidity, the statistical modeling of breakthrough time and volume is performed by means of RSM.

RSM models

Based on the experimental design results listed in the last three columns of Table 3, the RSM has been applied to determine the polynomial regression equations and to establish the relation between each one of the three output responses and the input factors.

Table 3

Orthogonal Central Composite Design of experimental and responses

Run No	**Input variables**[a]						**Responses**		
	Flow rate		Bed height		Relative humidity		Breakthrough time	Breakthrough volume	Pressure drop
	Q $(m^3 \cdot h^{-1})$	x_1	H (m)	x_2	φ $(\%)$	x_3	t_b $(min.)$	V_b $(m^3 \cdot kg^{-1})$	Δp (Pa)
1	2.00	1	0.2305	1	80.0	1	11.64	1.858	714.8
2	0.80	-1	0.2305	1	80.0	1	36.30	2.318	188.9
3	2.00	1	0.1375	-1	80.0	1	0.71	0.191	423.1
4	0.80	-1	0.1375	-1	80.0	1	10.44	1.118	102.5
5	2.00	1	0.2305	1	45.0	-1	9.98	1.593	711.5
6	0.80	-1	0.2305	1	45.0	-1	54.76	3.496	193.7
7	2.00	1	0.1375	-1	45.0	-1	4.66	1.247	418.6
8	0.80	-1	0.1375	-1	45.0	-1	24.55	2.628	105.9
9	2.19	α	0.1840	0	62.5	0	3.84	0.660	686.3
10	0.61	$-\alpha$	0.1840	0	62.5	0	48.41	2.319	87.8
11	1.40	0	0.2452	α	62.5	0	20.55	1.921	475.8
12	1.40	0	0.1228	$-\alpha$	62.5	0	3.26	0.683	230.4
13	1.40	0	0.184	0	85.5	α	5.30	0.582	351.8
14	1.40	0	0.184	0	39.5	$-\alpha$	14.14	1.555	348.4
15	1.40	0	0.184	0	62.5	0	8.65	0.951	348.9
16	1.40	0	0.184	0	62.5	0	8.40	0.923	354.6

[a] $\alpha = 1.316$

The experimental data (Table 3) were analyzed by the Multi Linear Regression (MLR) method to fit a second-order polynomial equation [17]:

$$Y = \beta_0 + \sum_{i=1}^{4} \beta_i \cdot x_i + \sum_{i=1}^{4} \beta_{ii} \cdot x_i^2 + \sum_{i=1}^{3} \sum_{j>i}^{4} \beta_{ij} \cdot x_i \cdot x_j + \varepsilon \quad (6)$$

where β_0, β_i, β_{ii}, and β_{ij} are regression coefficients (β_0 is a constant term, β_i is a linear effect term, β_{ii} is a squared effect term, β_{ij} and is an interaction effect term) and Y is the predicted response value. MLR is based on finding the regression model that minimizes the residual sum of squares of the response.

For each response, the regression coefficients corresponding to the coded and actual variables were determined as described herein further.

RSM model for breakthrough time (t_b)

In terms of coded variables, the model of the breakthrough time (t_b) is:

$$Log\left(Y_{t_b}\right) = 0.925 - 0.398x_1 + 0.304x_2 - 0.162x_3 + 0.082x_1 \cdot x_2 + 0.134x_2 \cdot x_3 + 0.116x_1^2 \quad (7)$$

subjected to $-1 \le x_i \le +1$; $\forall i = 1,2,3$.

In term of actual variables, the RSM model is:

$$Log\left(t_b\right) = 4.512 - 2.104M_V - 7.864H - 0.04\varphi + 2.925M_V \cdot H + 0.165H \cdot \varphi + 0.322M_V^2 \quad (8)$$

subjected to $0.8 \le Q \le 2$ [$m^3\ h^{-1}$]; $0.1375 \le H \le 0.2305$ [m] and $45 \le \varphi \le 80$ [%].

The significance of the regression coefficients in RSM-models was tested using the statistical Student's t test for a confidence interval of *99 %* [18]. Consequently, in Eqs. (7) and (8) only the significant terms were retained. However, the interaction between flow rate and bed height is significant only for a confidence interval of *95 %*.

The significance of the models was tested by the analysis of variance (ANOVA) that is the most reliable way to evaluate the quality of a RSM-model [19]. The ANOVA parameters for the breakthrough time are listed in Table 4.

The model F-ratio computed according to ANOVA is 77.35, a value much greater than the tabulated one ($F\text{-}tab_{(0.05,6,9)} = 3.374$). This pinpoints the statistical validity of the RSM model. Based on the F-ratio and degrees of freedom, the p-value can be computed. It is generally accepted that a model is statistically validated when model p-value is lower than *0.05* (model p-value *<0.0001*), respectively a model error is insignificant when the p-value of lack of fit is higher than *0.05* (lack of fit p-value = *0.0777*).

The estimated value of the determination coefficient (R^2 – correlation coefficient between experimental and predicted values by RSM-model) is 0.981, which is very close to that of statistical adjustment ($R_{adj}^2 = 0.968$), indicating that only the significant terms were included in the RSM-model. Moreover, the F-ratio

corresponding to the lack of fit is lower than F-tabulated ($F\text{-tab}_{(0.05,9,1)} = 238.882$) underlying an insignificance of the model error [20].

Table 4

Analysis of variance (ANOVA) for t_b response.

Source	***DF***[a]	***SS***[b]	***MS***[c]	***F-ratio***	***F-tab***	***p-value***	R^2	R^2_{adj}
Model	6	3.460	0.580	77.35	3.374	<0.0001	0.981	0.968
Residual	9	0.067	$7.446 \cdot 10^{-3}$					
Lack of Fit[d]	8	0.067	$8.366 \cdot 10^{-3}$	98.72	238.882	0.0777		
Pure Error[e]	1	$8.475 \cdot 10^{-5}$	$8475 \cdot 10^{-5}$					
Total	15	3.527						

[a] Degrees of freedom, [b] Sum of squares, [c] Mean square, [d] Model error, [e] Replicate error.

The statistical agreement between the experimental data and those predicted with RSM-model for t_b model is emphasized in Fig. 4a.

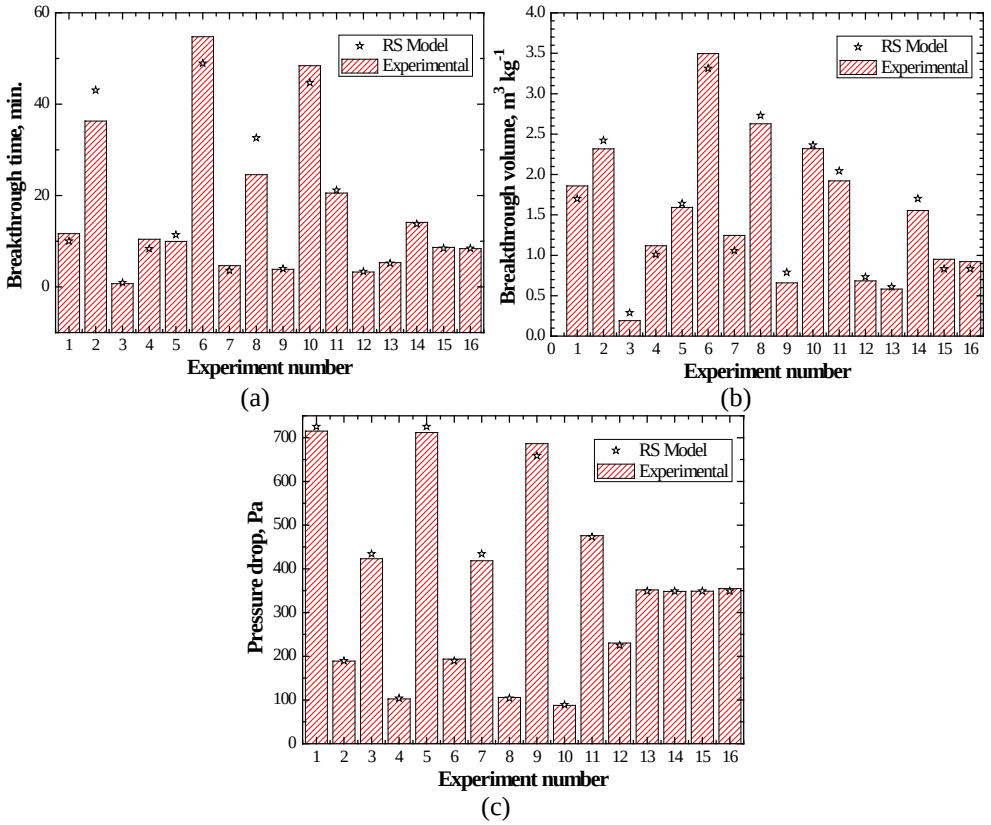

Fig. 4. Experimental and predicted values of (a) t_b response; (b) V_b response; (c) Δp response.

In Fig. 5 the response surface plots of breakthrough time are presented emphasizing the influence of the design variables upon this dependent variable.

As can be noticed, the decrease of flow rate and higher bed heights result in longer breakthrough times. Though the main effect of inlet relative humidity is lower, it is a significant one. Nevertheless the breakthrough time is an important indicator in gas separation approaches; the breakthrough volume is a more appropriate response for optimization problems.

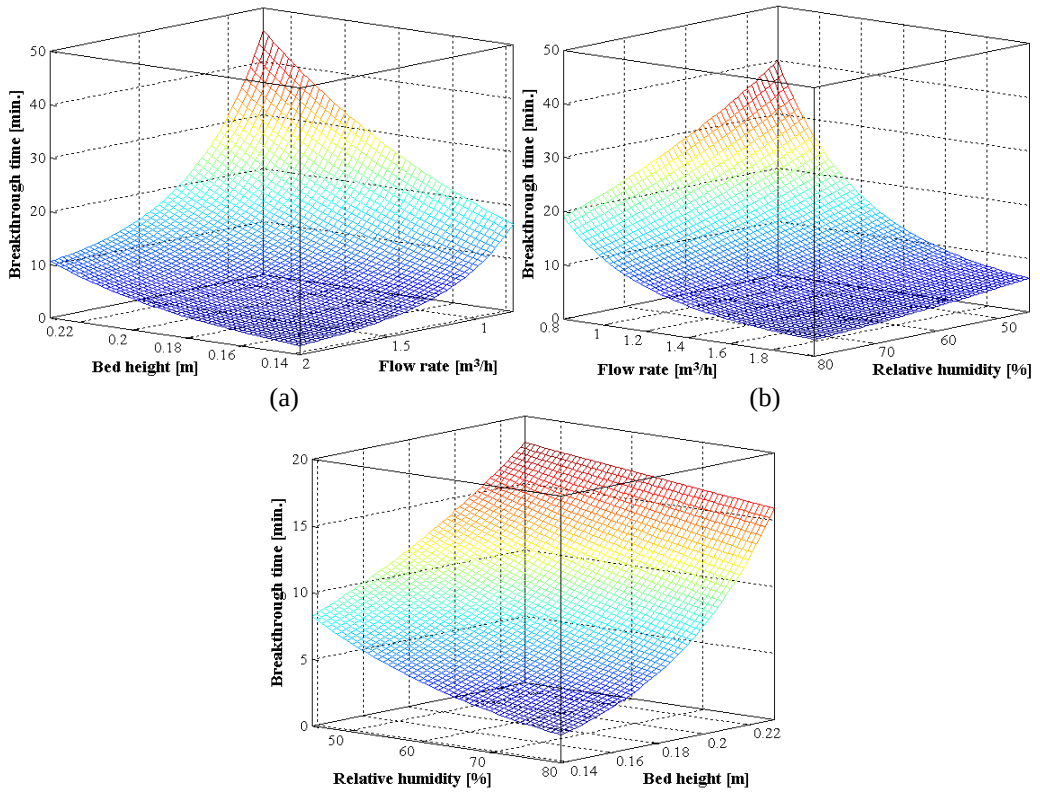

Fig. 5. Response surface plots of the breakthrough time as a function of (a) flow rate and bed height, $x_3=0$; (b) flow rate and relative humidity, $x_2=0$; (c) bed height and relative humidity, $x_1=0$.

RSM model for breakthrough volume (V_b)

The breakthrough volume (V_b) that takes into account the treated volume of gas per unity of adsorbent was calculated by means of Eq. (5). The obtained regression coefficients were tested with statistical Student's t test for a confidence interval of *99 %*.

In terms of the coded variables, the RSM-model is as follows:

$$Y_{V_b} = 0.829 - 0.598x_1 + 0.498x_2 - 0.415x_3 + 0.237x_1 \cdot x_3 + 0.207x_2 \cdot x_3 + 0.431x_1^2 + 0.322x_2^2 + 0.187x_3^2 \quad (9)$$

subjected to $-1 \le x_i \le +1;\ \forall i = 1,2,3.$

In term of actual variables, the RSM-model is:

$$V_b = 16.41 - 5.758M_V - 60H - 0.179\varphi + 0.023M_V \cdot \varphi + 0.254H \cdot \varphi + 1.196M_V^2 + 149.1H^2 + 0.0006\varphi^2 \quad (10)$$

subjected to $0.8 \le Q \le 2\ [m^3\ h^{-1}];\ 0.1375 \le H \le 0.2305\ [m]$ and $45 \le \varphi \le 80\ [\%]$.

The ANOVA analysis results are described in Table 5. In case of breakthrough volume, the model F-ratio is also much higher than model F-tabulated (F-tab$_{(0.05,8,7)}$ = 3.726), determination coefficient and R^2_{adj} are very close to unity, the F-ratio of the model error is lower than F-tabulated, p-value of the model is lower than *0.05*, while the p-value of lack of fit is higher than *0.05*. Thus, the statistical results presented in Table 5 indicate that the RSM-model suggested for volume breakthrough is adequate and the model error is insignificant. The statistical agreement between the experimental data and those predicted with RSM-model for V_b response is shown in Fig. 4b.

Table 5

Analysis of variance (ANOVA) for V_b response

Source	***DF***[a]	***SS***[b]	***MS***[c]	***F-ratio***	***F-tab***	***p-value***	R^2	R^2_{adj}
Model	*8*	*11.4700*	*1.433*	*45.49*	*3.726*	*<0.0001*	*0.981*	*0.960*
Residual	*7*	*0.2206*	*0.03151*					
Lack of Fit[d]	*6*	*0.2202*	*0.0367*	*92.98*	*233.986*	*0.07922*		
Pure Error[e]	*1*	$3.947 \cdot 10^{-4}$	$3.947 \cdot 10^{-4}$					
Total	*15*	*11.6906*						

[a] Degrees of freedom, [b] Sum of squares, [c] Mean square, [d] Model error, [e] Replicate error.

In Fig. 6 the response surface plots of V_b are shown and the influences of the independent variables upon this response are emphasized.

In comparison with the RSM-model for t_b response, in this case the main effect of inlet relative humidity becomes comparable with the other two factors considered. Moreover, while the interaction between flow rate and bed height becomes insignificant, the interactions of inlet relative humidity with the other two independent variables as well as the quadratic terms of inlet relative humidity and bed height become significant. In order to optimize the volume of treated gas in relation to energy consumption, one has to consider the pressure drop throughout the adsorbent bed height.

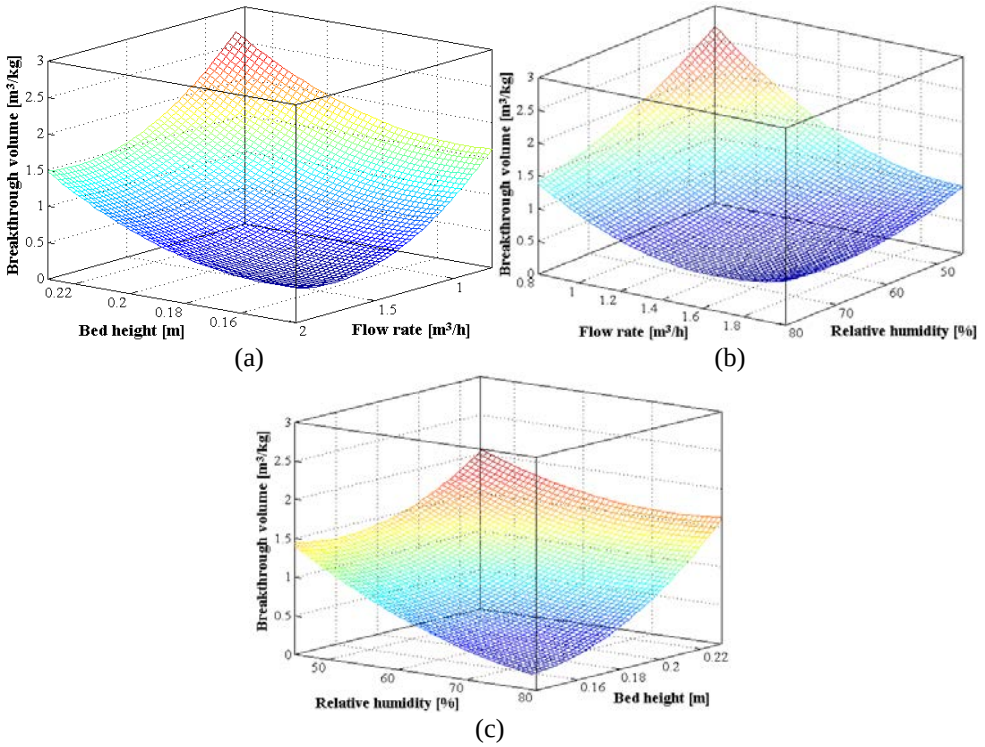

Fig. 6. Response surface plots of the breakthrough volume as a function of (a) flow rate and bed height, $x_3=0$; (b) flow rate and relative humidity, $x_2=0$; (c) bed height and relative humidity, $x_1=0$.

RSM model for pressure drop (Δp)

Δp was also considered as response and the obtained regression coefficients were tested with statistical t test for a confidence interval of *99 %*.

In terms of the coded variables, the RSM-model for Δp is as follows:

$$Y_{\Delta p} = 348.787 + 216.404x_1 + 94.132x_2 + 51.334x_1 \cdot x_2 + 14.346x_1^2 \quad (11)$$

subjected to $-1 \le x_i \le +1$; $\forall i = 1,2,3$.

In term of actual variables, the RSM-model for Δp is:

$$\Delta p = 23.432 - 89.449M_V - 551.54H + 1839.92M_V \cdot \varphi + 39.849M_V^2 \quad (12)$$

subjected to $0.8 \le Q \le 2\ [m^3\ h^{-1}]$ and $0.1375 \le H \le 0.2305\ [m]$.

The ANOVA analysis results are listed in Table 6. In case of pressure drop, due to the inlet relative humidity has no significant influence, the orthogonal central composite design proves to have an excessive number of experiments and consequently the model obtained has outstanding statistical significance and adequacy as shown in Table 6. The outstanding statistical agreement between the experimental data and those predicted with RSM-model for Δp response is underlined in Fig. 4c.

Table 6.

Analysis of variance (ANOVA) for Δp response

Source	***DF***[a]	***SS***[b]	***MS***[c]	***F-ratio***	***F-tab***	***p-value***	R^2	R^2_{adj}
Model	4	654246	163561	1187.75	3.357	<0.0001	0.997	0.994
Residual	11	1517.33	137.939					
Lack of Fit[d]	10	1495.23	149.523	6.77	241.882	0.291		
Pure Error[e]	1	22.098	22.098					
Total	15	655763						

[a] Degrees of freedom, [b] Sum of squares, [c] Mean square, [d] Model error, [e] Replicate error

In Fig. 7 the response surface plot of Δp is shown and the influence of the flow rate and bed height upon this response is emphasized. As can be noted, the pressure drop increases with adsorbent bed height and this effect becomes more pronounced at higher flow rates.

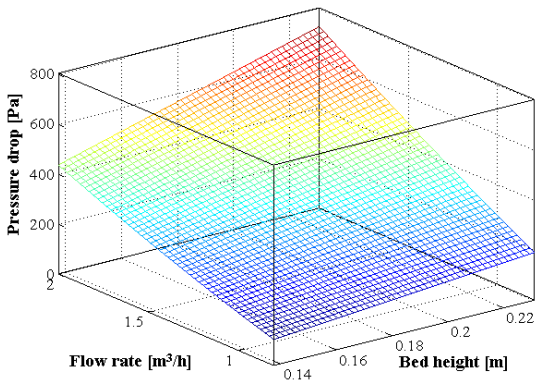

Fig. 7. Response surface plot of the pressure drop as a function of flow rate and bed height.

Analyzing the average relative error of these three responses, it can be concluded that the average relative errors of *11.74*, *10.78*, and *1.64%* were obtained for predictors of breakthrough time, breakthrough volume and pressure drop respectively.

Optimization

Taking into account the antagonist effects of flow rate and bed height on V_b and Δp responses, it is to be optimized the maximization of Y_{V_b} and the minimization of $Y_{\Delta p}$. For this aim, several optimization methods have been considered as described further.

Canonical analysis

The canonical analysis is a computing technique that allows one to find out whether a response has a global optimum point (stationary point) and whether this point is located within the valid region (region of experimentation). Since the RSM-models of the responses Y_{V_b} and $Y_{\Delta p}$ were found to be adequate for predictions, the canonical analysis was employed to determine the nature of the stationary point for these two responses. The suggested second-order approximations can be written in matrix form as follows:

$$\hat{Y} = b_0 + \bar{x}^T \cdot \bar{b}_L + \bar{x}^T \cdot \bar{\bar{B}} \cdot \bar{x} \tag{13}$$

where b_0 is intercept coefficient, $\bar{b}_L$ - slope coefficient and $\bar{\bar{B}}$ the second order coefficient. The stationary point of a response surface can be determined with the following equation:

$$\bar{x}_S = -\frac{1}{2}\left(\bar{\bar{B}}\right)^{-1}\bar{b}_L \tag{14}$$

The nature of the stationary point is defined by the canonical coefficients $\bar{\omega}$ that represent the eigenvalues of matrix $\bar{\bar{B}}$ and can be localized by solving the characteristic equation:

$$\det\left(\bar{\bar{B}} - \bar{\omega}\bar{\bar{E}}\right) = 0 \tag{15}$$

where $\bar{\bar{E}}$ is the unity matrix.

If all eigenvalues of $\bar{\bar{B}}$ are negative (positive), the response surface presents a maximum (minimum) in the stationary point. When eigenvalues (canonical coefficients) have mixed signs, the stationary point is a minimax or a saddle point [18].

The canonical forms obtained for breakthrough time, breakthrough volume and pressure drop can be written as follows:

$$\hat{Y}_{t_b} - 12.589 = -0.072\chi_1^2 + 0.133\chi_2^2 + 0.055\chi_3^2 \tag{16}$$

$$\hat{Y}_{V_b} - 1.768 = 0.097\chi_1^2 + 0.49\chi_2^2 + 0.353\chi_3^2 \tag{17}$$

$$\hat{Y}_{\Delta p} - 0.202 = 33.823\chi_1^2 - 19.477\chi_2^2 \tag{18}$$

where $\hat{Y}_{t_b,S} = 12.589$, $\hat{Y}_{V_b,S} = 1.768$ and $\hat{Y}_{\Delta p,S} = 0.202$ represent the values of the objective functions in the stationary points; χ_1, χ_2 and χ_3 are the canonical axes with origin in the stationary point.

The correctness of the canonical coefficients is confirmed by the validity of Eq. (19) that is equal to *0.116* for t_b response, *0.94* for V_b response and *14.346* for Δp response:

$$\sum_{i=1}^{n} b_{ii} = \sum_{i=1}^{n} \omega_{ii} \tag{19}$$

Due to the eigenvalues for t_b response have mixed signs, the stationary point $\bar{x}_{t_b,S} = [1.288 \quad 1.209 \quad -3.057]^T$ is a saddle point. In case of V_b, the canonical coefficients have positive signs and it can be concluded that the stationary point, $\bar{x}_{V_b,S} = [0.228 \quad -1.318 \quad 1.695]^T$, is a minimum point. However, the stationary points of breakthrough volume and time cannot be considered as optimal solutions due to these are located outside of the valid region. In case of Δp response, the objective function has a stationary point $\bar{x}_{\Delta p,S} = [-1.834 \quad -3.191]^T$ outside the valid region.

Since the breakthrough volume and pressure drop responses vary in different directions, in the search of the optimal solution it must be taken into account a compromise between the increase of volume of treated gas and decrease of pressure drop throughout the adsorbent fixed bed.

Optimization by Lagrange multipliers method

The optimization problem can be formulated mathematically as follows:

$$\min\left\{\hat{J}(x_1, x_2, x_3)\right\} \tag{20}$$

subjected to the restriction:

$$\hat{Y}_{V_b}(x1, x2, x3) - 2 \le 0 \tag{21}$$

where *2* $m^3 \cdot kg^{-1}$ represents the minimum volume of treated air imposed in accordance to the experimental region of independent variables investigated and the values of breakthrough volume obtained.

In order to determine the optimal solution within the valid ranges of the independent variables, two constraints on the coded variables x_1 and x_2 were taken into consideration ($x_1^2 - 1 \le 0$; $x_2^2 - 1 \le 0$), while x_3 was considered equal to *1*, value that corresponds to the most unfavorable situation (the highest concentration of adsorbate in gas).

In order to identify the optimal point of the objective function subjected to the restrictions mentioned above, the method of Lagrange multipliers was applied [18]. This method introduces new unknown scalar variables, named Lagrange multipliers, for each constraint. Thus, a Lagrange function *L* is to be developed:

$$L(x_1,\ldots.x_6,\lambda_1,\ldots,\lambda_3)=\hat{J}+\lambda_1\left[\left(\hat{Y}_{v_b}-V\right)+x_4^2\right]+\lambda_2\left(x_1^2-1+x_5^2\right)+\lambda_3\left(x_2^2-1+x_6^2\right) \quad (22)$$

where λ_1, λ_2, λ_3 are Lagrange multipliers, x_4, x_5, x_6 are fictive non-negative variables meant to transform the restrictions of inequality into equality ones. After differentiating in relation to each variable and multiplier, a system of equation was obtained. This system was solved using Minerr function included in MathCAD software.

Hence, the obtained optimal point to treat *2* $m^3 \cdot kg^{-1}$ of gas in terms of coded variables for $x_3 = 1$ is $\bar{x}^* = \{-1 \quad 0.71 \quad 1\}^T$ while the minimum value of pressure drop is *173.058 Pa*. To this optimal point it corresponds a breakthrough time of *33.92 min*.

The same results can be obtained by using the graphical method of overlapping the response surface of breakthrough volume and that of pressure drop at the maximum inlet relative humidity as shown in Fig. 8. Transforming the coded values into actual ones, the optimal flow rate is of *0.8* $m^3 \cdot h^1$ and optimal bed height of *0.217 m* allow to treat *2* $m^3 \cdot kg^{-1}$ of gas with a pressure drop of *173.058 Pa*.

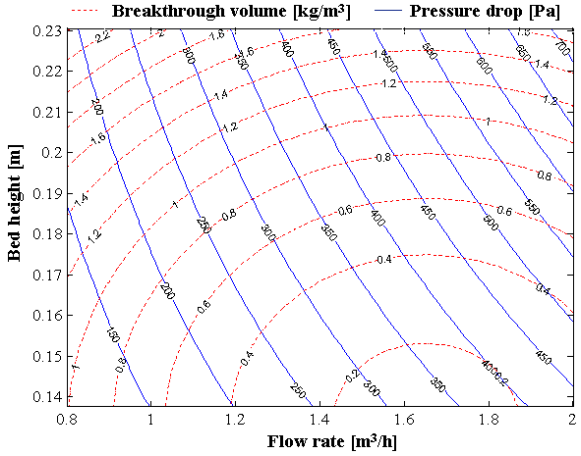

Fig. 8. Overlap contour plots of breakthrough volume and pressure drop response surfaces ($x_3 = 1$)

Multi-objective optimization by NBI algorithm

Calibration Generation package of Matlab software allows one to solve multi-objective optimization problems based on the Normal Boundary Intersection (NBI) algorithm developed by Das and Dennis [21] for generating Pareto surfaces in non-linear multi-objective optimization problems. This method is independent of the relative scales of the objective functions and provides an

evenly distributed set of points in the Pareto surface given an evenly distributed set of parameters [22], which is an advantage compared to the most common multi-objective approaches such as weighting method and the ε-constraint method [23].

Since the objectives of breakthrough volume and pressure drop functions are in conflict with each other, the main purpose of multi-objective optimization based on NBI algorithm was to find a set of Pareto-optimal solutions. Thus, maximizing the objective function of breakthrough volume and minimizing the objective function of pressure drop when $x_3 = 1$ (maximum inlet relative humidity), the set of Pareto optimal points were obtained as shown in Table 7.

As can be noted, the optimal conditions are located at the boundary of the experimental region, $\bar{x}^* = \{-1 \quad 1 \quad 1\}^T$, when the adsorption pilot plant treats *2.42* $m^3 \cdot kg^{-1}$ with a pressure drop of *189.63 Pa* in about *43 min*.

Table 7.

Set of Pareto optimal solutions for $x_3 = 1$.

No.	x_1^*	x_2^*	x_3^*	t_b, min.	Δp^*, Pa	V_b^*, $m^3 \cdot kg^{-1}$
1	-1	1	1	43.04	189.63	2.420
2	-1	0.844	1	37.86	182.94	2.217
3	-1	0.667	1	32.73	175.63	2.016
4	-1	0.504	1	28.64	168.40	1.830
5	-1	0.317	1	24.56	160.39	1.648
6	-1	0.114	1	20.80	151.73	1.478
7	-1	-0.107	1	17.34	142.24	1.321
8	-1	-0.356	1	14.14	131.60	1.183
9	-1	-0.644	1	11.16	119.27	1.073
10	-1	-1	1	8.33	104.03	1.010

In Fig. 9 is presented the selected Pareto optimal solutions of multi-objective optimization, pinpointing the dependences between the three factors and the two objective functions considered.

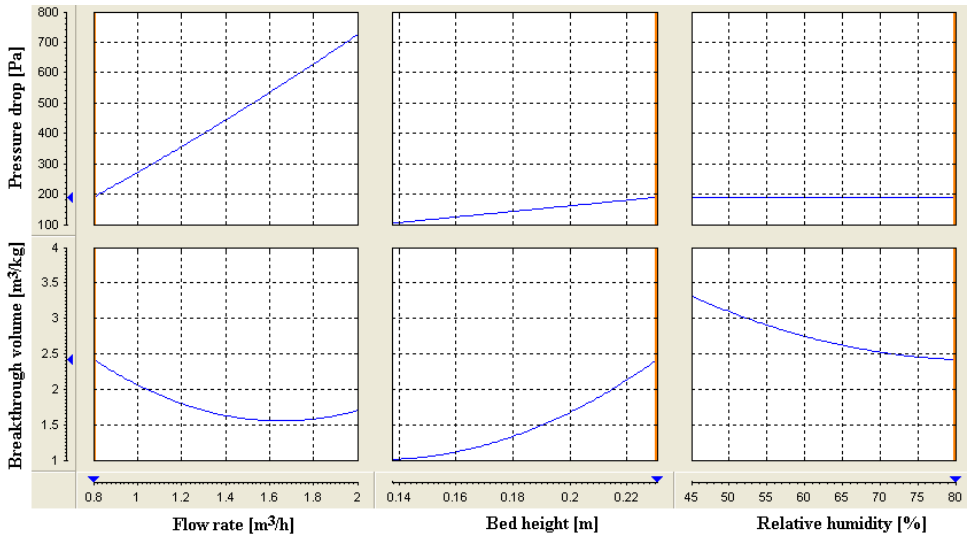

Fig. 9. Pareto optimal solution of multi-objective optimization by NBI algorithm.

6. Conclusions

Response Surface Modeling and Multi-objective optimization of a pilot plant for gas separation by adsorption in fixed bed was presented in this work. Water vapors and calcium chloride impregnated alumina were used as adsorbate and adsorbent respectively. The experimental investigations were carried out under non-isothermal and non-adiabatic conditions.

An orthogonal Central Composite Design allowed the mathematical modeling of the studied gas separation process on wide ranges of the considered process parameters. Based on these models, breakthrough time, breakthrough volume and pressure drop were predicted in the experimental region with average relative errors of 11.74, 10.78 and 1.64% respectively.

A thorough analysis of the resulted response surfaces was carried out through canonical analysis. Then, Lagrange multipliers method and multi-objective method based on the normal boundary intersection algorithm provided by Matlab software were used to determine the optimal operating parameters of the pilot-plant for gas separation by adsorption within the technical ranges of the operating parameters.

REFERENCES

[1] Daou, R., Wang, Z. K., Xia, Z.Z., Desiccant cooling air conditioning: a review. *Renew. Sust. Energy Rev.*, 10, (2006), 55–77.

[2] Rüthven, D.M., Farooq, S., Knaebel, K.S., *Pressure Swing Adsorption*, VCH Publishers, New York, 1994.

[3] Gordeeva, L., Grekova, A., Krieger, T., Aristov, Y.I., Composites “binary salts in porous matrix” for adsorption heat transformation, *Appl. Therm. Eng*., 50(2), (2013), 1633–1638.

[4] Daou, K., Wang, R.Z., Xia, Z.Z., Yang, G.Z., Experimental comparison of the sorption and refrigerating performances of a $CaCl_2$ impregnated composite adsorbent and those of the host silica gel. *Int. J. Refrigeration*, 30(1), (2007), 68-75.
[5] Freni, A., Russo, F. Vasta, S., Tokarev, M., Aristov, Y.I., Restuccia, G., An advanced solid sorption chiller using SWS−1L. *Appl. Therm. Eng*., 27(13), (2007), 2200-2204.
[6] Petrescu, S., Secula, M.S., Mathematical modeling of gas drying by adsorption. *Environ. Eng. Manag. J*., 7(3), (2008), 179-191.
[7] Diaconescu, R., Secula, M.S., Petrescu, S., Study of Gas Drying by Adsorption on Composite Materials Using Neural Networks. *Rev. Chim. (Bucharest*), 60 (10), (2009), 1065-1069.
[8] Secula, M.S., Diaconescu, R., Petrescu, S., Screening and Response Surface Modeling of Water Vapor Adsorption from Wet Air in Packed Bed of Silica gel using D-Optimal Design. *Stud. Univ. Babes-Bolyai, Chemia*, 54 (2), (2009), 133-144.
[9] Secula, M.S., Spiridon, M., Solomon, I., Petrescu, S., Response Surface Modelling of Water Vapor Adsorption in Fixed Bed of Impregnated Alumina Grains, *Rev. Chim. (Bucharest)*, 62(12), (2011), 1175-1179.
[10] Stoeckli, H.F., Characterization of microporous carbons by adsorption and immersion techniques. In: Patrick. J. (Ed.), *Porosity in Carbons – Characterization and Applications*. Arnold, London, 1995, 67–92.
[11] Stoeckli, H.F., Lopez-Ramon, M.V., Hugi-Cleary, D., Guillot. A., Micropore sizes in activated carbons determined from Dubinin–Radushkevich equation. *Carbon*, 39, (2001), 1115–1116.
[12] Sing, K.S.W., Everett, D.H., Haul, R.A.W., Moscou, L., Pierotti, R.A., Rouquerol, J., Siemieniewska, T., Reporting physisorption data for gas/solid systems – with special reference to the determination of surface area and porosity. IUPAC, *Pure Appl. Chem*., 57, (1985), 603–619.
[13] Kline, J., Moclintock, F.A., Describing uncertainties in single sample experiments. *Mech. Eng*., 1, (1953), 3-9.
[14] ASHRAE Handbook Fundamentals. American Society of Heating, Refrigerating and Air Conditioning Engineers, Atlanta, GA, USA, 1993.
[15] Perry, R.H., Green, D.W., Perry's chemical engineers handbook, 6th ed.: McGraw- Hill, New York, 1984.
[16] Lai, M.H., Chung, C.C., Chung, T.W., Experimental determination and predictions of breakthrough curves in a fixed bed of silica gel using the transfer unit approach. *Chem. Eng. Comm*. 187 (1), (2001), 185—198.
[17] Myer, R.H., Montgomery, D.C., Response Surface Methodology. Wiley, United States, 2002.
[18] Akhnazarova, S., Kafarov, V., Experiment Optimization in Chemistry and Chemical Engineering, Mir Publishers, Moscow, 1982.
[19] Bezerra, M.A., Santelli, R.E., Oliveira, E.P., Villar, L.S., Escaleira, L.A., Response surface methodology as a tool for optimization in analytical chemistry. *Talanta*, 76, (2008), 965–977.
[20] Cornel, J.A., How to Apply Response Surface Methodology, second ed., American Society for Quality Control, Milwaukee, Wisconsin, 1990.
[21] Das, I., and Dennis, J. E., Normal-Boundary Intersection: A New Method for Generating the Pareto Surface in Nonlinear Multicriteria Optimization Problems. *SIAM Journal on Optimization*, 8 (3), (1998), 631-657.
[22] Shukla, P.K., On the Normal Boundary Intersection Method for Generation of Efficient Front. Proceedings of the 7th international conference on Computational Science, Part I: ICCS 2007, Beijing, China, 2007, 310-317.
[23] Jia, Z., Ierapetritou, M.G., Generate Pareto optimal solutions of scheduling problems using normal boundary intersection technique. *Comput. Chem. Eng*. 31, (2007), 268–280.

NOVEL GRAPHITIC NANO-SIZED MATERIALS FOR VOLATILE ORGANIC COMPOUNDS ADSORPTION

Etelka DAVID, Ioan MAMALIGA*

Department of Chemical Engineering, "Gheorghe Asachi" Technical University of Iasi,
73 Prof. dr. doc. D. Mangeron Street, 700050 Iasi, Romania

Abstract

Because air is complex and heterogeneous, continuously evolving in time and space and in the same time is the source of life of humanity, is important to maintain it clean and fresh. The removal of various pollutants from the environment is a challenge, and adsorption techniques are usually thought to be more facile and effective. This review deals with the solid porous carbonaceous sorbents used to trap VOCs in air, and subsequent desorption techniques. Recent progress has shown that the graphene-based materials have a profound impact on electronic and optoelectronic devices, chemical sensors, nanocomposites and energy storage. This paper reviews the carbon nanomaterials that could integrate the new generation of gas sensors with superior performance.

Keywords: Volatile organic compound, Gas sensors, Graphite, Carbon nanotubes, Fullerene

"*If the facts don't fit the theory, change the facts.*" (Albert Einstein)

1. Introduction

Most people in developed countries spend up to 90% of their time indoors. Taking into account that each person inhales about 22 m^3 air per day, inhalation of indoor air is potentially the major determinant of human exposure to many pollutants. Inadequate ventilation can increase indoor pollutant levels by not bringing in enough outdoor air to dilute emissions from indoor sources and by not carrying indoor air pollutants out of the home. High temperature and humidity levels can also increase concentrations of some pollutants [1, 2].

Volatile organic compounds (VOCs) comprise an important group of chemicals that evaporate easily at room temperature, and are commonly present in

* Corresponding author: E-mail address: imamalig@ch.tuiasi.ro

indoor air. Some of them may cause short and long-term adverse health effects. Studies have found that levels of these chemicals average 2 – 5-fold higher indoors than outdoors. During and for several hours immediately after certain activities, such as paint stripping, levels may be 1000-fold the background outdoor levels. Studying VOC levels in new and old homes, Park and Ikeda [3] concluded that in new homes initial VOC levels decreased dramatically and were close to the mean values for older homes after one year. Also of the public microenvironments monitored, pubs and train stations were shown to have the highest concentration of most target VOCs. It was proved that seasonality is the most dominant pattern of indoor VOCs, founding the highest concentration during the winter months, which decrease from three to four times during summer [4].

Table 1. shows some of the most common VOCs determined in ambient air, distinguished by their capacity as ozone precursors [5].

Table 1

More frequent volatile organic compounds (VOCs) determined in environmental air samples

No.	VOCs with significant photochemical ozone-creation potential	Other VOCs	
1.	1-Pentene	1,1-Dichloroethylene	Chlorobenzene
2.	2-cis, trans-Pentene	Methylene chloride	1,1,1,2-Tetrachloroethane
3.	Isoprene	cis, trans-1,2-Dichloroethylene	Bromoform
4.	i-Hexene	1,1-Dichloroethane	1,1,2,2-Tetrachloroethane
5.	o,m,p-Xylene	2,2- Dichloropropane	1,2,3-Trichloropropane
6.	1,3,5-Trimethylbenzene	Bromochloromethane	Bromobenzene
7.	1,2,4Trimethylbenzene	Chloroform	2-Chlorotoluene
8.	1,4-Dichlorobenzene	1,1,1-Trichloroethane	4-Chlorotoluene
9.	i-Octane	1,2-Dichlorethane	1,3-Dichlorobenzene
10.	n-Heptane	1,1-Dichloropropene	1,2,3-Trimethylbenzene
11.	Toluene	Benzene	Trimethylbenzene
12.	n-Octane	Carbon tetrachloride	1,2-Dichlorobenzene
13.	Ethylbenzene	Trichloroethylene	1,2-Dibromo-3-chloropropane
14.	Styrene	1,2-Dichloropropane	
15.	Isopropylbenzene	Dibromomethane	1,2,4-Trichlorobenzen
16.	n-Propylbenzene	Bromodichloromethane	Naphthalene
17.	sec, tert-Butylbenzene	cis, trans 1,3-Dichloropropene	Hexachlorobutadiene
18.	p-Isopropyltoluene	1,1,2-Trichloroethane	1,2,3-Trichlorobenzene
19.	n-Butylbenzene	1,3-Dichloropropane	
20.	i-Pentane	Dibromochloromethane	
21.	n-Pentane	1,2-Dibromoethane	
22.	n-Hexane	Tetrachloroethene	

Of all these compounds the most common indoor VOCs which exhibit relatively higher concentration than others, detected in Europe are: benzene,

toluene, xylene, formaldehyde, phenols, acetates and some esters [6]. Some physical properties and concentrations of these VOCs are summarized in Table 2, which completes the list from our first review about adsorption of VOC on carbonaceous materials.

Table 2.

Physical properties and concentrations of five chosen VOCs

Type of VOC	Chemical formula	Molecular weight (g/mol)	Molecule diameter (Å)	Boiling point (°C)	Permissible exposure limit at 25°C, 760 torr (ppm)	Vapor pressure at 25°C (kPa)
Formaldehyde	CH_2O	30.03	2.43[c]	- 19.5	3[e]	517.69
Benzene	C_6H_6	78.11	4.5[a]	80.4	5[e]	12.7
o,m,p-Xylene	C_8H_{10}	106.16	6.7/7.1/7.4[d]	140	100[e]	1.1
Toluene	$C_6H_5CH_3$	92.14	5.80[b]	110.6	300[e]	3.79
Acetone	C_3H_6O	58.08	4.7[f]	50.5	1000[e]	30.6

a – [7] , b – [8] , c – [9], d – [10], e – [11], f – [12]

Stricter environmental regulations require that aromatics need to be removed before the effluents can be safely discharged into the environment and adsorptive separation is among the most effective means of achieving this goal being the simplest process to implement. The key step in an adsorption process is the choice of a solid adsorbent, and activated carbon is often the solid of choice because the graphitic nature of the pore walls offers two distinct advantages over other solid adsorbents: it is both hydrophobic and has high atom density (greater affinity for the adsorptive process) [13].

Although activated carbon is considered to be a satisfactory general adsorbent, the new applications demanded by advancing industrial technology, requires more and more sophisticated materials. Nonmicroporous carbon materials are an important kind of nanostructured materials. These materials are attractive because they join relatively high specific surface and uniform mesoporous diameter. These properties make these materials promising candidates for the adsorption of organic molecules, as well as supports for many catalytic phases [14].

2. General aspects of graphitic materials

Depending on the degree of crystallographic order, carbons based on the allotropic form of graphite, can be classified into graphitic carbons (which have a measurable crystallographic order) and non-graphitic carbons (without any measurable crystallographic order). The evolution of carbon based materials is represented in Figure 1.

The allotropes of carbon include:

- *diamond* is a rigid and isotropic 3D structure in which carbon atoms are bonded together in a tetrahedral lattice arrangement (sp^3 - based structure),
- *graphite* is a layered 3D structure where the carbon atoms are bonded in sheets of a hexagonal lattice (sp^2 - based structure),
- *graphene* is a 2D honeycomb lattice being the basic building block of graphitic materials,
- *fullerenes* are 0D carbon structures in which the carbon atoms are bonded together in spherical, tubular, or ellipsoidal formations to form an empty cage of sixty (C60) or more carbon atoms. The hybridization occurs, resulting in a $sp^{2+\varepsilon}$ form [15, 16].

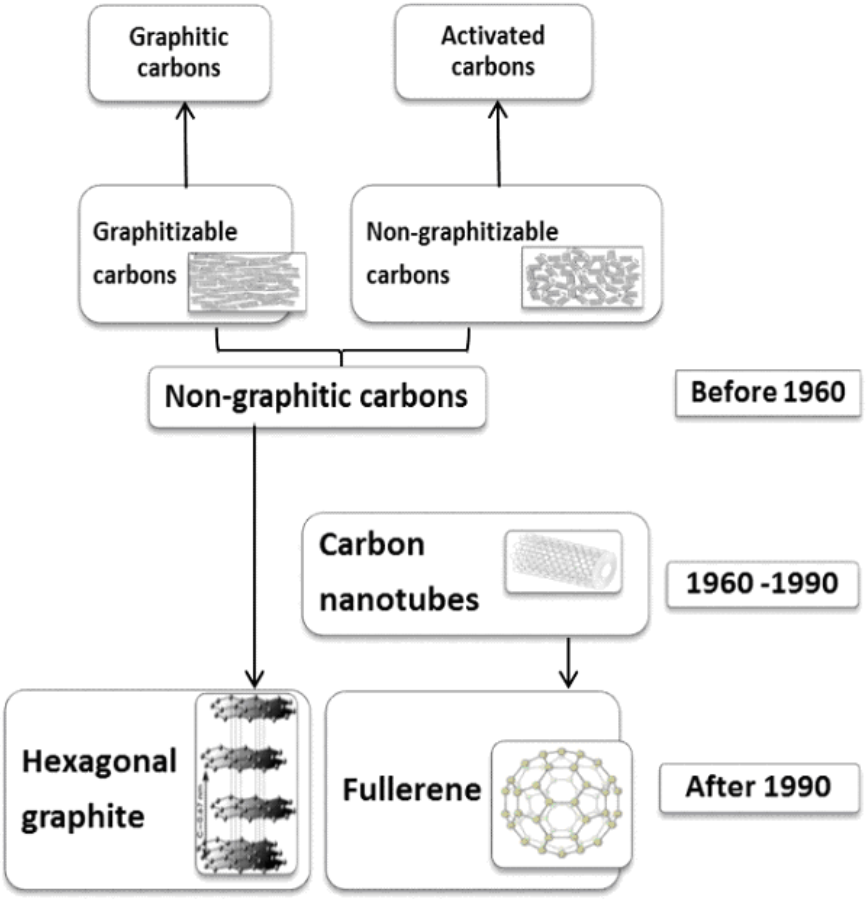

Fig. 1. Schematic representation of some of the carbon structures and their evolution.

On an atomic scale, the majority of carbons exhibit the allotropic form of graphite a sp^2-based structure, while diamond-like carbons, fullerenes and their derivatives, such as nanotubes, represent a shorter variety of carbon forms.

Graphite is the next allotrope of carbon after fullerene. It can be defined as an infinite three-dimensional crystal made of more than 10 stacked layers consisting of sp^2 hybridized carbon atoms, each carbon atom being connected to other three, making an angle of 120° with a bond length of 1.42 Å. In general, graphitic (graphite or graphene) nanoribbons are finite narrow strips, defined as a one-dimensional sp^2 hybridized carbon crystal cut out from the infinite 2D sheet [17, 18]. There are two structures that result after cutting a nanoribbon as follows (Fig. 2.2): armchair and zigzag, an armchair being an unrolled zigzag nanotube [19]. In particular, nanotubes with armchair chirality exhibit metallic characteristics whereas zigzag tubes, a semiconducting or semimetal behavior [20].

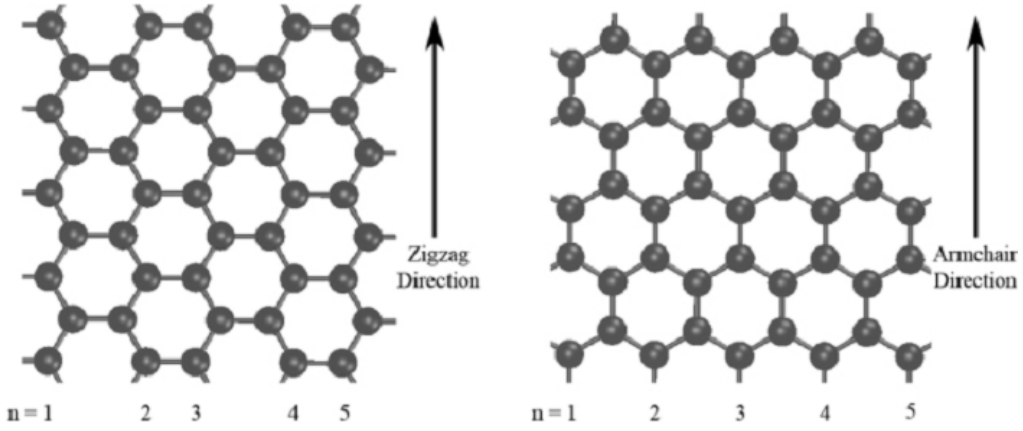

Fig. 2. Carbon nanoribbon.

Graphene, as a new member of carbon-based materials, has emerged as a promising nanoplatform with enormous potential for the research of various fields. It can be functionalized in order to enhance its specificity, loading capacity, solubility, biocompatibility, etc. The most common chemical moieties, carboxylic (-COOH) and hydroxyl (-OH) groups, can be covalently created on the graphene surface using strong acids and/or oxidants. Theoretically, graphene (or ‘2D graphite’) has been studied for sixty years, and is widely used for describing properties of various carbon-based materials. [18, 21].

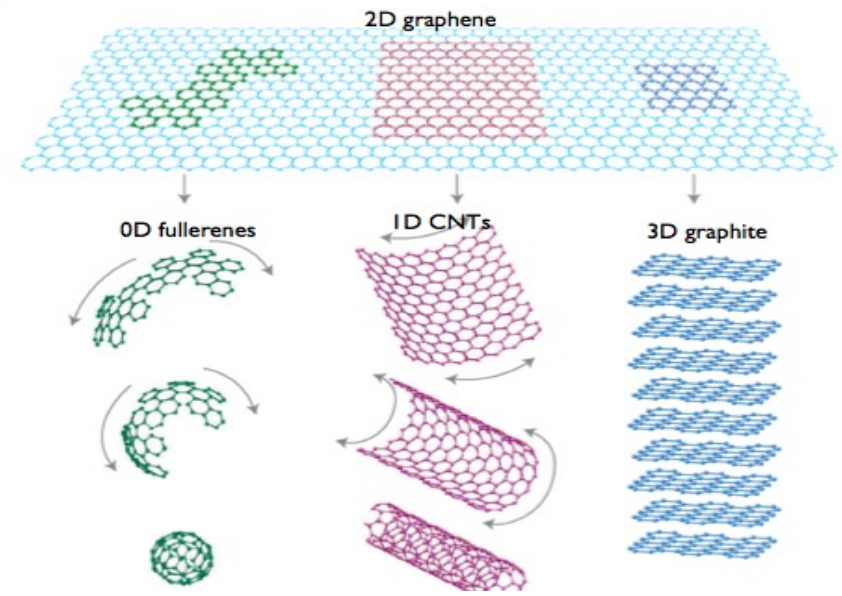

Fig. 3. Molecular models of different types of sp^2 hybridized carbon nanostructures exhibiting different dimensionalities. [22]

More generally, graphene represents a conceptually new class of materials that are only one atom thick and, on this basis, offers new inroads into low-dimensional physics that has never ceased to surprise and continues to provide a fertile ground for applications [18].

3. Adsorption on novel graphitic materials

In the last few years there has been an explosion in the number of published papers dealing with nanomaterials for gas sensing. There is a need for simple, sensitive and stable electronic sensors suited for trace detection in a wide spectrum of applications. Carbon materials with inherent nanoscale features have potential for becoming ideal components for the next generation of autonomous sensor technology, since they combine excellent detection sensitivity with interesting transduction properties in a single layer of material [15]. Their exceptional sensitivity allows the detection of toxic gases in concentrations as small as 1 part per billion (ppb). This and even higher levels of sensitivity are sought for industrial, environmental and military monitoring [23].

3.1. Carbon nanotubes

Carbon nanotubes (CNTs) - members of the fullerene structural family, are one-dimensional macromolecules, originally discovered by Iijima in 1991. Their name is derived from their long, hollow structure with the walls formed by graphene sheets. These sheets are rolled at specific and discrete ("chiral") angles, and the combination of the rolling angle and radius determines whether the individual nanotube shell is, metallic or semiconducting. The ends of CNTs are sealed with fullerene like hemispherical molecules. Depending upon the number of graphene sheets rolled, there are two categories of carbon nanotubes (Fig. 4.):

- single-walled carbon nanotubes (SWCNTs) consisting mainly of graphite sheets with only one carbon layer and with pores in the microporous range (diameter 0.4–2 nm),
- multiwalled carbon nanotubes (MWCNTs), which consist of at least two layers and have pores specially in mesopore range (2–100 nm) [24].

Both SWCNT and MWCNT possess high tensile strengths, are ultra-light weight and have excellent mechanical, thermal and chemical stability. Their reported surface areas range between 150 and 1500 m^2/g, which is a basis for serving as good sorbents. In combination with their metallic- and semi-conductive electronic properties, this remarkable array of features has seen a plethora of applications proposed, of which in the field of analytical chemistry is one of the most important. In this field CNT are increasingly used as sorbents and as separation phases [25-27].

Due to their highly porous and hollow structure, relatively large specific surface areas and easily modified surfaces, much attention has been paid to the adsorption of various inorganic and organic pollutants by CNTs in environmental treatment. CNTs are now synthesized at larger scales (more than 3000 metric tons/year), and 28 used in many electronic, medical, space and military applications [28].

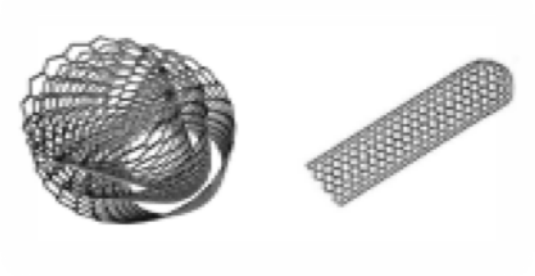

Fig. 4. Carbon-based nanomaterials: SWCNT (right), and MWCNT (left) [29].

Physical and chemical properties of the carbon nanotubes can be controlled through the synthesis processes used for their production. The three main methods for CNT synthesis are arc discharge (with the lowest yield), laser ablation (the most expensive), and chemical-vapor deposition (CVD). CVD seems to be the most common approach and various versions of it has been used for scale up, in which synthesis is carried out at relatively low temperature, with high yields and purity [30-32].

Carbon nanotubes have been reported to be an excellent material for solid-state gas sensors [18]. Various hydrocarbons can be chosen as carbon sources to produce CNTs, such as xylene, toluene, acetylene, methane, etc. These different carbon sources strongly influence the morphology and the quality of the CNTs obtained by varying the involved decomposition processes and carbon feed mechanisms [33].

3.1.1. Single walled carbon nanotubes (SWCNT)

Due to their remarkable and unique mechanical, electrical, optical and thermal properties, SWCNTs have been one of the most popular nanomaterials after fullerenes. Because of the broad application fields of carbon nanomaterials (CNM), the annual production capacity of SWCNTs was estimated to have reached 4500 t in 2011 [34].

Table 3.

Properties of the pristine single-walled carbon nanotubes

Property	Value	Unit	Ref.
C-Purity	> 98	%	[29]
Average diameter	1 – 2	nm	[29]
Length	10 – 20	μm	[29]
Bulk density	1.3 – 1.5	g/cm^3	[29]
BET surface area	400 - 1000	m^2/g	[29]
Tensile Strength	13 – 53	GPa	[29]
Elastic Modulus	~1	TPa	[35]
Electrical Conductivity	>106	S/m	[35]

Two types of SWCNT were tested regarding the adsorption of toluene at ambient pressure, vapor concentrations ranging from 10^{-4} to 0,95 and isothermal conditions of 25, 37, 50 °C. The samples contained 95 – 98 wt.% SWCNTs (EA95), and 80 wt.% SWCNTs (CVD80) respectively. Each sample was heated to desorb volatile, materials then cooled at room temperature and its dry weight was recorded. Vapors of known concentrations were then continuously passed through the sample chamber. Adsorption equilibrium was assumed to exist when no increase in mass was observed for 30 min. The maximum adsorption capacity for

toluene was measured at 35 ppm, for sample EA95 – 108 mg/g, and for CVD80 – 80 mg/g [36].

According to Chin *et al.* [37] solution pH shows no significant influences on the adsorption capacity of oxidized SWCNTs for toluene but it is seriously affected by the acid oxidation of the membrane.

CNT sorbent characteristics were tested using as-prepared MWCNT with non-tubular carbons (NTC), purified MWCNT, and SWCNT, for the preconcentration of volatile organic compounds (toluene) with concentration of the analytes in the range 9 – 12 ppm at a flow rate of 3 mL/min, and the amount of sorbent being 20 mg. The results showed that SWCNT had the highest adsorption capacity in terms of breakthrough volume. This is attributed to the smaller diameter, which led to the higher specific area [38].

It was reported in literature that SWCNTs of lower diameter present higher adsorption capacity towards benzene and the experimental results obtained, suggested that the adsorption capacity of the CNTs towards benzene is very weak. The achieved concentration factors were too low compared to other carbon materials [29].

The behavior of closed-end and open-end CNTs by controlling the annealing temperature were compared in the adsorption of different alkanes, including benzene. The results showed that the alkane coverage increases by 50%, when opening the CNT tube ends. Thus, the initial adsorption probability increases [39].

On the other hand Chin et al. [37] compared adsorption of various substituted non-polar benzene derivates on SWCNT with and without oxidation to investigate the influence of sorbate properties on interaction with CNTs. The adsorption experiments were carried out in a shaker at 25°C and 150 rpm for 28 h. The effects of temperature on the equilibrium adsorption were examined at 293, 303, and 313 K. Regarding the solutions pH values the authors pointed out, that at high pH, the ionized oxygen-containing surface groups bind with water molecules via hydrogen bonding and the adsorption sites are occupied. Therefore, the adsorption capacity for benzene decreases at high pH values. Also the adsorption of benzene decreased after oxygen-containing functional groups were introduced on the surface of SWCNTs.

Adsorption on SWCNTs is a combination of adsorption [i] in the hollow space inside nanotubes, [ii] in the interstitial spacing between three or more neighboring nanotubes, [iii] on the grooves present on the periphery of a nanotube bundle, and [iv] on the curved surface on the periphery of a bundle [36].

Based on the excellent sensing properties of graphene, Quang et al. [40] studied the response of graphene based quartz crystal microbalance (QCM) sensor to some VOCs, including acetone vapors at room temperature. The adsorption of molecular adsorbates on SWCNT was found to be concentrated on the oxidation

defect sites (carboxylic acid). The response of the fabricated sensor has shown good reproducibility and reversibility for acetone concentrations of 100 and 200 ppm. The result demonstrated that the graphene-coated QCM sensor has the highest selectivity with ethanol vapor and that the humidity effects are non-negligible. Therefore, a humidity sensor is needed as a feedback source for the gas sensor in order to cancel interference in the future.

3.1.2. Multiwalled carbon nanotubes (MWCNT)

MWCNTs are polymers of pure carbon and can be reacted and manipulated using the rich chemistry of carbon. This provides opportunity to modify the structure and to optimize their usage, allowing innovative applications especially in materials processing and energy management. Three properties of MWCNTs are specifically interesting for the industry:

- electrical conductivity (as conductive as copper),
- mechanical strength (up to 20 times stronger than steel and 5 times lighter),
- thermal conductivity (same as that of diamond and more than five times that of copper).

A combination of these impressive properties enables a whole new variety of useful and beneficial applications. Table 4. summarizes some physical and chemical properties of MWCNTs.

Table 4.

Properties of the multiwalled carbon nanotubes.

Property	Value	Unit	Ref.
C-Purity	> 98	%	[29]
Number of walls	2 - 15	-	[29]
Outer mean diameter	13 - 36	nm	[29]
Inner diameter distribution	2 - 6	nm	[29]
Length	>10	μm	[18]
Bulk density	1.8 – 2.0	g/cm^3	[35]
BET average surface area	200	m^2/g	[29]
Total pore volume	1.05	mL/g	[29]
V micro	0.0425	mL/g	[29]
V meso	0.706	mL/g	[29]
Tensile Strength	10 – 60	GPa	[35]
Elastic Modulus	0.3 – 1	TPa	[35]

Guo and coworkers and Lu and coworkers oxidized carbon nanotubes in nitrosulfuric acid and decorated them with metal particles - Pd, Ni, Au, and Pd, by a reduction method for detecting benzene and for discriminating acetone and

benzene. Among the different metals studied, Rh led to the highest benzene response [41, 42].

Based on this approach, Leghrib and coworkers [43] used oxygen plasma treated MWCNT decorated with metal particles for the recognition of benzene vapors. They concluded that metal nanoparticles transfer significant amount of charge upon adsorption of a target molecule at room temperature and it provides a selective detection of benzene at trace levels (50 ppb). One year later, they further investigated gas sensing properties using nano-clusters that donate or accept a significant amount of charge upon adsorption of a target molecule, so as to affect electron transport in the nanotube. They decorated plasma-treated carbon nanotubes with discrete metal nanoparticles (Rh and Pt) for the recognition of benzene vapors with high sensitivity and selectivity. Surface treatment and metal decoration were conducted using plasma post-discharge at atmospheric pressure and room temperature. The tested concentrations for benzene were 50, 100, 200 and 500 ppb. As a result the use of benzene-sensitive and benzene-insensitive metal-decorated multiwalled carbon nanotubes can provide selective detection of molecular benzene at trace levels with a detection limit below 50 ppb even in changing humidity backgrounds and in the presence of interfering species such as carbon monoxide, hydrogen sulphide and nitrogen dioxide [44].

In conclusion, functionalization of the carbon nanomaterial surface (decorated with metal or metal oxide nanoparticles or by grafting functional groups) is a practical way to increase sensitivity, minimize unwanted effects (moisture interference) and tune selectivity [45].

The performance of nonmicroporous carbon structures (MWCNT with < 1 wt% of metallic impurities) was evaluated for the adsorption of some representative VOCs by inverse gas chromatography (IGC). Measurements were carried out in the temperature range of 200 – 250°C by using samples between 0.2 and 0.6 g of carbon materials. The results showed that increasing molecular sizes lead to higher adsorption capacity, this parameter being higher for cyclic forms (benzene and cyclohexane) than for aliphatic ones (*n*-hexane) [14].

Two carbon multiwall nanotubes, CNT1 and CNT2, with purity higher than 95 wt.% having similar diameters and lengths were tested for the adsorption of benzene vapors. The average pore width and the average thickness of the CNT2 (11.2 and 28 nm) was higher than those for CNT1 (7.3 and 18.8 nm). All measurements were performed in an isothermal oven in the temperature range of 303, 333, and 363 K. The results showed that adsorption capacities of CNT1 for all organic vapors were less than the corresponding values for CNT2 at 303K, the best obtained value for benzene was 25.5 L/g [46].

The adsorption of benzene can occur on the external wall surface of the CNT, in the grooves and the interstitial sites through π-π interaction or through capillary condensation in its internal pores. In the case of MWCNTs, the layer-to-

layer spacing of 0.34 nm is generally smaller than the radius of gyration of organic vapours, so most organic chemicals, such as benzene are too large to be adsorbed between the MWCNT layers [47]

Shih *et al*. [46] studied, besides benzene, acetone vapors adsorption on two types of CNT with different pore widths (7.3 and 11.2 nm) and thickness (18.8 and 28 nm). The adsorption measurements were performed in an isothermal oven at three temperatures (303, 333, 363 K). The micropore (<2 nm) volume for CNT1 (0.00614 cm^3/g) is only slight more than CNT2 (0.00222 cm^3/g). The highest adsorption rate (516.4 L/g) was found on the sample with larger pore widths and thickness and also with higher micropore volume.

Hafaiedh and coworkers [48] have studied the potential of oxygen plasma treated multiwalled carbon nanotubes for the detection of VOCs at room temperature. The samples were synthesized by chemical vapor deposition and their purity was higher than 95%. The nanotubes were up to 50 nm in length and their outer and inner diameters ranged from 3 to 15 nm and 3 to 7 nm, respectively. A uniform functionalization with oxygen was applied to the as provided carbon nanotubes in order to improve their dispersion and surface reactivity. The functionalized carbon nanotubes were dispersed in an organic vehicle stirred during 20 min at room temperature and air-brushed onto alumina sensor substrates. The substrates consisted of interdigitated gold electrodes at the front side, and a platinum heating resistor at the back side. The results showed that oxygen plasma treated MWCNT sensors are more sensitive to toluene than to benzene vapors which could be attributed to the presence of a methyl group in the former molecule. Also they observed a stronger interaction between MWCNTs and acetone molecules than that of CNTs and benzene or toluene molecules.

The application of carbon nanotubes is still hampered by difficult manipulation of electronic properties, or the unsatisfactory stability under high temperature or oxidation. The lack of solubility and the difficult manipulation in any solvents have imposed great limitations to the use of CNT [49].

To endow CNTs for all kinds of applications, Meng and coll. summarized several methods of functionalization by integrating other functional groups or materials onto their surface. According to them, a functionalized nanotube exhibit improved mechanical, optical or electrical properties that are different from those of the original nanotube [50].

To compare the adsorption capacity of heat-modified and acid-modified CNTs, Norzilah and coworkers [51] studied the behavior of phenol on two types of CNTs with different morphologies produced by CVD method using acetone (CNT-A) and ethanol (CNT-E) as carbon source. It was found that acid and heat modifications contribute to the elimination of catalyst particles. Also heat modification reduces the oxygen functional groups on CNTs. The optimum pH for adsorption of phenol for as-synthesized CNT-A is at pH = 8 and for as-

synthesized CNT-E is at pH = 4. The phenol adsorption isotherms at room temperature show that the heat-treated CNTs have the highest adsorption capacity (0.183 mol/kg = 17.2 mg/g), contributing by the basicity surface, in spite of their low surface area.

Many studies have shown that via a functionalization of carbon nanotube sidewalls, a better chemical bonding between a specific chemical species and the nanotube can be reached and the selectivity of the adsorption process can be enhanced.

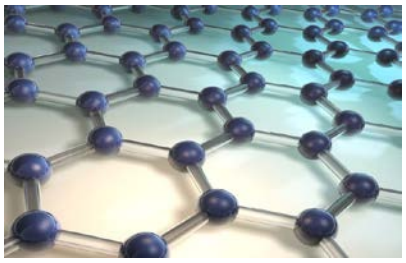

3.2. Graphene

The recent definition of graphene can be given as a two-dimensional monolayer of carbon atoms, which is the basic building block of graphitic materials of all other dimensionalities. It is often called the ‘‘mother of all graphitic materials’’ since the graphite or nanotubes are just derivatives of graphene with other dimensionality [18].

Graphene can be wrapped up into 0D fullerenes, rolled into 1D nanotubes or stacked into 3D graphite (Fig. 2.3). Graphene is a chemicaly inert planar monolayer of carbon atoms arranged into a two-dimensional honeycomb lattice with sp^2 hybridized and a carbon–carbon bond length of 0.142 nm. It has strong mechanical, thermal, and electrical properties, with a theoretical value of specific surface area at 2630 m^2/g [22].

Graphene can be obtained through various physical and chemical routes which include micromechanical cleavage, chemical vapor deposition, epitaxial growth on silicon carbide, arc discharge, unzipping of carbon nanotubes, electrochemical synthesis, total organic synthesis, chemical reduction of grapheme oxides, and plasma discharge etching of graphite [52]. Mechanical cleavage of graphite was the initial method to produce single-layer graphene sheets; however, this approach has no control over the number of layers and is an inefficient process that is not suitable for large scale production. Epitaxial growth of graphene layers requires high temperatures and ultrahigh vacuum, which is costly and thus may limit the application of graphene. Chemical vapor deposition recently has been reported to produce large-area graphene films, but a purification process may be needed to eliminate the catalyst particles and obtain clean graphene sheets [53].

The possibility of using graphene as a highly sensitive gas sensor was reported. Its 2D structure makes every carbon atom a surface atom so that electron transport through graphene can be highly sensitive to adsorbed molecules. For instance, mechanically exfoliated graphene has demonstrated a potential ability to detect gases down to the single molecular level. It was shown that the increase in,

graphene charge carrier concentration, induced by adsorbed gas molecules, can be used to make highly sensitive sensors that even have the possibility of detecting individual molecules [23]. Further theoretical predictions suggest that by creating artificial pores (nitrogen or hydrogen funtionalized pores) in grapheme can increase its permeability and permeation-selectivity [54].

Chemically reduced graphene oxide (i.e. graphene sheet decorated with oxygen functional groups) has been also reported as a useful material for developing gas sensors. It is produced by Hummers method from flake graphite, has disrupted conjugation in the graphene plane, and abundant functional groups, such as epoxide, hydroxyl, carboxyl and carbonyl, on its surfaces. These oxygen-containing groups could form strong complexes with metal ions, and allow the graphene oxide to act as a sesnsitive adsorbent. Also because of the π-π interaction between the graphene and the organic molecules, pristine graphene had a much higher adsorption capacity than graphene oxide [52]. Graphene oxide (GO) is much easier to process than graphene, and offers the possibility to tailor the amount of functional groups by controlling the degree of reduction. Robinson *et al*. [55] demonstrated that reduced graphene oxide using hydrazine can be used as the active material for high-sensitive gas sensors. It has shown excellent performance for detection of acetone. They suggested that partial reduction of graphene oxide to graphene is necessary because the process leaves a functionalized surface (with active oxygen defects) that shows stronger reactivity to the target analytes.

A year later Lu and coworkers [53] pointed out that this method involves toxic chemicals and the introduction of extra nitrogen functional groups on graphene surface may slow down the sensing response. Hence they synthesized GO by the oxidative treatment of purified natural graphite which was partially reduced via thermal treatment in Ar flow with temperatures as low as 200 °C. The miniaturized gas sensor based on the reduced GO exhibited great room-temperature sensing properties.

Graphite oxide (GO) silylated by 3-aminopropylmethyldiethoxysilane (samples of 100 mg) were used as an adsorbent of formaldehyde at very low concentration (~2 ppm) from gas phase at 30 °C. The amounts of adsorbed formaldehyde on silyalted GO were calculated to be 36.1 – 91.2 mg/g. Also it was observed that the amount of adsorbed formaldehyde became lower for the samples with higher contents of silicon (accordingly higher content of amino groups C=N). This indicates these materials, containing amino groups, are promising adsorbents of formaldehyde at low concentration [56, 57].

Many theories and experiments have showed the existence of defects, in graphene and carbon nanotubes. These defects can affect the magnetic and electronic properties of the carbon-based materials. The surface of vacancy-defect containing sites of graphene was compared to the perfect one, regarding

adsorption. It was found out that oxygen molecule preferred to be chemisorbed on the graphene surface containing vacancy-defect sites [58].

Also the interactions between H_2CO and pure, N-doped and Ti-doped graphene sheets were investigated using the same theory. The results showed that between pure graphene sheet and H_2CO molecule was a weak interaction. Regarding N-doped graphene sheet, H_2CO molecule was little affected by N doped atom. Finally the most stable adsorption process took place on Ti-doped graphene through oxygen atom [59].

Zhou and coworkers [60] performed a density functional theory (DFT) study on the adsorption of formaldehyde on perfect and vacancy-defected graphene (VG) doped with B, N, and S. The vacancy was created by removing a C atom from the perfect graphene. The results indicated that the presence of vacancy, enhanced the interaction between graphene and H_2CO molecule while the H_2CO molecule still presented physisorption on VG with relatively small adsorption energy. After introducing different dopants (B, N, and S), chemisorptions of H_2CO were observed on the doped configurations. Therefore, B- and S-doped graphene could also be potentially used as good sensors.

Based on the theory that two graphene layers stack directly on top of each other make strong covalent bonds, when the distance between planes is 1,56 nm [61], Krasnenko and colab. [62] have found that the geometry optimization process depends on the starting position of the benzene molecule and graphene layer. At a short separating distance of 1.56 Å, strong covalent bonding are formed between graphene sheet and benzene molecule whereas at a greater distance of about 3.3 Å weak van der Waals interactions were noticed.

3.3. Fullerenes

Fullerene (buckmintsterfullerene - C_{60}) discovered by Kroto *et al*. in 1985, are the only molecular solids in the realm of carbon materials. They consists of 60 carbon atoms with diameter about 1 nm. The C_{60} molecule has 32 faces with 12 pentagons and 20 hexagons. The C_{60} molecule which is basically neutral and spinning freely under ambient conditions, has two distinct bonding types with hexagon–hexagon edges (C=C bond ~0.140 nm) and hexagon–pentagon edges (C-C bond ~0.147 nm) [63].

The fullerene and fullerene-related molecules present unique structural and electronic properties, having remarkable reactivity and electron acceptor character and a high molecular symmetry. Addition of radicals to the fullerene molecules leads to symmetry reduction to C_{60} [64, 65]. In the same time high purity and crystallinity of the C_{60} indicates a lack of microporosity [66].

Fig. 5. Fullerene structure.

Adsorption studies on fullerene have been carried out with a variety of objectives in terms of adsorbates which included inert gases, organic vapors or even reactive gases. Most of the work devoted to fullerene as adsorbents included aliphatic compounds (alkanes, alkyl halides, ethers, esters, ketones, alcohols) and aromatic compounds with different substituents [64]. Chao and Shih used piezoelectric quartz crystal membrane coated with fullerene to study the adsorption and interaction between various organic molecules and fullerene. The selectivity of C_{60} for the chosen polar organic molecules seemed to be in the following order: carboxylic acids > aldehydes > amines > alcohols > ketones. They also concluded that physical adsorption occurs for polar molecules whereas nonpolar organic molecules exhibit a much stronger adsorption on fullerene [67].

More recently $C_{60}Pd_n$ polymer-like materials were prepared and reacted with toluene at ambient temperature, without additional energy sources and at low concentration (1000 ppb, value closed to the actual toluene concentration in the environment). There was observed the strong adsorption capacity of toluene molecules toward $C_{60}Pd_n$. Theoretical studies also suggested that π-electrons of C_{60} of toluene overlap through the d-orbitals of a Pd atom, should open the route to fullerene materials as adsorbents for harmful gases [68].

Despite all, there is a drawback that should be considered about fullerene. Because every atom in a fullerene is a surface atom, electron transport through these materials can be highly sensitive to adsorbed molecules. This phenomenon has subsequently enabled the fabrication of sorption-based sensors, capable of detecting trace levels of vapor using conventional low-power electronics [55].

Considering the characteristics of the different carbon nanomaterials, graphene offers similar interaction properties with target molecules than that of large-diameter CNTs (generally multiwalled carbon tubes) [18].

4. Conclusions

Gas molecule sensors are playing increasingly important roles in controlling chemical processes and monitoring environmental mediums. Recently, graphene sheets have been proven to have more effective sorbency than activated carbon. Along with a high mechanical strength (strongest nanomaterial), and high thermal conductivity (25 x silicon), the pore structure of graphene materials is set to open a wide range of exciting applications in gas separation or fluid purification. Due to their high levels of sensitivity, graphene nanosheets (GNSs) could be applied as ideal candidates for detection of different gases existing in various environments.

Novel and eco-friendly functionalization technologies are also very important. Using non-toxic and cost-effective precursors, the prepared graphene nanosheets based composites are more attractive. More research concerning the application of graphene-metal composites in pollutant removal is expected.

Patterned into quasi-one-dimension materials, graphene-based materials with low aggregation and high specific surface areas show high adsorption capacities for organic pollutants, especially benzene-containing compounds. They also are used in many ways for environmental remediation and pollutant removal. They can be used to reduce the pollutant concentration by adsorption, decompose pollutants to less toxic molecules (mainly applicable to organic pollutants and persistent organic pollutants), and reduce low-valency species (mainly applicable to toxic high-valency metal ions). Although graphene cannot be synthesized on a large scale and inexpensively, there is no doubt that graphene or graphene-based materials will be easily and inexpensively produced in large quantities in the near future. The outstanding physicochemical properties of graphene and graphene-based materials will play a very important role in environmental pollution management in the future.

"*Nothing in life is to be feared, it is only to be understood.*
Now is the time to understand more, so that we may fear less." (Marie Curie)

REFERENCES

[1] Barro R., Regueiro J., Llompart M., Garcia-Jares C., Analysis of industrial contaminants in indoor air: Part 1. Volatile organic compounds, carbonyl compounds, polycyclic aromatic hydrocarbons andpolychlorinated biphenyls – A review, *Journal of Chromatography A*, 1216, (2008), 540-566.

[2] Caselli M., Gennaro G., Saracino M.R., Tutino M., Indoor contaminants from newspapers: VOCs emissions in newspaper stands, *Environmental Research*, 109, (2009), 149-157.

[3] Park J.S., Ikeda K., Variations of formaldehyde and VOC levels during 3 years in new and older homes, *Indoor Air*, 16, (2006), 129-135.

[4] Rehwagen M., Schlink U., Herbarth O., Seasonal cycle of VOCs in apartments, *Indoor Air*, 13, (2003), 283-291.

[5] Ras M.R., Borrull F., Marce R.M., Sampling and preconcentration techniques for determination of volatile organic compounds in air samples, *Trends in Analytical Chemistry*, 28, (2009), 96-109,

[6] Meng Y., Removal of volatile organic compounds from indoor air using regenerative activated carbon fiber cloth, UMI Dissertation Publishing, Michigan, 2008.

[7] Freude D., Size, mass and kinetics of molecules, *Molecular Physics*, 2004, Chapter 2, 1-19.

[8] Dehdashti A., Khavanin A. Rezaei A., Assilian H., Motalebi M., Application of microwave irradiation for the treatment of adsorbed volatile organic compounds on granular activated carbon, *Iranian Journal of Environmental Health Science and Engineering*, 8(1), (2011), 85-94.

[9] Pei J., Zhang J.S., Critical review of catalytic oxidization and chemisorption methods for indoor formaldehyde removal., *HVAC & R Research*, 17, (2011), 476-503.

[10] Zhang W.M., Chen J.-L., Pan B.-C., Zhang Q.-X., Competitive and cooperative adsorption behaviors of phenol and aniline onto nonpolar macroreticular adsorbents, *Journal of Environmental Sciences*, 17(4), (2005), 529-534.

[11] Occupational Safety & Health Administration (OSHA), Permissible Exposure Limit (PEL) - An allowable exposure level in workplace air - Regulatory Limits, 2006.

[12] Tsai J.-H., Chiang H.M., Huang G.Y., Chiang H.L., Adsorption characteristics of acetone, chloroform and acetonitrile on sludge-derived adsorbent, commercial granular activated carbon and activated carbon fibers, *Journal of Hazardous Materials*, 154(1-3), 2008, 1183-1191.

[13] Klomkliang N., Do D.D., Nicholson D., Tangsathitkulchai C., Wongkoblap A., Multilayer adsorption of benzene on graphitized thermal carbon black — The importance of quadrupole and explicit hydrogen in the potential model, *Chemical Engineering Science*, 69, (2012), 472–482.

[14] Díaz E., Ordóñez S., Vega A., Adsorption of volatile organic compounds onto carbon nanotubes, carbon nanofibers, and high-surface-area graphites, *Journal of Colloid and Interface Science*, 305(1), (2007), 7-16.

[15] Llobet E., Gas sensors using carbon nanomaterials: A review, *Sensors and Actuators B: Chemical*, 179, (2013), 32-45.

[16] Menéndez-Díaz J.A., Martín-Gullón I., Types of carbon adsorbents and their production, *Interface Science and Technology*, 7, (2006), 1-48.

[17] Terrones M., Botello-Méndezb A.R., Campos-Delgadoc J., López-Uríasd F., Vega-Cantúd Y.I., Rodríguez-Macíasd F.J., Elías A.L., Munoz-Sandovald E., Cano-Márquezd A.G., Charlierb J.C., Terrones H., Graphene and graphite nanoribbons: morphology, properties, synthesis, defects and applications, *Nano Today*, 5, (2010), 351 – 372.

[18] Geim A.K., Novoselov K.S., The rise of grapheme, *Nature Materials*, 6, (2007), 183-191.

[19] Delibozov N., Analysis of graphene nanoribbons passivated with gold, copper and indium, *International Journal of Theoretical and Applied Nanotechnology*, 1, (2013), 41-46.

[20] Tascon J.M.D., *Novel carbon adsorbents*, National Institute of Carbon, INCAR-CSIC, Oviedo, Spain, 2012.

[21] Wang H., Yuan X., Wu Y., Huang H., Peng X., Zeng G., Zhong H., Liang J., Ren M., Graphene-based materials: Fabrication, characterization and application for the decontamination of wastewater and wastegas and hydrogen storage/generation, *Advances in Colloid and Interface Science*, 195 -196, (2013), 19-40.

[22] Singh V., Joung D., Zhai L., Das S., Khondaker S.I., Seal S., Graphene based materials: past, present and future, *Progress in Materials Science*, 56(8), (2011), 1178–1271.

[23] Schedin F., Geim A.K., Morozov S.V., Hill E.V., Blake P., Katsnelson M.I., Novoselov K.S., Detection of Individual gas molecules adsorbed on graphene, *Nature Materials*, 6, (2007), 652–655.

[24] Inagaki M., Carbon Nanotubes: Synthesis and Formation, Chapter 2, *Advanced Materials Science and Engineering of Carbon*, 154, (2014), 15-40.

[25] Smart S.K., Cassady A.I., Lu G.Q., Martin D.J., The biocompatibility of carbon nanotubes, *Carbon*, 44, (2006), 1034-1047.

[26] Fraczek A., Menaszek E., Paluszkiewicz C, Blazewicz M., Comparative in vivo biocompatibility study of single and multi-wall carbon nanotubes, *Acta Biomaterialia*, 4, (2008), 1593–1602.

[27] Green M.J., Behabtu N., Pasquali M., Adams W.W., Nanotubes as polymers. *Polymer*, 50(21), (2009), 4979-4997.

[28] Apul O.G., Karanfil T., Adsorption of Synthetic Organic Contaminants by Carbon Nanotubes: A Critical Review, *Water Research*, 68(1), (2015), 34-55.

[29] Huffer Thorsten, Sorption of non-ionic organic compounds by carbon-based nanomaterials – Systematic characterization, modeling, and application - Dissertation, Duisburg-Essen University, 2014.

[30] Mittal M., Kumar A., Carbon nanotube (CNT) gas sensors for emissions from fossil fuel burning, A review, *Sensors and Actuators B: Chemical*, 203, (2014), 349–362.

[31] Vairavapandian D., Vichchulada P., Lay M.D., Preparation and modification of carbon nanotubes: review of recent advances and applications in catalysis and sensing, *Analytica Chimica Acta*, 626, (2008), 119-129.

[32] Han Z.J., Rider A.E., Fisher C., Van Der Laan T., Kumar S., Levchenko I., Ostrikov K., Biological application of carbon nanotubes and grapheme, *Carbon Nanotubes and Graphene* - Second Edition, 2014.

[33] Li H., He D., Li T., Genestoux M., Bai J., Chemical kinetics of catalytic chemical vapor deposition of an acetylene/xylene mixture for improved carbon nanotube production, *Carbon*, 48, (2010), 4330 –4342.

[34] DeVolder M.F.L., Tawfick S.H., Baughman R.H., Hart A.J., Carbon nanotubes: present and future commercial applications, *Science*, 339, (2013), 535–539.

[35] Schulz M.J., Shanov V.N., Yin Z., *Nanotube Superfiber Materials*- Changing Engineering Design, Massachusetts, USA, 2014.

[36] Agnihotri S., Rood M.J., Rostam-Abadi M., Adsorption equilibrium of organic vapors on single-walled carbon nanotubes, *Carbon*, 43, (2005), 2379–2388.

[37] Chin C.J.M., Shih M.W., Tsai H.J., Adsorption of nonpolar benzene derivatives on single-walled carbon nanotubes, *Applied Surface Science*, 256(20), (2010), 6035-6039.

[38] Hussain C.M., Mitra S., Micropreconcentration units based on carbon nanotubes (CNT), *Analytical and Bioanalytical Chemistry*, 339(1), (2011), 75-89.

[39] Burghaus U., Effect of carbon nanotubes crystal structure on adsorption kinetics of small molecules, *Journal of Thermal Analysis and Calorimetry*, 106, (2011), 123-128.

[40] Quang V.V., Hunga V.N., Tuanb L.A., Phanb V.N., Huy T.N., Quy N.V., Graphene-coated quartz crystal microbalance for detection of volatile organic compounds at room temperature, *Thin Solid Films*, 568, (2014), 6-12.

[41] Guo M., Pan M., Chen J., Mi Y., Zhang X., Chen Y., Palladium modified multi-walled carbon nanotubes for benzene detection at room temperature. *Chinese Journal of Analytical Chemistry*, 34, (2006), 1755-1758.

[42] Lu Y., Partridge C., Meyyappan M., A carbon nanotubes sensor array for sensitive gas discrimination using principal component analysis. *Journal of Electroanalytical Chemistry*, 593, (2006), 105–110.

[43] Leghrib R., Felten A., Demoisson F., Reniers F., Pireaux J.J., Llobet E., Room-temperature, selective detection of benzene at trace levels using plasma-treated metal-decorated multiwalled carbon nanotubes, *Carbon*, 48(12), (2010), 3477-3484.

[44] Leghrib R., Dufour T., Demoisson F., Claessens N., Reniers F., Llobet E., Gas sensing properties of multiwall carbon nanotubes decorated with rhodium nanoparticles, *Sensors and Actuators B: Chemical*, (2011), 974-980.

[45] Zilberman Y., Ionescu R., Feng X., Muellen K., Haick H., Nanoarray of polycyclic aromatic hydrocarbons and carbon nanotubes for accurate and predictive detection in real-world environmental humidity, *American Chemical Society Nano*, 5(8), (2011), 6743-6753.

[46] Shih Y., Li M., Adsorption of selected volatile organic vapors on multiwall carbon nanotubes, *Journal of Hazardous Materials*, 154, (2008), 21-28.

[47] Lahlou H., Leghriba R., Llobeta E., Vilanova X., Correig X., Development of a gas pre-concentrator based on carbon nanotubes for benzene detection, *Procedia Engineering*, 25 (2011), 239–242.

[48] Hafaiedh I., Elleucha W., Clementb P., Llobet E., Abdelghani A., Multi-walled carbon nanotubes for volatile organic compound detection, *Sensors and Actuators B: Chemical*, (2013), 344-350.

[49] Tasis D., Tagmatarchis N., Bianco A., Prato M., Chemistry of carbon nanotubes, *Chemical Reviews*, 106, (2006), 1105–1136.

[50] Meng L., Fu C., Lu Q., Advanced technology for functionalization of carbon nanotubes, *Progress in Natural Science*, 19(7), (2009), 801-810.

[51] Norzilah A.H., Fakhrul-Razi A., Choong T.S.Y., Luqman A.C., Surface modification effects on CNTs adsorption of methylene blue and phenol, *Journal of Nanomaterials*, 2011, (2011), 1-18.

[52] Lu K., Zhao G.X., Wang X.K., A brief review of graphene-based material synthesis and its application in environmental pollution management, *Chinese Science Bulletin*, 57, (2012), 1223-1234.

[53] Lu G., Ocola L.E., Chen J., Gas detection using low-temperature reduced graphene oxide sheets, *Applied Physics Letters*, 94, (2009), 083111.

[54] Berry V., Impermeability of graphene and its applications, *Carbon*, 62, (2013), 1-10.

[55] Robinson J.T., Perkins F.K., Snow E.S., Wei Z., Sheehan P.E., Reduced grapheme oxide molecular sensors, *Nano Letters*, 8(10), (2008), 3137-3140.

[56] Matsuo Y., Nishino Y., Fukutsuka T., Sugie Y., Removal of formaldehyde from gas phase by silylated graphite oxide containing amino groups, *Carbon*, 46, (2008), 1162-1163.

[57] Wang S., Sun H., Ang H.M., Tadé M.O., Adsorptive remediation of environmental pollutants using novel graphene-based nanomaterials, *Chemical Engineering Journal*, 226, (2013), 336-347.

[58] Yu J.G., Yu L.Y., Yang H., Liu Q., Chen X.H., Jiang X.Y., Chen X.Q., Jiao F.P., Graphene nanosheets as novel adsorbents in adsorption, preconcentration and removal of gases, organic compounds and metal ions, *Science of the Total Environment*, 502, (2014), 70-79.

[59] Zhang H.P., Luoa X.G., Lina X.Y., Lub X., Lengc Y., Song H.T., Density functional theory calculations on the adsorption of formaldehyde and other harmful gases on pure, Ti-doped, or N-doped graphene sheets, *Applied Surface Science*, 283, (2013), 559-565.

[60] Zhou Q., Yuan L., Yang X, Fu Z., Tang Y., Wang C., Zhang H., DFT study of formaldehyde adsorption on vacancy defected grapheme doped with B, N, and S, *Chemical Physics*, 440, (2014), 80-86.

[61] Andres P.L., Ramırez R., Verges J.A., Strong covalent bonding between two graphene layers, *Physical Review B*, 77, (2008), 045403.

[62] Krasnenko V., Kikas J., Brik M.G., Modification of the structural and electronic properties of graphene by the benzene molecule adsorption, *Physica B*, 407, (2012), 4557–4561.

[63] Rhee J.H., Byeongchul H., Sharma S.C., Electronic structure and electrical properties of Na-doped C_{60} thin films, *Thin Solid Films*, 517(2), (2008), 522-524.

[64] Bottani E.J., Tascón J.M.D., *Adsorption by Carbons*, CSIC, National Institute of Carbon, Oviedo, Spain, 2008.

[65] Sabirov D.S., Bulgakov R.G., Reactivity of fullerenes family towards radicals in terms of local curvature, *Computational and Theoretical Chemistry*, 963, (2011), 185-190.

[66] Gusev V.Y., Ruetsch S., Popeko L.A., Popeko I.E., Nitrogen and argon adsorption and SEM characterization of C_{60} and C_{60}/C_{70} fullerenes: Comparison with graphite, *Physical Chemistry B*, 103, (1999), 6498-6503.

[67] Chao Y.C., Shih J.S., Adsorption study of organic molecules on fullerene with piezoelectric crystal detection system, *Analytica Chimica Acta*, 374 (1998), 31-38.

[68] Hayashi A., Yamamoto S., Suzuki K., Matsuoka T., The first application of fullerene polymer-like materials, $C_{60}Pd_n$, as gas adsorbents, *Journal of Materials Chemistry*, 17 (2004), 2633-2637.

GAS-LIQUID ABSORPTION OF VOLATILE ORGANIC COMPOUNDS FROM GAS STREAMS IN A PACKED-BED COLUMN: MODELLING AND SIMULATION

Violeta Alexandra ION, Oana Cristina PÂRVULESCU* and Tănase DOBRE

Department of Chemical and Biochemical Engineering, University Politehnica of Bucharest, 1-7 Polizu Street, 011061, Bucharest, Romania

Abstract
Gas-liquid absorption in a packed-bed column is a simple, regenerative and recuperative technique which is widely used for separation of volatile organic compounds (VOCs) species from gas streams. A case study on modelling of acetone absorption from an air stream into clean water flowing through Raschig rings packing has been presented. Simulations were conducted in order to emphasize the effect of operational parameters on absorption performances. An increase in gas flow rate and a decrease in liquid flow rate reduced the acetone separation efficiency, whereas an increase in flow rate of both fluids improved the overall mass transfer.

Keywords: Absorption, Acetone, Modelling, Packed column, Volatile organic compound

1. Introduction

Malodorous and/or toxic VOCs are mainly generated by chemical, petrochemical, pharmaceutical, cosmetics, food, electronics industries as well as by the use of solvents and fossil fuels [1-7]. Nowadays, the control of VOCs emissions is an important concern in the prevention and remediation of air pollution. There are various control techniques, including adsorption, absorption, condensation, membrane separation as recuperative ones, and bio-filtration, thermal, catalytic and photocatalytic oxidation as destructive, each of them with its limitations [1-20]. The choice of a suitable VOCs control technique depends on different factors, *e.g.* nature and concentration of VOC species in the gas stream, gas flow rate, process safety, space constrains, species recuperation, investment and operational costs [4,12,14,16,19].

Gas-liquid absorption is a simple, safe, regenerative and recuperative technique which is frequently used both in the theoretical studies and industrial

* Corresponding author. Email address: oana.parvulescu@yahoo.com (O.C. Pârvulescu)

applications [1-13,15-18]. It involves the transfer of one or more VOC species from a gas phase into a liquid absorbent (solvent). Absorption performances, commonly evaluated as VOC separation efficiency and overall mass transfer kinetics, depends on nature and concentration of VOC species in the feed gas, absorbent nature, absorption reactor type, gas and liquid flow rate, process temperature and pressure [5,9,15-17].

The selection of an appropriate liquid absorbent is essential for obtaining optimal process performances. An ideal absorbent should have a high absorption capacity, a low vapor pressure in order to reduce its losses, a low viscosity and a high VOC diffusion coefficient, respectively, as well as it ought to be noncorrosive, nontoxic, nonflammable, inexpensive, chemically and thermally stable [5,9,12,13,18]. Taking into account these criteria, various absorbents were tested, *e.g.* water [4,5,15,16], silicon oil [12] and water-silicon oil mixture [9,10], vegetable oil [4], lubricant oil [4], ionic liquids [13], polyglycols [12], alkylphthalates [8,12], alkyladipates [11,12,17,18] and aqueous solutions of alkyladipates [2]. Water is an efficient absorbent for removal of hydrophilic VOC species, whereas organic liquids and their solutions are used as absorbents for hydrophobic species.

Packed-bed columns with counter-current flows of gas and liquid are widely employed to remove VOCs from gas streams [5,9,10,12,15,16,18]. Many researches in the related literature has aimed at studying the effect of characteristic operational parameters of packed columns on absorption performances [5,9,15,16,18]. An increase in absorption efficiency with liquid flow rate increasing and gas flow rate decreasing as well as an improvement of overall mass transfer at higher values of flow rate of both fluids were reported [15,16,18].

This paper presents a theoretical study on the modelling and simulation of VOC species absorption from a gas into a liquid stream using a countercurrent packed-bed column. The process was particularized for acetone removal from air by absorption into clean water passing through a packing consisting of Raschig rings.

2. Mathematical model

A countercurrent packed-bed absorption column is schematically shown in Fig. 1, where the gas and liquid flow rates are expressed as molar flow rates of inert fluid and the concentrations of *i* VOC species as molar ratios. The simplifying assumptions of the model are as follows:

- steady state;
- transfer of *i* species from gas into liquid phase;
- countercurrent plug flow of liquid and gas phase;

- axial dispersion of liquid phase;
- negligible absorbent vaporization (constant inert liquid flow rate);
- negligible gas solubility in the liquid (constant inert gas flow rate);
- linear interphase equilibrium relationship (Henry's law) between the molar fractions of *i* species in the gas and liquid phase, *i.e.*:

$$y_i^* = m_{xy} x_i \tag{1}$$

- isothermal and isobaric conditions.

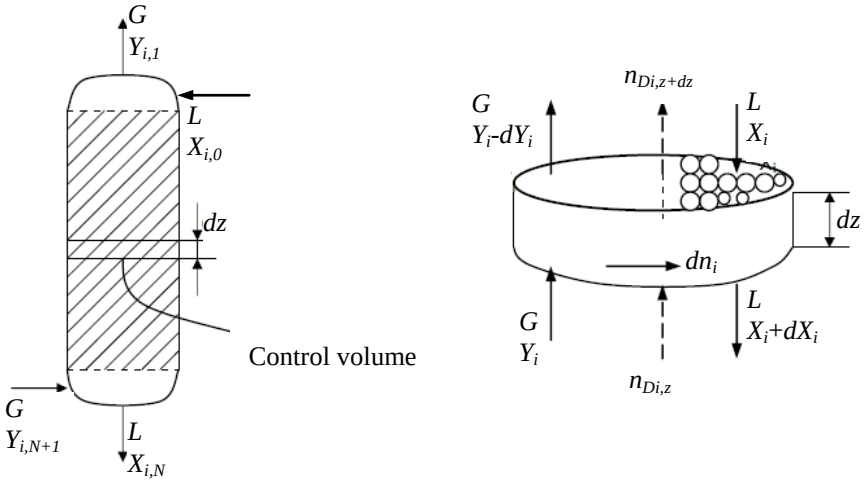

Fig. 1. Scheme of: (a) countercurrent packed-bed absorption column, (b) control volume in the absorption column.

Mathematical model describing the transfer of *i* species from gas into liquid phase consists of the following system of equations and restrictions:

- equation of mass balance of *i* species in the gas phase (for the control volume shown in Fig. 1b):

$$GY_i = G(Y_i - dY_i) + dn_i \;\Leftrightarrow\; GdY_i = dn_i \tag{2}$$

- equation of mass transfer kinetics of *i* species for the gas phase:

$$dn_i = K_{Yi}\sigma S(Y_i - Y_i^*)dz \tag{3}$$

- relationship of interphase equilibrium of *i* species:

$$Y_i^* = m_{XY} X_i \tag{4}$$

where m_{XY} can be expressed depending on Henry's constant, m_{xy}, as follows:

$$m_{XY} = \frac{\frac{y_i^*}{1-y_i^*}}{\frac{x_i}{1-x_i}} = \frac{\frac{m_{xy}x_i}{1-m_{xy}x_i}}{\frac{x_i}{1-x_i}} = \frac{m_{xy}(1-x_i)}{1-m_{xy}x_i} = \frac{m_{xy}\left(1-\frac{X_i}{1+X_i}\right)}{1-m_{xy}\frac{X_i}{1+X_i}} = \frac{m_{xy}}{1+X_i(1-m_{xy})} \quad (5)$$

- equation of mass balance of *i* species in the liquid phase (for the control volume shown in Fig. 1b):

$$LX_i + dn_i + n_{Di,z} = L(X_i + dX_i) + n_{Di,z+dz} \quad (6)$$

- equations expressing the molar flow of *i* species due to the axial dispersion of the liquid phase at *z* and *z+dz* distances from the column bottom, respectively:

$$n_{Di,z} = -D_l S(1-\varepsilon_g-\varepsilon_s)\frac{\rho_l}{M_l}\frac{d(X_i+dX_i)}{dz} \quad (7)$$

$$n_{Di,z+dz} = -D_l S(1-\varepsilon_g-\varepsilon_s)\frac{\rho_l}{M_l}\frac{dX_i}{dz} \quad (8)$$

- boundary conditions (according to the notations in Fig. 1a):

$$z=0 \qquad Y_i = Y_{i,N+1} \qquad X_i = X_{i,N} \quad (9)$$

$$z=H \qquad Y_i = Y_{i,1} \qquad X_i = X_{i,0} \quad (10)$$

Coupling equations (2)-(5), a first order differential equation describing the concentration profile of *i* species in the gas phase along the column can be written as:

$$\frac{dY_i}{dz} = \frac{K_{Yi}\sigma S}{G}\left(Y_i - \frac{m_{xy}X_i}{1+X_i(1-m_{xy})}\right) \quad (11)$$

Equations (3), (7) and (8) substituted in Eq. (6) lead to a second order differential equation expressing the transfer of *i* species into the liquid phase, *i.e.*:

$$\frac{d^2X_i}{dz^2} + \frac{LM_l}{D_l\rho_l S(1-\varepsilon_g-\varepsilon_s)}\frac{dX_i}{dz} - \frac{K_{Yi}\sigma M_l(Y_i-Y_i^*)}{D_l\rho_l(1-\varepsilon_g-\varepsilon_s)} = 0 \quad (12)$$

Accordingly, characteristic mathematical model of *i* species absorption into the liquid phase consists of the independent differential equations (11) and (12) along with the boundary conditions (9) and (10). Aiming at simplifying the solving procedure, a first order differential equation has been used instead of Eq. (12). Considering the mass balance of *i* species for the inferior part of the absorption column (Fig. 1a), Eq. (6) becomes:

$$LX_i + GY_{i,N+1} - GY_i = LX_{i,N} - D_l S(1-\varepsilon_g-\varepsilon_s)\frac{\rho_l}{M_l}\frac{dX_i}{dz} \quad (13)$$

By rearranging its terms, Eq. (13) turns into a first order differential equation describing the concentration profile of *i* species in the liquid phase along the column, *i.e.*:

$$\frac{dX_i}{dz} = \frac{M_l}{D_l \rho_l S(1-\varepsilon_g-\varepsilon_s)}\left[G(Y_i - Y_{i,N+1}) - L(X_i - X_{i,N})\right] \tag{14}$$

Commonly, in calculation concerning the design of a countercurrent packed-bed absorption column, the values of inert gas flow rate, G, inlet molar ratio of *i* species in the gas phase, $Y_{i,N+1}$, outlet molar ratio of *i* species in the gas phase (or separation factor, φ), $Y_{i,1}$, inlet molar ratio of *i* species in the liquid phase, $X_{i,0}$, are given, whereas the ones of inert liquid flow rate, L, and outlet molar ratio of *i* species in the liquid phase, $X_{i,N}$, must be calculated. The mass balance around the absorption column shown in Fig. 1a leads to the following relationship for determining the L/G ratio:

$$\frac{L}{G} = \frac{Y_{i,N+1} - Y_{i,1}}{X_{i,N} - X_{i,0}} \tag{15}$$

The minimum value of L, L_{min}, corresponds to the maximum value of $X_{i,N}$, *i.e.* that which is in equilibrium with $Y_{i,N+1}$, so that, taking into account Eq. (4), Eq. (15) becomes:

$$\frac{L_{min}}{G} = \frac{Y_{i,N+1} - Y_{i,1}}{\frac{Y_{i,N+1}}{m_{XY}} - X_{i,0}} \tag{16}$$

For dilute systems, it can be assumed that $Y_i \approx y_i$ and $X_i \approx x_i$, accordingly, based on Eqs. (1) and (4), $m_{XY} \approx m_{xy}$ and Eq. (16) can be written as:

$$\frac{L_{min}}{G} = \frac{Y_{i,N+1} - Y_{i,1}}{\frac{Y_{i,N+1}}{m_{xy}} - X_{i,0}} \tag{17}$$

The values of inert liquid flow rate, L, are usually between 1.1 L_{min} and 2 L_{min} [5,9,10]. In the case of inexpensive solvents, it is recommended to operate at a high inert liquid flow rate ($1.6L_{min} \le L \le 2L_{min}$) in order to decrease the column height and, consequently, to reduce the investment cost as well as to facilitate the maintenance and control [5].

3. Case study

Acetone (*i* VOC species) absorption from an air stream into water using a countercurrent packed-bed column was predicted based on the following data:

- packing: ceramic Raschig rings (diameter: d_R=0.025 m; void fraction: ε_V=0.74 m^3/m^3; specific surface: σ=204 m^2/m^3; solid surface fraction: ε_s=0.21 m^2/m^2);
- gas surface fraction: ε_g=0.74 m^2/m^2;
- liquid surface fraction: $\varepsilon_l = 1 - \varepsilon_s - \varepsilon_g = 0.05$ m^2/m^2 (corresponding to a thin liquid film down-flowing along the walls of the Raschig rings);
- column diameter: D=1 m;
- temperature: t=21°C;
- pressure: p=101325 Pa;
- inlet gas mass flow rate: G_{mg}=0.9 kg/s;
- inlet VOC mass concentration in the gas phase: $\gamma_{gi,N+1}$=0.035 kg_i/m^3;
- inlet VOC mass concentration in the liquid phase: $\gamma_{li,0}$=0 kg_i/m^3;
- VOC separation efficiency: φ=99 %;
- VOC diffusion coefficients in the gas and liquid phase [21]: D_{ig}=1.1×10^{-5} m^2/s and D_{il}=1.1×10^{-9} m^2/s;
- linear interphase equilibrium relationship [5]: $y_i^* = m_{xy} x_i = 1.4 x_i$;
- gas and liquid physical properties summarized in Table1.

Table 1.

Physical properties of gas and liquid phase at t=21 °C and p=101325 Pa

No.	Name	Symbol	Value		Unit
			Gas phase	Liquid phase	
1	Density	ρ	1.2	998	kg/m^3
2	Dynamic viscosity	η	1.8×10^{-5}	0.98×10^{-3}	kg/(m s)
3	Molar mass	M	29	18	kg/kmol

Characteristic parameters of mathematical model consisting of equations (9)-(11) and (14) were obtained according with the following algorithm:

1. Determination of inlet molar fractions of i species in the gas and liquid phase, $y_{i,N+1}$ and $x_{i,0}$, depending on inlet mass concentrations, $\gamma_{gi,N+1}$ and $\gamma_{li,0}$, operation pressure, p, temperature, t, liquid density, ρ_l, molar masses of liquid, M_l, and i species, M_i:

$$y_{i,N+1} = \frac{\gamma_{gi,N+1} R (t + 273.15)}{M_i p} \tag{18}$$

$$x_{i,0} = \frac{\gamma_{li,0} M_l}{\rho_l M_i} \tag{19}$$

2. Calculation of inert gas flow rate, G, depending on inlet molar fraction of i species in the gas phase, $y_{i,N+1}$, inlet gas mass flow rate, G_{mg}, and gas molar mass, M_g:

$$G = (1 - y_{i,N+1}) \frac{G_{mg}}{M_g} \tag{20}$$

3. Calculation of inlet molar ratios of i species in the gas and liquid phase based on inlet molar fractions:

$$Y_{i,N+1} = \frac{y_{i,N+1}}{1 - y_{i,N+1}} \tag{21}$$

$$X_{i,0} = \frac{x_{i,0}}{1 - x_{i,0}} \tag{22}$$

4. Determination of outlet molar ratio of i species in the gas phase, $Y_{i,1}$, depending on separation efficiency, φ, and inlet molar ratio of i species in the gas phase, $Y_{i,N+1}$:

$$Y_{i,1} = \left(1 - \frac{\varphi}{100}\right) Y_{i,N+1} \tag{23}$$

5. Estimation of minimum inert liquid flow rate, L_{min}, from Eq. (17):

$$L_{min} = G \frac{Y_{i,N+1} - Y_{i,1}}{\frac{Y_{i,N+1}}{m_{xy}} - X_{i,0}} \tag{24}$$

6. Selection of operation inert liquid flow rate, L, *i.e.*:

$$L = 2L_{min} \tag{25}$$

7. Determination of inlet liquid mass flow rate, G_{ml}, depending on L, M_l and $x_{i,0}$:

$$G_{ml} = \frac{LM_l}{1 - x_{i,0}} \tag{26}$$

8. Calculation of outlet molar ratio of i species in the liquid phase, $X_{i,N}$, based on mass balance around the absorption column (Fig. 1a):

$$X_{i,N} = X_{i,0} + \frac{G}{L}\left(Y_{i,N+1} - Y_{i,1}\right) \tag{27}$$

9. Estimation of partial gas mass transfer coefficient of i species in units corresponding to molar concentration, k_{ig} (m/s), according to the following relationship:

$$Sh_g = 0.45 \,\mathrm{Re}_g^{0.65} \, Sc_g^{0.33} \tag{28}$$

where:

$$\mathrm{Re}_g = \frac{\rho_g w_g d_e}{\eta_g} \tag{29}$$

$$w_g = \frac{G_{mg}}{S\rho_g} = \frac{4G_{mg}}{\pi D^2 \rho_g} \tag{30}$$

$$d_e = 4\frac{\varepsilon_V}{\sigma} \tag{31}$$

$$Sc_g = \frac{\eta_g}{\rho_g D_{ig}} \tag{32}$$

$$Sh_g = \frac{k_{ig} d_e}{D_{ig}} \tag{33}$$

10. Determination of partial gas mass transfer coefficient of *i* species in units corresponding to molar fraction, k_{yi} (kmol/(m^2 s)), depending on k_{ig} and operation conditions, *i.e. p* and *t*:

$$k_{ig}\left(c_{ig} - c_{ig}^*\right) = k_{yi}\left(y_i - y_i^*\right) = \frac{k_{yi} R(t + 273.15)}{p}\left(c_{ig} - c_{ig}^*\right) \Rightarrow$$

$$k_{yi} = k_{ig}\frac{p}{R(t + 273.15)} \tag{34}$$

11. Determination of partial gas mass transfer coefficient of *i* species in units corresponding to molar ratio, k_{Yi} (kmol$_g$/(m^2 s)), depending on k_{yi}, m_{XY} (calculated with Eq. (5)) and molar ratios of *i* species in the liquid and gas phase (X_i and Y_i):

$$k_{Yi}\left(Y_i - Y_i^*\right) = k_{yi}\left(y_i - y_i^*\right) = k_{yi}\left(\frac{Y_i}{1+Y_i} - \frac{Y_i^*}{1+Y_i^*}\right) \Rightarrow$$

$$k_{Yi} = \frac{k_{yi}}{\left(1+Y_i\right)\left(1+Y_i^*\right)} = \frac{k_{yi}}{\left(1+Y_i\right)\left(1+m_{XY}X_i\right)} \tag{35}$$

12. Estimation of partial liquid mass transfer coefficient of *i* species in units corresponding to molar concentration, k_{il} (m/s), according to the following relationship:

$$Sh_l = 0.0026\,\mathrm{Re}_l^{0.72}\,Sc_l^{0.50} \tag{36}$$

where:

$$\mathrm{Re}_l = \frac{G_{ml}}{S\sigma\eta_l} \tag{37}$$

$$Sc_l = \frac{\eta_l}{\rho_l D_{il}} \tag{38}$$

$$Sh_l = \frac{k_{il}}{D_{il}}\left(\frac{\eta_l^2}{g\rho_l^2}\right)^{1/3} \tag{39}$$

13. Determination of partial liquid mass transfer coefficient of *i* species in units corresponding to molar fraction, k_{xi} (kmol/(m^2 s)), depending on k_{il}, ρ_l and M_l:

$$k_{il}\left(c_{il} - c_{il}^*\right) = k_{xi}\left(x_i - x_i^*\right) = \frac{k_{xi}M_l}{\rho_l}\left(c_{il} - c_{il}^*\right) \Rightarrow$$

$$k_{xi} = k_{il}\frac{\rho_l}{M_l} \tag{40}$$

14. Determination of partial liquid mass transfer coefficient of *i* species in units corresponding to molar ratio, k_{Xi} (kmol$_l$/(m^2 s)), depending on k_{xi}, m_{XY} (calculated with Eq. (5)), X_i and Y_i:

$$k_{Xi}\left(X_i - X_i^*\right) = k_{xi}\left(x_i - x_i^*\right) = k_{xi}\left(\frac{X_i}{1+X_i} - \frac{X_i^*}{1+X_i^*}\right) \Rightarrow$$

$$k_{Xi} = \frac{k_{xi}}{\left(1+X_i\right)\left(1+X_i^*\right)} = \frac{k_{xi}}{\left(1+X_i\right)\left(1+\frac{Y_i}{m_{XY}}\right)} \tag{41}$$

15. Determination of total gas mass transfer coefficient of *i* species in units corresponding to molar ratio, K_{Yi} (kmol$_g$/(m^2 s)), depending on partial mass transfer coefficients, k_{Yi} and k_{Xi}, and m_{XY}:

$$K_{Yi} = \frac{1}{\frac{1}{k_{Yi}} + \frac{m_{XY}}{k_{Xi}}} \tag{42}$$

16. Estimation of axial dispersion coefficient, D_l, using the following correlation:

$$Sh_D = 0.527\,\mathrm{Re}_{lD}^{0.50}\,Ga_{lD}^{0.33} \tag{43}$$

where:

$$\mathrm{Re}_{lD} = \frac{\rho_l w_{lD} d_R}{\varepsilon\eta_l} \tag{44}$$

$$w_{lD} = \frac{G_{ml}}{S\rho_l} = \frac{4G_{ml}}{\pi D^2\rho_l} \tag{45}$$

$$Ga_{lD} = \frac{g d_R^3 \rho_l \left(\rho_l - \rho_g\right)}{\eta_l^2} \tag{46}$$

$$Sh_D = \frac{D_l \rho_l}{\eta_l} \tag{47}$$

4. Results and discussions

Characteristic mathematical model of absorption process described by ordinary differential equations (11) and (14) along with boundary conditions (9) and (10), whose parameters were calculated based on Eqs. (18)-(47), was solved using the fourth order Runge-Kutta method starting from z=0. It was obtained that a VOC separation efficiency of 99 % could be attained for a packing height of 5.43 m. Characteristic values of model parameters included in Eqs. (9)-(11) and (14) are summarized in Table 2, where $K_{Yi,mn}$ represents the mean value of K_{Yi} between z=0 and z=H.

Simulations were further conducted in order to highlight the effect of molar flow rate of inert fluid on the absorption performances evaluated in terms of VOC separation efficiency and mass transfer kinetics. Separation efficiency, φ, was estimated based on Eq. (23) depending on $Y_{i,1}\big|_{z=H=5.43m}$, whereas mass transfer kinetics was expressed as mean value of overall gas mass transfer coefficient of i species, $K_{Yi,mn}$, calculated using Eq. (42).

Table 2.

Model parameters in Eqs. (9)-(11) and (14)

No.	Name	Symbol	Value	Unit
1	Inlet molar ratio of *i* species in the gas phase	$Y_{i,N+1}$	0.0148	$kmol_i/kmol_g$
2	Inlet molar ratio of *i* species in the liquid phase	$X_{i,0}$	0	$kmol_i/kmol_l$
3	Outlet molar ratio of *i* species in the gas phase	$Y_{i,1}$	1.478×10^{-4}	$kmol_i/kmol_g$
4	Outlet molar ratio of *i* species in the liquid phase	$X_{i,N}$	0.0053	$kmol_i/kmol_l$
5	Molar flow rate of inert gas	G	0.0306	$kmol_g/s$
6	Molar flow rate of inert liquid	$L=2L_{min}$	0.0848	$kmol_l/s$
7	Overall gas mass transfer coefficient of *i* species	$K_{Yi,mn}$	2.909×10^{-4}	$kmol_g/(m^2 s)$
8	Axial dispersion coefficient	D_l	0.0022	m^2/s
9	Packing height	H	5.43	m

4.1. The effect of liquid flow rate

The results of simulations conducted at various values of molar flow rate of inert liquid, L, for G=0.0306 $kmol_g/s$ and H=5.43 m, *i.e.* concentration profiles of i species along the column, $Y_i(z)$ and $X_i(z)$, which are compared in Fig. 2, highlight a decrease in Y_i and X_i with L increasing. Curves illustrated in Fig. 3

referring to the effect of L on process performances emphasize that φ and $K_{Yi,mn}$ increase with L, the dependency between φ and L being polynomial (Eq. (48)), whereas $K_{Yi,mn}$ increases with L according to a power law (Eq. (49)). Moreover, φ varies between 90 and 99 % and $K_{Yi,mn}$ from 2.464×10^{-4} to 2.909×10^{-4} $kmol_g/(m^2 s)$ for L ranging in the field [0.0636-0.0848] $kmol_l/s$, *i.e.* for $1.6L_{min} \le L \le 2L_{min}$.

$$\varphi = -7000L^4 + 2000L^3 - 200L^2 + 11.695L - 0.212 \quad (48)$$

$$K_{Yi,mn} = 12.486L^{0.59} \quad (49)$$

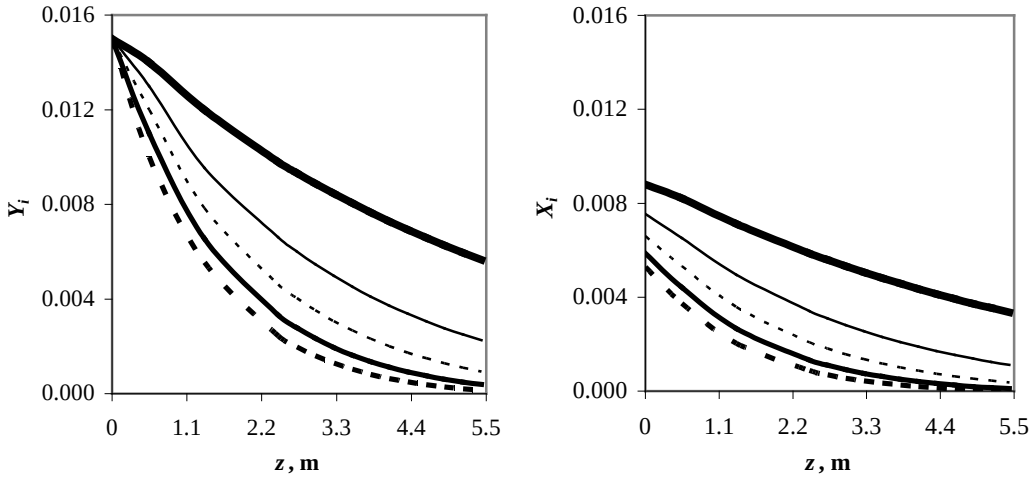

Fig. 2. Variation of molar ratios of *i* species in the gas and liquid phase, Y_i and X_i, along the column ($0 \le z \le H$) at various molar flow rate of inert liquid, L (▪▪▪ $2L_{min}$, ─ $1.8L_{min}$, ⋯ $1.6L_{min}$, — $1.4L_{min}$, ▬ $1.2L_{min}$), for L_{min}=0.0424 $kmol_l/s$, G=0.0306 $kmol_g/s$ and H=5.43 m.

4.2. The effect of gas flow rate

The concentration profiles of *i* species along the column, $Y_i(z)$ and $X_i(z)$, simulated at various values of molar flow rate of inert gas, G, for $L=2L_{min}$=0.0848 $kmol_l/s$ and H=5.43 m, which are shown in Fig. 4, reveal an increase in Y_i and X_i with G. Curves depicted in Fig. 5 highlight that φ has a polynomial decrease with G (Eq. (50)), whereas $K_{Yi,mn}$ increases with G according to a power law (Eq. (51)). Moreover, values of φ between 99 and 90 % and of $K_{Yi,mn}$ from 2.909×10^{-4} to 3.015×10^{-4} $kmol_g/(m^2 s)$ are obtained for G varying from 0.0306 $kmol_g/s$ (G_{min}) to 0.0397 $kmol_g/s$ ($1.3G_{min}$).

$$\varphi = -10.741G^2 + 0.672G - 0.0007 \quad (50)$$

$$K_{Yi,mn} = 4.440G^{0.12} \quad (51)$$

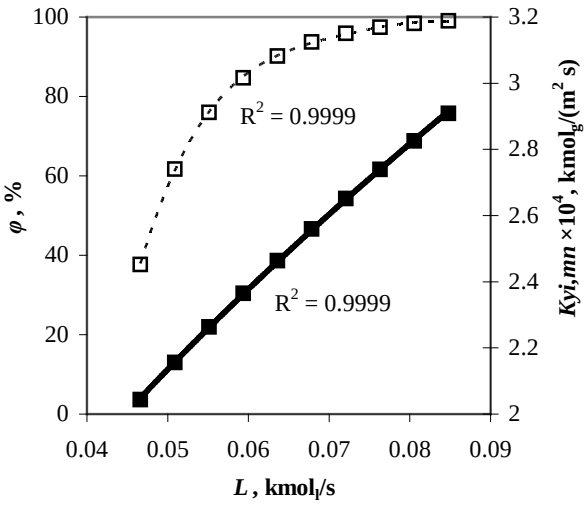

Fig. 3. Effect of molar flow rate of inert liquid, $1.1L_{min} \le L \le 2L_{min}$, on VOC separation efficiency, φ (□ Eq. (23), ⋯ Eq. (48)) and overall gas mass transfer coefficient, $K_{Yi,mn}$ (■ Eq. (42), ─ Eq. (49)), for L_{min}=0.0424 kmol$_l$/s, G=0.0306 kmol$_g$/s and H=5.43 m

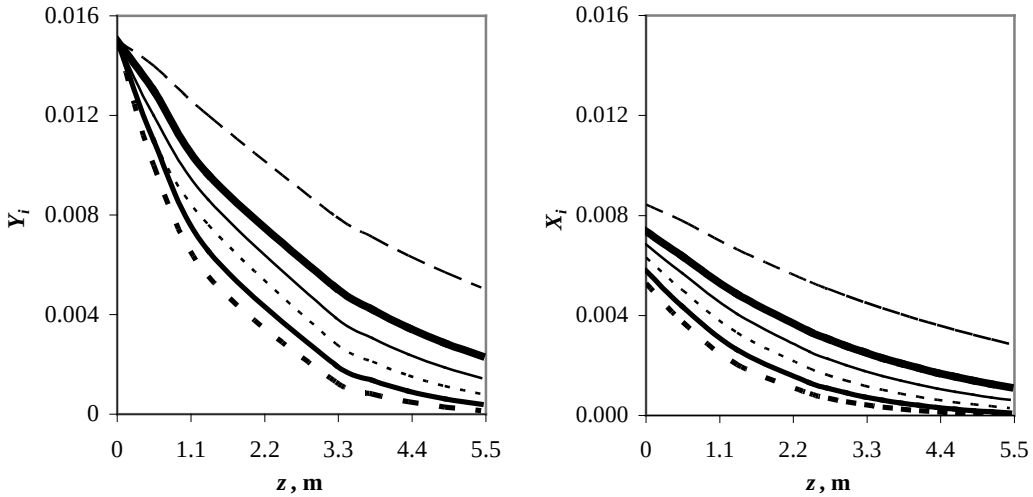

Fig. 4. Variation of molar ratios of i species in the gas and liquid phase, Y_i and X_i, along the column ($0 \le z \le H$) at various molar flow rate of inert gas, G (▪▪▪ G_{min}, ─ $1.1G_{min}$, ⋯ $1.2G_{min}$, — $1.3G_{min}$, ▬ $1.4G_{min}$, – – $1.6G_{min}$), for G_{min}=0.0306 kmol$_g$/s, L=$2L_{min}$=0.0848 kmol$_l$/s and H=5.43 m.

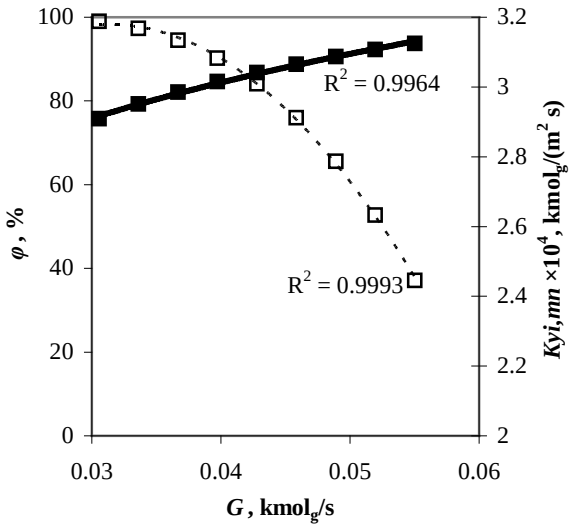

Fig. 5. Effect of molar flow rate of inert gas, $1.1G_{min} \leq G \leq 1.8G_{min}$, on VOC separation efficiency, φ (□ Eq. (23), ⋯ Eq. (50)) and overall gas mass transfer coefficient, K_{Yi} (■ Eq. (42), ─ Eq. (51)), for G_{min}=0.0306 $kmol_g/s$, $L=2L_{min}$=0.0848 $kmol_l/s$ and H=5.43 m

5. Conclusions

A theoretical study on the modelling and simulation of *i* VOC species absorption from a gas into a liquid absorbent (solvent) using a countercurrent packed-bed column was presented. Absorption performances, evaluated as VOC separation efficiency and overall mass transfer kinetics, depends on nature and concentration of VOC species in the feed gas, solvent nature, packing type and dimension, column diameter, gas and liquid flow rate, process temperature and pressure. A case study on acetone removal from air by absorption into clean water passing through a packing consisting of Raschig rings was considered.

A model for predicting the acetone concentration in the fluid phase along the column and the packing-bed height needed to attain specified separation efficiency as well as an algorithm for calculating the model parameters were presented. A packing-bed height of 5.43 m and a minimum value of molar flow rate of inert liquid (L_{min}) of 0.0424 $kmol_l/s$ were obtained starting from the following data: inlet acetone mass concentration in the gas phase of 0.035 kg_i/m^3, ceramic Raschig rings with a diameter of 0.025 m, column diameter of 1 m, inlet air mass flow rate of 0.9 kg/s, separation efficiency of 99 %, operation temperature of 21 °C and pressure of 101325 Pa.

Simulations were performed in order to evaluate the effect of process parameters on absorption performances for a packing-bed height of 5.43 m. An increase in air flow rate and a decrease in water flow rate diminished the separation efficiency, whereas an increase in flow rate of both fluids improved the

overall mass transfer, according to data reported in the related literature. Moreover, for an inlet air mass flow rate of 0.9 kg/s, separation efficiencies over 90 % were attained for molar flow rates of inert liquid between $1.6L_{min}$ and $2L_{min}$.

The model could be applied for absorption of any VOC species from a gas stream into any solvent type using countercurrent columns with different types and dimensions of packing and under various operation conditions. For a specified value of VOC separation efficiency and an inexpensive solvent, it is recommended to operate at molar flow rates of inert liquid between $1.6L_{min}$ and $2L_{min}$ in order to obtain enhanced performances in terms of VOC separation efficiency and overall mass transfer kinetics as well as of investment costs due to a decrease in packing height.

Acknowledgements

This work was supported by the Sectorial Operational Programme Human Resources Development (SOP HRD), financed from the European Social Fund and the Romanian Government under the contract number POSDRU/159/1.5/S/137390/.

Nomenclature

d_e	equivalent diameter of packing, m
d_R	diameter of Raschig ring, m
D	column diameter, m
D_l	axial dispersion coefficient, m^2/s
G	molar flow rate of inert gas, $kmol_g/s$
G_m	mass flow rate, kg/s
H	packing height, m
k_i	partial mass transfer coefficient of *i* species in units corresponding to molar concentration, m/s
$k_{y/xi}$	partial gas/liquid mass transfer coefficient of *i* species in units corresponding to molar fraction, $kmol/(m^2 s)$
$k_{Y/Xi}$	partial gas/liquid mass transfer coefficient of *i* species in units corresponding to molar ratio, $kmol_{g/l}/(m^2 s)$
K_{Yi}	overall gas mass transfer coefficient of *i* species in units corresponding to molar ratio, $kmol_g/(m^2 s)$
L	molar flow rate of inert liquid, $kmol_l/s$
m_{xy}	slope of interphase equilibrium line referring to molar fraction, $y_i^* = m_{xy} x_i$
m_{XY}	characteristic variable of interphase equilibrium relationship referring to molar ratio, $Y_i^* = m_{XY} X_i$
M	molar mass, kg/kmol
n_i	molar flow rate of *i* species transferred from gas to liquid, $kmol_i/s$

$n_{Di,z}$	molar flow rate of *i* species due to the axial dispersion of the liquid phase, at *z* distance from the column bottom, $kmol_i/s$
R	universal gas constant, R=8314 J/(kmol K)
S	column cross-sectional area, m^2
w	superficial velocity, m/s
x_i	molar fraction of *i* species in the liquid phase, $kmol_i/kmol$
X_i	molar ratio of *i* species in the liquid phase, $kmol_i/kmol_l$
x_i^*	equilibrium molar fraction of *i* species in the liquid phase, $kmol_i/kmol$
X_i^*	equilibrium molar ratio of *i* species in the liquid phase, $kmol_i/kmol_l$
y_i	molar fraction of *i* species in the gas phase, $kmol_i/kmol$
Y_i	molar ratio of *i* species in the gas phase, $kmol_i/kmol_g$
y_i^*	equilibrium molar fraction of *i* species in the gas phase, $kmol_i/kmol$
Y_i^*	equilibrium molar ratio of *i* species in the gas phase, $kmol_i/kmol_g$
z	axial coordinate, m

Dimensionless numbers

Ga	Galilei number
Re	Reynolds number
Sc	Schmidt number
Sh	Sherwood number

Greek letters

γ_i	mass concentration of *i* species, kg_i/m^3
ε	surface fraction, m^2/m^2
ε_V	void fraction, m^3/m^3
η	dynamic viscosity, kg/(m s)
ρ	density, kg/m^3
σ	active specific surface, m^2/m^3
φ_i	separation efficiency of *i* species

Subscripts

D	relative to axial dispersion
g	relative to gas
i	index designating VOC species
l	relative to liquid
min	minimum
mn	mean
N	relative to liquid outlet
N+1	relative to gas inlet
s	relative to solid
z	relative to *z* distance in the column
0	relative to liquid inlet
1	relative to gas outlet

Superscripts

*	relative to equilibrium

REFERENCES

[1] Ambrozek, B., Zwarycz-Makles, K., Theoretical and experimental studies of the recovery of volatile organic compounds from waste air streams in the thermal swing adsorption system with closed-loop regeneration of adsorbent, *Energy Conversion and Management*, 85, (2014), 646–654.

[2] Darracq, G., Couvert, A., Couriol, C., Amrane A., Le Cloirec, P., Kinetics of toluene and sulfur compounds removal by means of an integrated process involving the coupling of absorption and biodegradation, *Journal of Chemical Technology and Biotechnology*, 85, (2010), 1156–1161.

[3] Kim, K.J., Kang, C.S., You, Y.J., Chung, M.C., Woo, M.W., Jeong, W.J., Park, N.C., Ahn, H.G., Adsorption–desorption characteristics of VOCs over impregnated activated carbons, *Catalysis Today*, 111, (2006), 223-228.

[4] Ozturk, B., Yilmaz, D., Absorptive removal of volatile organic compounds from flue gas streams, *Process Safety and Environmental Protection*, 84, (2006), 391–398.

[5] Rahbar, M.S., Kaghazchi, T., Modeling of packed absorption tower for volatile organic compounds emission control, *International Journal of Environmental Science and Technology*, 2, (2005), 207-215.

[6] Shah, I.K., Pré, P., Alappat, B.J., Effect of thermal regeneration of spent activated carbon on volatile organic compound adsorption performances, *Journal of the Taiwan Institute of Chemical Engineers*, 45, (2014), 1733–1738.

[7] Yu, F.D., Luo, L., Grevillot, G., Electrothermal swing adsorption of toluene on an activated carbon monolith: Experiments and parametric theoretical study, *Chemical Engineering and Processing: Process Intensification*, 46, (2007), 70–81.

[8] Bourgois, D., Vanderschuren, J., Thomas, D., Determination of liquid diffusivities of VOC (paraffins and aromatic hydrocarbons) in phthalates, *Chemical Engineering and Processing*, 47, (2008), 1357–1364.

[9] Dumont, E., Darracq, G., Couvert, A., Couriol, C., Amrane, A., Thomas, D., Andrès, Y., Le Cloirec, P., VOC absorption in a countercurrent packed-bed column using water/silicone oil mixtures: Influence of silicone oil volume fraction, *Chemical Engineering Journal*, 168, (2011), 241–248.

[10] Dumont, E., Darracq, G., Couvert, A., Couriol, C., Amrane, A., Thomas, D., Andrès, Y., Le Cloirec, P., Hydrophobic VOC absorption in two-phase partitioning bioreactors; influence of silicone oil volume fraction on absorber diameter, *Chemical Engineering Science*, 71, (2012), 146–152.

[11] Hadjoudj, R., Monnier, H., Roizard, C., Lapicque, F., Measurements of diffusivity of chlorinated VOCs in heavy absorption solvents using a laminar falling film contactor, *Chemical Engineering and Processing*, 47, (2008), 1478–1483.

[12] Heymes, F., Manno-Demoustier, P., Charbit, F., Fanlo, J.L., Moulin, P., A new efficient absorption liquid to treat exhaust air loaded with toluene, *Chemical Engineering Journal*, 115, (2006), 225–231.

[13] Jiang, Y., Guo, C., Liu, H., Magnetically rotational reactor for absorbing benzene emissions by ionic liquids, *China Particuology*, 5, (2007), 130–133.

[14] Li, R., Xu, J., Wang, L., Li, J., Sun, X., Reduction of VOC emissions by a membrane-based gas absorption process, *Journal of Environmental Sciences*, 21, (2009), 1096–1102.

[15] Lin, C.C., Wei, T.Y., Hsu, S.K., Liu, W.T., Performance of a pilot-scale cross-flow rotating packed bed in removing VOCs from waste gas streams, *Separation and Purification Technology*, 52, (2006), 274–279.
[16] Marki, E., Lenti, B., Vatai, Gy., Bekassy-Molnar, E., Clean technology for acetone absorption and recovery, *Separation and Purification Technology*, 22-23, (2001), 377-382.
[17] Mhiri, N., Monnier, H., Falk, L., Intensification of the G/L absorption in microstructured falling film application to the treatment of chlorinated VOC's. Part III: Influence of gas thickness channel on mass transfer, *Chemical Engineering Science*, 66, (2011), 5989–6001.
[18] Monnier, H., Falk, L., Lapicque, F., Hadjoudj, R., Roizard, C., Intensification of G/L absorption in microstructured falling film. Application to the treatment of chlorinated VOC's – part I: Comparison between structured and microstructured packings in absorption devices, *Chemical Engineering Science*, 65, (2010), 6425–6434.
[19] Park, B., Hwang, G., Haam, S., Lee, C., Ahn, I.S., Lee, K., Absorption of a volatile organic compound by a jet loop reactor with circulation of a surfactant solution: Performance evaluation, *Journal of Hazardous Materials*, 153, (2008), 735–741.
[20] Tokumura, M., Nakajima, R., Znad, H.T., Kawase, Y., Chemical absorption process for degradation of VOC gas using heterogeneous gas–liquid photocatalytic oxidation: Toluene degradation by photo-Fenton reaction, *Chemosphere*, 73, (2008), 768–775.
[21] Cussler, E.L., Diffusion: Mass transfer in fluid systems (3rd ed.), Cambridge University Press, New York, 2009.

KINETIC STUDY ON THE CONTROLLED RELEASE OF RIFAMPICIN

Paula POSTELNICESCU, Anca Madalina DUMITRESCU* and Evelina DRAGOMIR

[1]Departament of Chemical and Biochemical Engineering, University Politehnica of Bucharest, 1-7 Polizu Street, 011061, Bucharest, Romania

Abstract
In order to decrease the dosing frequency in a treatment, controlled release preparations of drugs are very important. The anti tubercular drugs are usually administrated as oral dosage forms. Among these drugs rifampicin, which is a semi synthetic hydrazine, is well absorbed from gastrointestinal tract and has a short biological half life. The aim of this paper is to simulate the release kinetics of rifampicin from natural polymeric microcapsules in intestinal fluid, by diffusional models. In order to illustrate the validity of the selected mathematical models, comparisons with experimental profiles obtained in simulated intestinal fluid and reported in the recent literature are presented.

Keywords: Rifampicin, Kinetics, Controlled release, Oral dosage forms, Microcapsules.

1. Introduction

The aim of controlling the drug delivery is to achieve more effective therapies while eliminating potential for both under- and overdosing. Controlled delivery systems include the maintenance of drug levels within a desired range, the need for fewer administrations, optimal use of drug and increased patient compliance [1].

In the design of drug delivery system, it is necessary to study and optimize the drug delivery profile specific for the release kinetics.

Over the past three decades, because the oral dosage forms are generally made of polymers in which the drug is dispersed, the controlled release from a polymeric matrix was a problem of special interest in the area of pharmacokinetics. Based on encouraging results, the recent trend is to shift from synthetic towards natural polymers [2].

The anti-tubercular drugs are usually administrated as oral dosage forms. In order to decrease the dosing frequency in a treatment, controlled release preparations of drugs are very important. Amongst the anti-tubercular drugs, rifampicin which is a

*Corresponding author: E-mail address: a_dumitrescu@chim.upb.ro (Anca Dumitrescu)

semi-synthetic hydrazine, is well absorbed from gastrointestinal tract and have a short biological half life of 2-5 hours [3]. In the last several years, many different types of controlled release formulations have been developed to improve clinical efficacy of drug and patient compliance [3]-[7]. Our research was based on the experimental results reported by Sarfaraz and co-workers for the release of rifampicin from biodegradable microcapsules prepared with sodium alginate and Carbopol 974P as coating polymers in different ratios [6]. The aim of this paper is to simulate the release kinetics of rifampicin in intestinal fluid, by using diffusional models.

2. Diffusional models for drug release

Assuming the hypothesis that drug release is controlled by diffusion, the kinetics can be simulated considering the classical unsteady state Fick's diffusion equation having appropriate boundary conditions, the Higuchi model and Baker-Lonsdale model.

2.1 Fick's diffusion equation

For the radial diffusion (spherical forms) and constant diffusivity, the equation takes the form:

$$\frac{\partial C}{\partial t} = \frac{D}{r^2} \cdot \frac{\partial}{\partial r}\left[r^2 \frac{\partial C}{\partial r} \right] \tag{1}$$

By considering the transport resistance in the external liquid layer:

$$-D\frac{\partial C}{\partial r} = h\left(C_S - C_\infty\right) \tag{2}$$

The amount of drug released after a period of time t, M_t, as a fraction of the corresponding quantity after infinite time, M_∞, is calculated from the equation [8]:

$$\frac{M_\infty - M_t}{M_\infty} = \sum_{n=1}^{\infty} \frac{6K^2}{\gamma_n\left(\gamma_n^2 + K^2 - K\right)} exp\left(-\frac{\gamma_n^2}{R^2} D \cdot t \right) \tag{3}$$

with the dimensionless number K:

$$K = \frac{h \cdot R}{D} \tag{4}$$

where the γ_ns are the roots of:

$$\gamma_n \cot \gamma_n = 1 - K \tag{5}$$

When the value of the mass transfer coefficient can be considered infinite, the drug concentration on the surface reaches its value at equilibrium as soon as the dosage form is put in contact with the liquid [8].
In this case, the kinetics of the drug release is described as follows [8]:

$$\frac{M_\infty - M_t}{M_\infty} = \frac{6}{\pi^2} \cdot \sum_{n=1}^{\infty} \frac{1}{n^2} \cdot exp\left(-\frac{n^2 \cdot \pi^2}{R^2} D \cdot t \right) \tag{6}$$

2.2. Higuchi model

The Higuchi equation describes the release of a drug from a matrix system as a square root of a time dependent process, based on a Fickian diffusion [9-11].

$$M_t = A\sqrt{D \cdot (2C_0 - C_S) C_S \cdot t} = k_H \sqrt{t} \tag{8}$$

The parameter of the model is the release rate constant, k_h, which reflects the design variables of the system.

2.3. Baker-Lonsdale model

This model was developed from the Higuchi equation and describes the drug controlled release from a spherical matrix [11].

$$\frac{3}{2}\left[1 - \left(1 - \frac{M_t}{M_\infty} \right)^{\frac{2}{3}} \right] - \frac{M_t}{M_\infty} = k \cdot t \tag{9}$$

The parameter of the model is the release rate constant k.

3. Results

By fitting the experimental data reported by Sarfaraz and co-workers [6], we established the effective diffusivities of rifampicin from the microcapsules with

characteristics given in Table 1, considering the hypothesis that the value of the mass transfer coefficient is infinite (the release medium is well stirred) [12]. On the basis of the calculated effective diffusivities, the predictions of the mathematical model were calculated. The standard errors of all models were established by using the equation [13]:

$$e = \frac{\left\| M_{exp} / M_{\infty} - M_{calc} / M_{\infty} \right\|_2}{\sqrt{N - p}} \tag{10}$$

The values of the calculated effective diffusivities are presented in Table 2.

Tabel 1

Characteristics of the microcapsules [6]

Microcapsules	**Mean particle size (μm)**	**Coat composition (Sodium alginate: Carbopol 974P)**
MC1	444.79	1:1
MC2	467.43	1:2
MC3	486.52	1:3

Table 2

The effective diffusivities of rifampicin and the standard errors of the model

Microcapsules	**$D_{eff} \cdot 10^{13}$ (m^2/s)**	**e**
MC1	1.88	0.02419
MC2	1.25	0.03240
MC3	1.00	0.06660

All the figures are related to the microcapsules MC2, having a rifampicin content of 10.81±0.27 %.

Fig.1 shows the release behaviour of rifampicin from microcapsules with the mean diameter d = 467.43 μm.

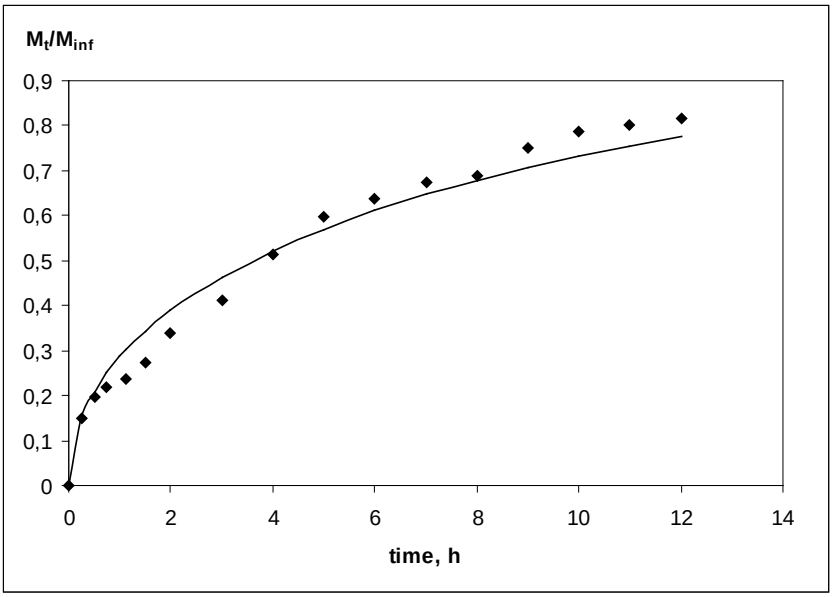

Fig.1. Release profiles of rifampicin from microcapsules with d= 467.43μm.

♦ *Experimental profile determined in simulated intestinal fluid (pH 7.4); - Predictions of the diffusional model*

Applying the Higuchi model for the same experimental results, the established values of parameter k_h and the standard errors of the model are presented in Table 3.

Table 3

The release rate constants of Higuchi model and the standard errors of the model

Microcapsules	**k_h, $h^{-0.5}$**	**e**
MC1	0.2543	0.0819
MC2	0.2443	0.0254
MC3	0.2414	0.0541

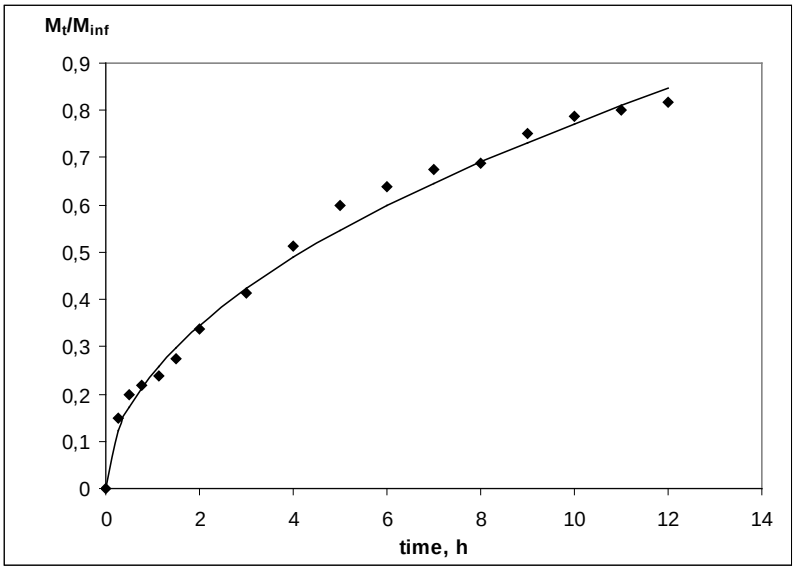

Fig. 2. Release profiles of rifampicin from microcapsules with d= 467.43μm.

♦ Experimental profile determined in simulated intestinal fluid (pH 7.4); - Predictions of Higuchi model

Fitting the experimental data by using Baker-Lonsdale model, we established the values of the release constant k.

The values of the release constant of Baker-Lonsdale model and the standard errors of this model are given in Table 4.

Table 4

The release constants of Baker-Lonsdale model and the standard errors of the model

Microcapsules	**k, h^{-1}**	**e**
MC1	0.0243	0.0278
MC2	0.0175	0.0458
MC3	0.0154	0.0800

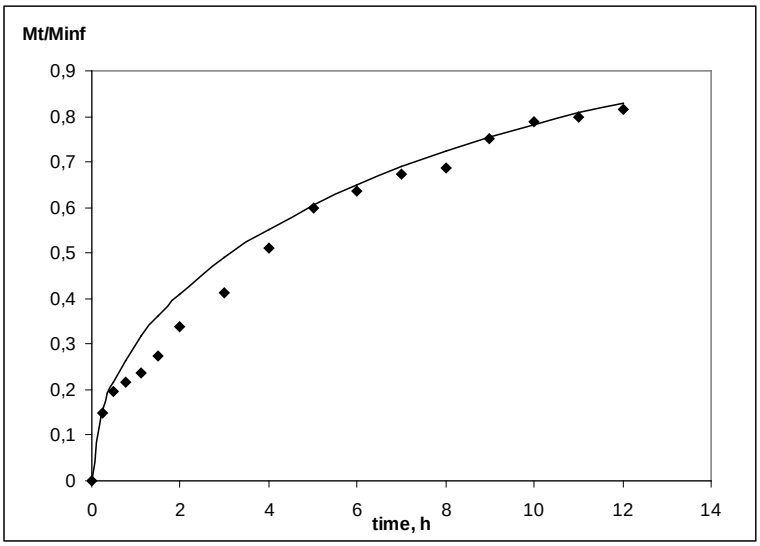

Fig. 3. Release profiles of rifampicin from microcapsules with d= 467.43μm.
♦ Experimental profile determined in simulated intestinal fluid (pH 7.4); - Predictions of Baker-Lonsdale model

4. Conclusions

Based on the experimental data from the recent literature and hypothesized drug release mechanisms, appropriate mathematical models were used to predict the release kinetics of rifampicin in order to optimize the oral administration of this drug.

According to the simulation results, the hypothesis that rifampicin release from natural polymeric microcapsules in intestinal fluid is controlled by diffusion is valid.

The Fick's diffusion model gives the best predictions because the interval of the standard errors is smaller by comparison with those obtained with Higuchi and Baker-Lonsdale models.

Notations

C - drug concentration

C_0 - drug initial concentration

C_s - drug solubility

C_e - drug concentration at liquid interface at equilibrium

D – diffusivity

D_{eff} – effective diffusivity

h – mass transfer coefficient

k_h - release rate constant for the Higuchi model in the dissolution medium

M_t - amount of drug released after a period of time *t*

M_∞ - amount of drug released after infinite time

N- number of the experimental points

p- number of the model parameters

R - radius

t – time

$\|\bullet\|_2$ - Euclidean norm

REFERENCES

[1] Khan, M.A. and Shefeeq, T., Role of Mathematical Modeling in Controlled Drug Delivery, *J. Sci. Res.*, 1(3), (2009), 539-550.

[2] Raizada, A., Bandari, A., Kumar, B., Polymers in Drug Delivery: A Review, *International Journal of Pharma. Research & Development-Online"*, IJPRD/2010/PUB/ARTI/VOV-2/ISSUE-8/OCT/002.

[3] Sabitha, P., Vijaya Ratna, J., Ravindra Reddy, K., Design and Evaluation of Controlled Release Chitosan-Calcium Alginate Microcapsules of Anti Tubercular Drugs for Oral Use, *Int. J. Chem. Tech. Res.*, 2(1), (2010), 88-98.

[4] Prashanti, G., Formulation and Evaluation of Mucoadhesive Microcapsules of Rifampicin, *IOSR J Pharm.*, 3(4), (2013), 10-14.

[5] Patel, B.K., Parikh, R.H., and Aboti, P.S., Development of Oral Sustained Release Rifampicin Loaded Chitosan Nanoparticles by Design of Experiment, *J Drug Delivery*, http://dx.doi.org/10.1155/2013/370938, (2013).

[6] Sarfaraz, M.D., Hiremath, D., and Chowdary, K.P.R., Formulation and Characterization of Rifampicin Microcapsules, *Indian J Pharm Sci*., 72(1), (2010), 101-105.

[7] Hiremath, S.P., and Saha R.N., Design and Study of Rifampicin Oral Controlled Release Formulations, *Drug Delivery*, **11**(5), (2004), 311-315.

[8] Vergnaud, J.M., and Roşca, I.D., *Assesing Bioavalability of Drug Delivery Systems*. Taylor & Francis Group, New York, 2005.

[9] Higuch, T., Mechanism of Sustained Action Medication, Theoretical Analysis of Rate of Release of Solid Drugs Dispersed in Solid Matrices, *Journal of Pharmaceutical Sciences*, 52, (1963), 1145-1149.

[10] Mathiowitz, E., *Encyclopedia of Controled Drug Delivery*, John Wiley&Sons, New York, 1999.

[11] Costa, P., Sousa Lobo, J. M., Modeling and Comparison of Dissolution Profiles, *Eur. J. Pharm. Sci.*, 13, (2001) 123-133.

[12] Postelnicescu, P., Dumitrescu, A. M., Josceanu, A. M., and Dragomir, E., Controlled Release of Rifampicin and Isoniazid from Oral Dosage Forms, *18th Romanian International Conference on Chemistry and Chemical Engineering*, September 4- 7, 2013 Sinaia Romania, S4 pp.24-27.

[13] Maria, G., Berger, D., Nastase, S., Luta, I., Kinetic Studies on the irinotecan release based on structural properties of functionalized mesoporous-silica supports, *Micropor. Mesopor. Mater*.,149, (2012), 25-35.

SUPERABSORBENT MATERIALS FOR AGRICULTURAL USES STARTING FROM BACTERIAL CELLULOSE

Anicuța STOICA-GUZUN, Marta STROESCU[*], Gabriela ISOPENCU, Sorin Ion JINGA, Tănase DOBRE

University "Politehnica" of Bucharest, Faculty of Applied Chemistry and Materials Science, Polizu 1-3, Bucharest, 011061, Romania

Abstract
Superabsorbent polymer materials were obtained starting from bacterial cellulose (BC) using biopolymers such as: gelatin, alginate, chitosan, and carboxymethyl cellulose. These composites were characterized using Fourier transform infrared spectroscopy (FTIR), scanning electron microscopy (SEM) and swelling measurements. The highest swelling degree was obtained for the composite BC- carboxymethyl cellulose.

Keywords: Superabsorbent polymer, Bacterial cellulose, Biopolymers

1. Introduction

Superabsorbent polymer (SAP) materials are hydrogels that can absorb and retain water or aqueous solutions up to thousands of times their own dry weight. Due to their excellent hydrophilic properties and high swelling rate SAPs have been used in many applications, the most known being those in the medical area (especially as infant diapers and antibacterial materials) and also in the agricultural field to improve soil water retention and other soil properties. Furthermore, SAPs could be used also as delivery materials for drugs, fertilizers or other active substances [1-6]. SAPs could be divided into two main classes; synthetic and natural. Most of the superabsorbent materials which are currently in use are produced from acrylic acid (AA) or its salts, and acrylamide (AM) using different polymerization techniques. These cross-linked polymers have very high swelling degree (1000 g water/g SAP), but have also some drawbacks, because they are non-biodegradable and are obtained starting from petroleum. For these reasons there is a growing interest for developing new SAPs starting from biodegradable polymers such as cellulose and its derivatives, starch, chitin, and chitosan [7-9]. Bacterial cellulose (BC), which is synthesized by *Acetobacter xylinum*, is a biopolymer which consists in a nanofiber network structure which confers a lot of interesting properties like as: high water holding capacity, high crystallinity and a high tensile strength. For this reason BC has been used alone or in different combinations, chemically modified or not, for different technical and biomedical applications [10, 11]. Its use for the obtaining superabsorbents materials starts from its capacity to absorb very high quantity of water in its structure. The aim of this paper is to present the results obtained using BC and different biopolymers

[*]Corresponding author: e-mail address: marta_stroescu@yahoo.com (Marta Stroescu)

(such as alginate, chitosan, gelatin and sodium carboxymethyl cellulose) in order to enhance water holding capacity and mechanical strength of bacterial cellulose.

2. Experimental

Materials and chemicals

All chemicals are commercially available, being of analytical grade (purchased from Sigma-Aldrich) and used without further purification. All solutions were prepared using high quality deionized water.

Production and purification of bacterial cellulose membranes

Bacterial cellulose (BC) membranes were produced by *Acetobacter* sp. isolated from traditionally fermented apple vinegar in Microbiology Laboratory of Chemical and Biochemical Engineering Department of University Politehnica of Bucharest. After 7-10 days, BC pellicles were separated from medium, rinsed with deionized water and then boiled in 0.1 M NaOH at 90°C for 30 minutes to remove the attached bacterial cells from the cellulose pellicles. Finally the membranes were rinsed with deionized water until neutral pH.

Preparation of composite films BC-biopolymers

The wet BC pellicles were placed between two sheets of filter paper to remove excessive water on them. Then they were immersed in different biopolymer solutions for 2 h at room temperature. After that, the membranes were withdrawn from the vessel and the excess of the biopolymer solution was removed using filter paper. Some of the samples were also immersed in different cross-linker solutions. As biopolymers, to prepare the immersion solutions, were used: gelatin (GL), alginate (ALG), chitosan (CTS), and carboxymethyl cellulose (CMC). As cross-linker calcium chloride (only for alginate solution) and epichlorohydrin (EPC) for the other biopolymers were used. The BC-biopolymer impregnated membranes were then dried at room temperature for 48 hours. The experimental conditions for all the samples obtained are presented in Table 1.

Characterization of BC-biopolymer composites

The morphology of bacterial cellulose composites was observed using a HITACHI S-2600N scanning electron microscope operating at 15-25 kV at a magnification of 5000-60000 K. All specimens were coated with gold before SEM observation.

FTIR spectroscopy

FTIR spectrometer (Jasco FT/IR6200), equipped with a DLATGS detector and a KBr/germanium as beam splitter, was used during FTIR spectra acquisition.

The spectra were the average of 50 scans recorded at a resolution of 4 cm^{-1} in the range from 4000 to 500 cm^{-1}.

Swelling tests

Swelling tests were conducted using water as contact liquid. Composite films were dried to constant weight, cut into 2 cm × 2 cm square shapes and then immersed in distilled water for two hours. The experiments were done in triplicate. Swelling degree (SD) was obtained by measuring the initial weight (m_0) and the weight of sample in swollen state (m_τ), using equation (1):

$$SD\,(\%) = \left(m_\tau - m_0\right)/m_0 \quad (1)$$

Table 1.

The composition of the BC-biopolymer films

Sample	Biopolymer solution	Conc. (%)	Cross-linker used	Conc.
GEL1	gelatin	1.00	-	-
GEL2		10	-	-
CTS1	chitosan	0.50		
CTS2		1.00		
CTS1CL		0.50	EPC	
CTS2CL		1.00	EPC	
ALG1	alginate	0.50	-	-
ALG2		1.00	-	-
ALG1CL		0.50	$CaCl_2$	
ALG2CL		1.00	$CaCl_2$	
CMC1		0.25	-	-
CMC2		0.50	-	-
CMC3		0.75	-	-
CMC4		1.00	-	-
CMC5		0.10		
CMC6		0.20		
CMC1CL		0.25	EPC	
CMC2CL		0.50	EPC	
CMC5CL		0.10	EPC	
CMC6CL		0.20	EPC	

3. Results and discussions

The morphology of all composites was studied using SEM technique. In Fig.1 are presented only some examples for composites CTS1, CTS2CL, ALG1

and ALG1CL. The images revealed that all composites present a good compatibility between the components.

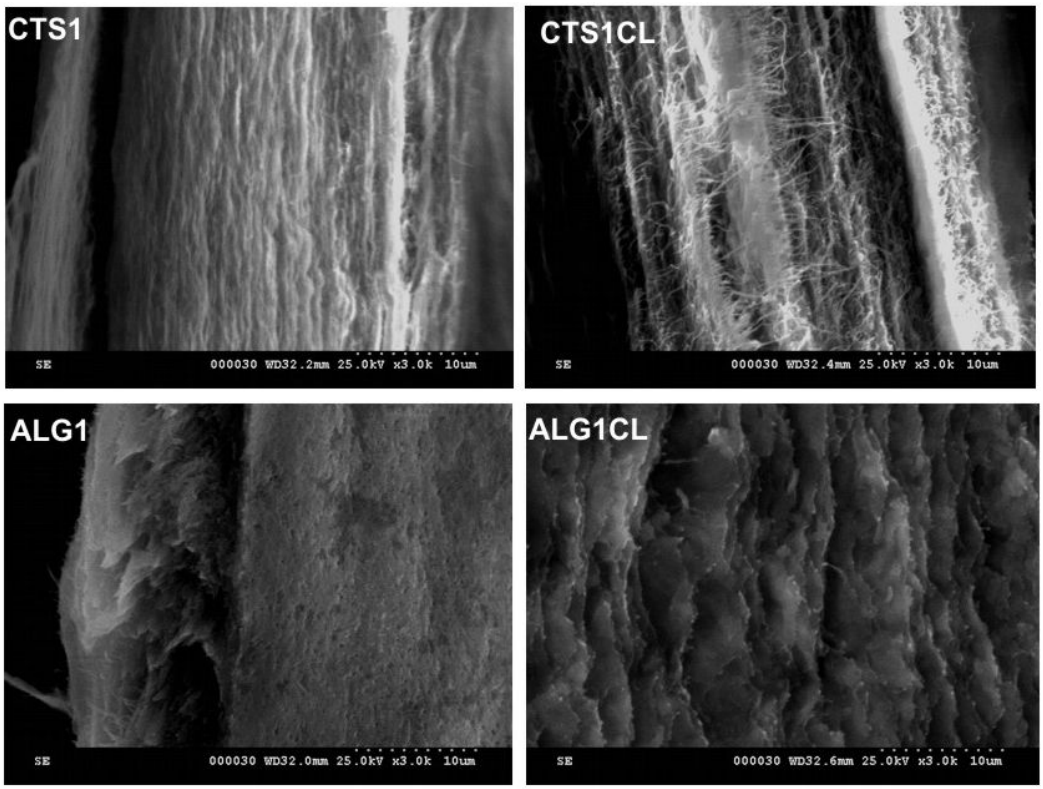

Fig.1. SEM images of composites BC-chitosan (CTS1 and CTS1CL) and BC-alginate (ALG1 and ALG1CL).

FTIR spectra analysis

Figure 2 presents FT-IR spectra of the composite BC–CMC (CMC2) and pure BC. As one could see, the first spectrum has characteristic adsorption peaks of bacterial cellulose at 3339 cm^{-1} (O-H stretching vibration), at 2917 cm^{-1} (C-H stretching vibration), at 1638 cm^{-1} (water molecules in the amorphous region) and others which are characteristic also to the backbone of cellulose. The composite BC-CMC spectrum presents only small shifts in comparison with BC spectrum. The peak due to the presence of COO^- (at around 1600−1640 cm^{-1}) is possible to be overlapped on the characteristic peak of water molecules in the amorphous region observed at 1638 cm^{-1} [12]. From the FTIR spectrum of BC-CMC composite one could also observe a good compatibility between the two components.

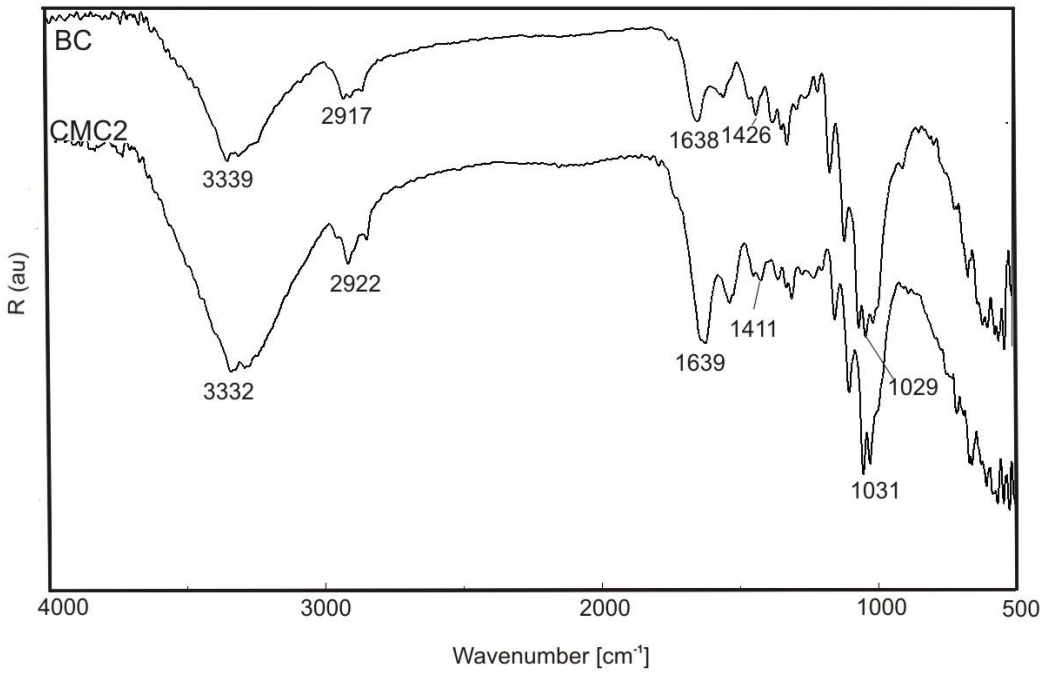

Fig.2. FTIR spectrum of the composite BC-CMC (CMC2).

Swelling studies of the BC-composites

The swelling degree for the samples BC with gelatin, alginat and chitosan, cross-linked or not, is presented in Fig.3. The highest swelling degree was obtained for BC-CTS composite CTS1 (starting immersion solution containing 0.5% CTS). In Fig.4 the evolution in time of the swelling degree of BC-CMC composites CMC1-CMC4 is depicted.

From Fig 4 one can see that the highest swelling degree was obtained for composite sample CMC1, for which the concentration of CMC in the immersion solution was 0.25%, and the lowest was obtained for the composite CMC4 obtained from the highest concentrated immersion solution (1%).

Other composites were obtained using CMC solutions, but after BC impregnation, these composites were immersed in EPC alcoholic solutions for cross-linking. SEM images of a BC-CMC composite, without cross-linker and with cross-linker, are presented in Fig 5.

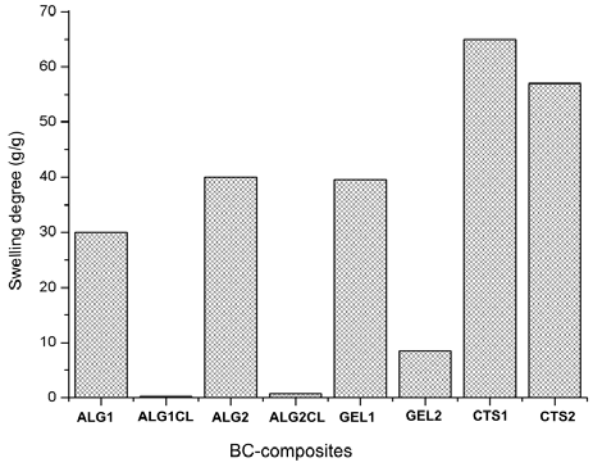

Fig 3. Swelling degree for BC-composites with alginate, gelatin and chitosan (the sample are noted as in Table 1).

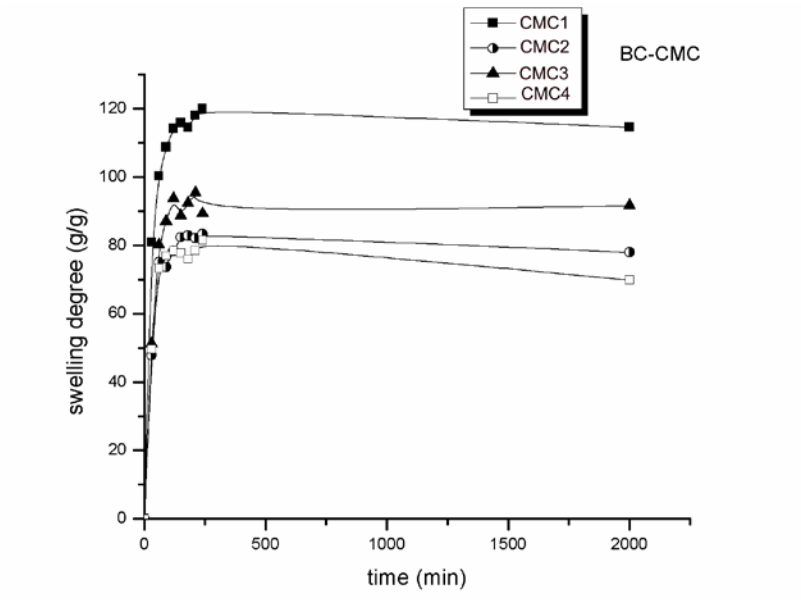

Fig.4. Swelling degree of BC-CMC composites versus time.

In Fig.5 one can see that the structure of the composite CMC2CL is more compact than the composite without cross-linker, and this is an expected result because the cross-linker must create new linkage between the components. The swelling degree is also decreasing for the cross-linked composites, because their structure is more rigid. Due to the fact that the best results were obtained for the composite CMC1, new immersion solutions were tested, containing 0.1% and

0.2% CMC. The best results for swelling degree were obtained for the composite CMC6 (immersion solution 0.2% CMC).

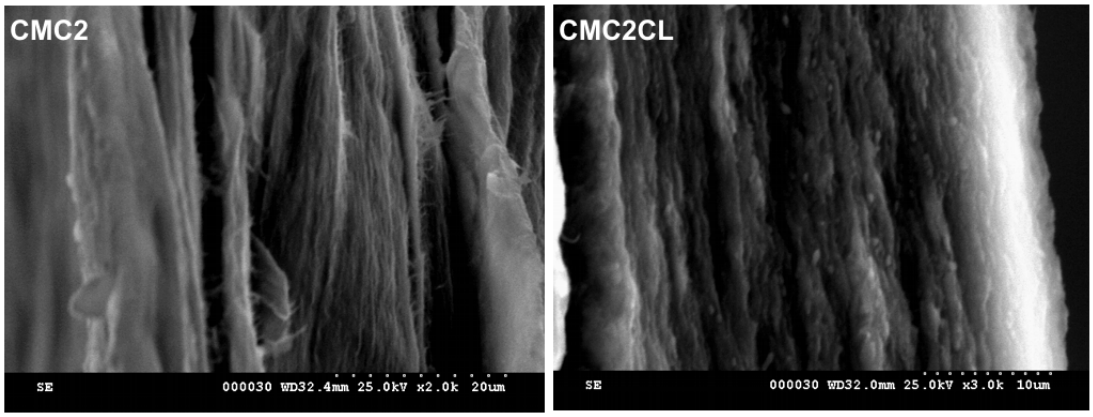

Fig.5. SEM images of composites BC-CMC (CMC2 and CMC2CL).

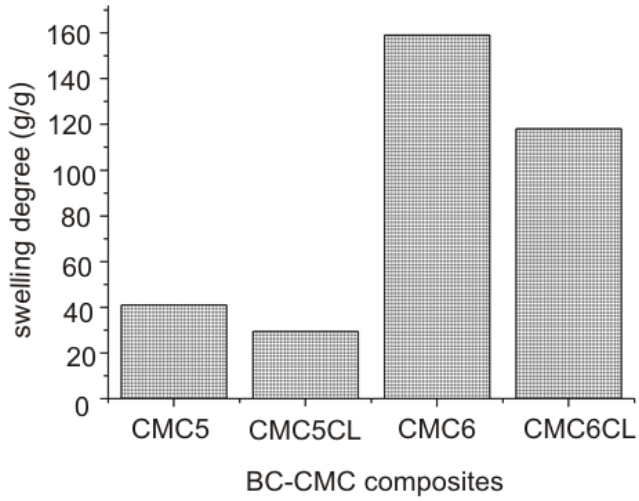

Fig.6. Sweeling degree of BC-CMC composites with and without cross-linking.

The composites CMC5 and CMC6 were modified also by immersion in the cross-linker solution of EPC. The comparison between swelling degrees for the cross-linked and not cross-linked BC-CMC composites is presented in Fig 6. As it was expected the cross-linking reduced the swelling degree of the composites.

4. **Conclusions**

New composites between BC and different biopolymers were obtained using the immersion method. The biopolymers tested for BC impregnation were gelatin,

sodium alginate, chitosan and carboxymethyl cellulose. The swelling degree of these composites was measured in order to obtain superabsorbent materials biodegradable and with agricultural uses. Some of the samples were also cross-linked with different cross-linkers. The best results were obtained for the composite CMC 6 prepared by immersion BC into a solution of 0.2% CMC. The crosslinking decreases the swelling degree, but enhances the mechanical resistance of the samples. The composites were also characterized using SEM and FTIR. A good compatibility between the components was observed.

Acknowledgement

Financial support from UEFSCDI–Romania (Research Grant–SABIOM-No. 114/2012) is gratefully acknowledged.

REFERENCES

[1] H. Ge, S. Wang, Thermal preparation of chitosan–acrylic acid superabsorbent: Optimization, characteristic and water absorbency. *Carbohydrate Polymers*, 113, (2014), 296–303.

[2] B. Ni, M. Liu, S. Lü, Multifunctional slow-release urea fertilizer from ethylcellulose and superabsorbent coated formulations. *Chemical Engineering Journal*, 155, (2009), 892–898.

[3] K. Hemvichian, A. Chanthawong, P. Suwanmala, Synthesis and characterization of superabsorbent polymer prepared by radiation-induced graft copolymerization of acrylamide onto carboxymethylcellulose for controlled release of agrochemicals. *Radiation Physics and Chemistry*, 103, (2014), 167–171.

[4] P. Schexnailder, G. Schmidt, Nanocomposite polymer hydrogels. *Colloid Polymer Science*, 287, (2009), 1–11.

[5] Yan Bao, Jianzhong Ma, Na Lib, Synthesis and swelling behaviors of sodium carboxymethyl cellulose-g-poly(AA-co-AM-co-AMPS)/MMT superabsorbent hydrogel. *Carbohydrate Polymers*, 84, (2011), 76–82.

[6] Lan Wu, Mingzhu Liu, Rui Liang, Preparation and properties of a double-coated slow-release NPK compound fertilizer with superabsorbent and water-retention. *Bioresource Technology*, 99, (2008), 547–554.

[7] C. Chang, B. Duan, J. Cai, L. Zhang, Superabsorbent hydrogels based on cellulose for smart swelling and controllable delivery, *European Polymer Journal*, 46, (2010), 92–100.

[8] H. Bidgoli, A. Zamani, M. J. Taherzadeh, Effect of carboxymethylation conditions on water binding capacity of chitosan-based superabsorbents. *Carbohydrate Research*,

[9] P. Chen, W. Zhang, W. Luo, Y. Fang, Synthesis of Superabsorbent Polymers by Irradiation and Their Applications in Agriculture. *Journal of Applied Polymer Science*, 93, (2004), 1748–1755.

[10] W. Czaja, A. Krystynowicz, S. Bielecki, R.M. Jr. Brown, Microbial cellulose the natural power to heal wounds. *Biomaterials*, 27, (2006), 145–151.

[11] W. Hu, S. Chen, J.Yang, Z. Li, H. Wang, Functionalized bacterial cellulose derivatives and nanocomposites, *Carbohydrate Polymers*, 101, (2014), 1043– 1060.

[12] H.L. Abd El-Mohdy, Radiation initiated synthesis of 2-acrylamidoglycolic acid grafted carboxymethyl cellulose as pH-sensitive hydrogel. *Plastic and Polymer Technology (PAPT)*, 3, (2014), 1–9.

EXPERIMENTAL STUDY FOR THE DESIGN OF ASPHALT MIXTURES BY RECOVERING FCC SPENT CATALYSTS

Iuliana ANDREI (IGNAT) and Claudia I. KONCSAG*

"Ovidius" University of Constanța, Department of Chemical Engineering and Technology, 900527, Constanța, Romania,

Abstract
The aim of this work was to investigate the potential use of waste catalysts from Fluid Catalytic Cracking (FCC) units as material for the asphalt mixtures. The design of an asphalt mixture consists in selecting an aggregate, filler, an asphalt binder and then their optimum combination. In this experimental study, the asphalt and the aggregate were previously selected, and the spent catalyst had to replace part of filler to a point that the characteristics of the mixture shouldn't be degraded. The grading of the mineral mix with FCC spent catalyst in different concentrations was checked. Then asphaltic mixtures were worked out with this mineral mix and the main characteristics were compared with standards: the apparent density, the water absorption, and stability. The FCC spent catalyst adding leads to the improvement of the stability and creep but should be limited at 3% wt. catalyst in the mineral aggregate, because a higher concentration will lead to worsening the grading, the water absorption capacity and creep.

Keywords: Asphalt mixture, Spent catalyst, Waste recovery

1. Introduction

Large amounts of waste accumulating from industry lead to environmental problems. Concerns of the public have obliged industrial companies to search for recovering solutions.

The spent FCC catalysts are zeolytic aggregates grading between 20-100μm, with bulk density: 0.5-0.67 g/cm^3, pore volume: 0.18-0.51 cm^3/g and specific area: 110-460 m^2/g.

Ex situ regeneration (rejuvenation), in fact a recycling option, is performed in specialized facilities at the catalyst producer [1]. But only part of the waste is regenerated nowadays.

A second option is to use the spent catalyst in constructions, in concrete formulae [2-6]. The main problem in this application is the chloride induced corrosion [7].

In search for new fillers or aggregates for asphalt mixture [8-10], the spent catalysts were taken into account. A study performed on spent catalysts of different types [11] revealed that catalysts of larger size can be used as aggregates and fine zeolytic catalysts could serve as fillers. Al Shaisi *et al* [11] recommended the use of FCC spent catalyst up to 5.5 % from the total aggregate.

*Corresponding author: email address:ckoncsag@yahoo.com (Claudia Koncsag)

In the present work, the authors checked the possibility to use FCC catalyst as filler in asphalt mixture without affecting the specifications of the mineral mixture [12] or of the final product specification [13].

2. Materials and methods

For this study, the following materials were used: aggregates, filler, FCC spent catalyst and asphalt. The aggregates are natural rocks crushed proceeding from the Piatra Roșie quarry in Cerna, Tulcea county, Romania. The aggregate grading is shown in Table 1. The filler is calcium carbonate from Murfatlar manufacture, with characteristics presented in Table 2.

Table 1.

Grading of the aggregates used in the experiment

Materials	Sort	Passing through sieve of …mm , %									
		25	16	8	4	2	1	0.63	0.20	0.10	0.063
Broken stone 16/25 mm	16 / 25	98.5	11.7								
Broken stone 8/16 mm	8 / 16	100	95.7	4.0							
Broken stone 4/8 mm	4 / 8	100	100	98.4	12.7	0.8					
Sand 0/4 mm	0 / 4	100	100	100	95.5	64.3	40.8	30.3	13.5	8.2	5.8

Table 2.

Characteristics of the filler used in the experiment

Characteristics	Standard method	Standard requirement	Experimental value	Category
Carbonates content, % wt.	SREN 196-21	Min. 90	98.5	CC90
Water content, %	SREN 1097-5	Max. 1	0.24	-
Grading, % passing through sieve: -2 mm	SREN 933-10	100	100	-
-0,125 mm		85 - 100	93.7	-
- 0,063 mm		70 - 100	91.0	-
Real density, g/cm3	SREN 1097-7	-	2.561	-
Void fraction in the dried compact filler, %	SREN 1097-4	Max. 4	0.172	-
Bulk density, g/cm3	SREN 1097-4	Max. 0,2	2.35	-
Solubility in water, %wt.	SREN 1744-1	Max.10	4.2	-
Blain trial, m^2/kg	SREN 196-6	Max.140	123	-

In Fig. 1 the grading curve of the usual mineral mixture containing 96% wt aggregate and 4% wt filler is presented.

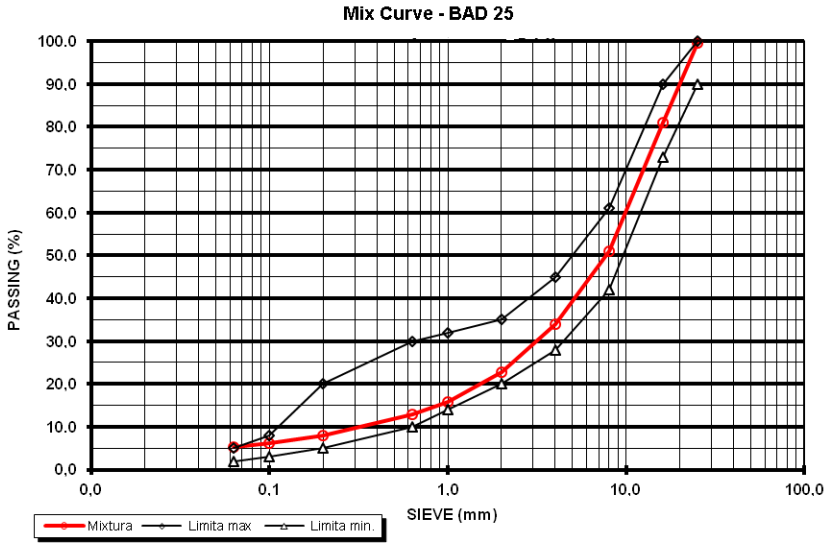

Fig.1. Grading curve for the mixture BAD 25 used in asphaltic mixtures.

The asphalt is ESSO type from Italy with characteristics presented in Table 3.
The FCC spent catalyst proceeding from an oil refinery has the characteristics presented in Table 4 and will replace a part of the filler.

Table 3.

Characteristics of the asphalt ESSO type 50-70$^{1}/_{10mm}$

Characteristics	Unit	Standard 12591/2009	Experimental results
Penetration at 25 ºC	1/10mm	50 - 70	58.8
Softening point	ºC	46 - 54	48.5
Ductility at 25 ºC	Cm	Min.100	>150
Frass breaking point	ºC	Max. -8	-8
Density la 20 ºC	g/cm^3	-	1.0475
Density la 15 ºC	g/cm^3	-	1.051
Weight loss at 163 ºC	%	≤ 0.5	0.253

Table 4.

Characteristics of the FCC spent catalyst

Characteristics	Unit	Standard SR EN 13043	Experimental results
Grading,-dimensions under: 0.063 mm 0.020 mm 0.010 mm	%	 100 80....100 70...100	 99.2 95.6 91.1
Moisture	% wt	max 1,0	3.5
Apparent density	g/cm^3	-	0.9

In this study, the BAD 25 mixture was modified by replacing 25 %, 50%, 75% and 100 % respectively of filler with the FCC spent catalyst. The new mineral mixtures grading was then performed. Then, a ratio of 4.2 % asphalt will be used, for all the asphalt mixtures in this experiment. This ratio was previously determined as an optimum for the initial mineral mixture described in Fig. 1. For preparing the asphalt mixture, the mineral materials were warmed up to 140ºC, the aggregate and filler were intimately mixed to form an homogeneous mass and then the asphalt warmed up to 165^{o}C was added. The mixture was blended until the complete wetting of mineral mixture. From this asphalt mixture, test specimens were prepared for the Marshall stability test, creep, apparent density and water absorption tests. The pile Marshall (Fig. 2) was used to produce specimens.

Fig.2. The pile driver Marshall for the manufacture of test specimens.

The specimens were kept at 20^{o}C for 24 hours before performing tests. Apparent density and water absorption determinations were performed following the standards AND 605/2013 and SR EN 13108 /2009.
For stability and creep, the tests specimens were kept at 60^{o}C for 1-3 h, depending on the specimen's thickness. The determinations were performed with the Marshall press, following the standard AND 605/2013 procedure.
For each determination of apparent density, water absorption, creep and stability, three specimens were manufactured and the experimental determination was made in triplicates.

3. Results and discussions

By replacing 25%, 50%, 75% and 100% respectively of filler with the FCC spent catalyst; this means 1%, 2% 3% and 4% wt. respectively in the BAD 25 mixture. New aggregates were obtained with grading framed between the minimum and maximum limits, as seen in Table 5.
The particles size is framed inside limits because FCC catalyst has a particle size distribution similar to the original filler. So, the differences between the new aggregates and the original mixture grading are very small and the mixture characteristics are not damaged by adding the catalyst. Also, there are some differences among all these mixtures due to their manufacture: first, the filler and the FCC catalyst are mixed and then this mixture is mixed with the rock. Small differences at the weighing are normal.

Table 5.

The aggregate grading of mixture BAD 25, replaced with FCC spent catalyst in proportion of 1%, 2%, 3%, and 4% wt.

Sieve, mm	Limits, %	Particle size distribution, for the mixture BAD25	Particle size distribution, for 1% wt. FCC catalyst	Particle size distribution, for 2% wt. FCC catalyst	Particle size distribution, for 3% wt. FCC catalyst	Particle size distribution, for 4% wt. FCC catalyst
25	90-100	99.7	99.7	99.8	99.8	99.8
16	73-90	84.6	84.5	84.6	84.8	84.7
8	42-61	55.1	54.9	55.0	55.0	55.0
4	28-45	39.9	40.9	41.8	41.8	41.8
2	20-35	28.2	28.2	28.3	28.6	28.5
1	14-32	18.8	18.9	19.5	19.3	19.5
0.63	10-30	14.8	14.8	15.7	15.7	15.5
0.2	5-20	8.9	8.9	9.1	9.1	9.1
0.1	3-8	6.2	6.1	6.5	6.7	6.6
0.063	2-5	5.3	4.8	4.8	4.3	3.7

Further, for every set of trials, the asphalt specimens manufactured with the original mineral mixture were tested in parallel with the specimens made with spent catalyst. This ensured exactly the same experimental conditions for a good comparison of results.
The average characteristics of the asphalt mixture made with the original BAD 25 mineral mixture were the following:
-apparent density: 2.352 ± 0.028 g/cm^3
-water absorption: 4.4 ± 0.5 % wt
-stability: 8.705 ± 0.820 kN
-creep: 3.64 ± 0.83 mm
-stability/creep ratio: 2.39 ± 0.44 kN/mm

As seen in Fig. 3, adding FCC spent catalyst will increase the apparent density of the aggregate, this being a positive influence, because the original BAD 25 has the density slightly over the minimum (an average of 2.352 comparing with min.2.250 imposed by the standard AND 605/2013). The increasing of the aggregate's apparent density with the percentage of FCC catalyst added (despite of its low apparent density) can be explained by the high void fraction and small particles of the FCC catalyst; this means that the aggregate particles arrangement will be more compact after mixing with FCC catalyst.

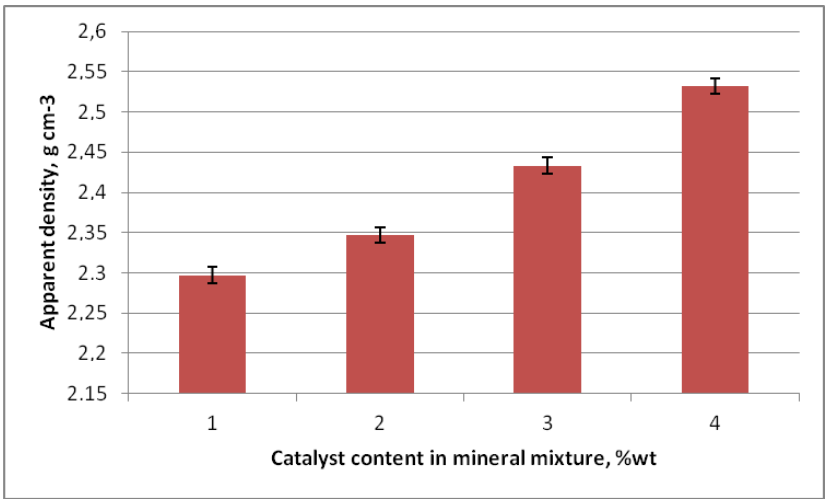

Fig.3. The influence of added FCC catalyst on the apparent density of the mineral mixture.

The effect of the catalyst replacing filler in the asphalt mixture can be seen in Fig. 4. Replacement of the filler with FCC spent catalyst should be limited to max.75% wt. (max. 3% wt. in the mineral mixture), because adding more would

lead to trespass the limit of water absorbed in the asphalt mixture: at 4% wt FCC spent catalyst in the mineral mixture, the average water absorption was 7% wt. comparing with max. 6% imposed by the standard AND 605/2013.

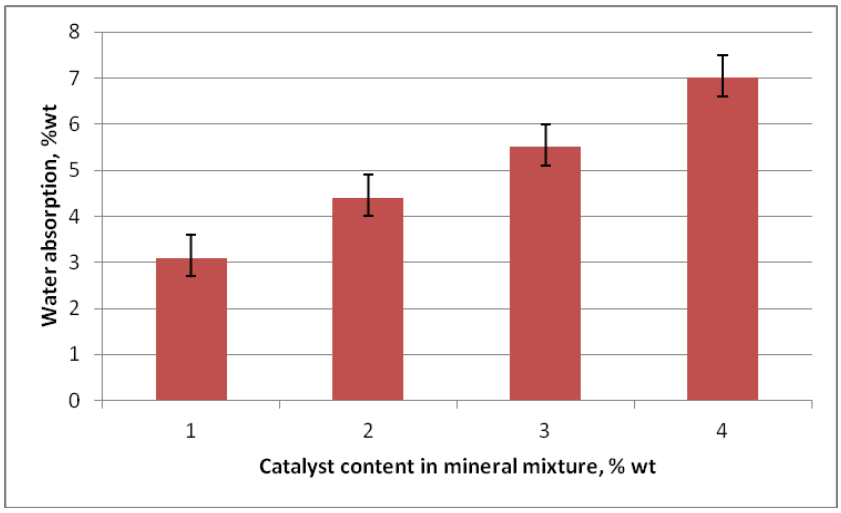

Fig.4. The influence of added FCC catalyst on the water absorption in the asphalt mixture.

The tests for the stability and creep show how the asphalt carpet acts at high traffic loads. The results of these tests are presented in Fig. 5 and Fig. 6.

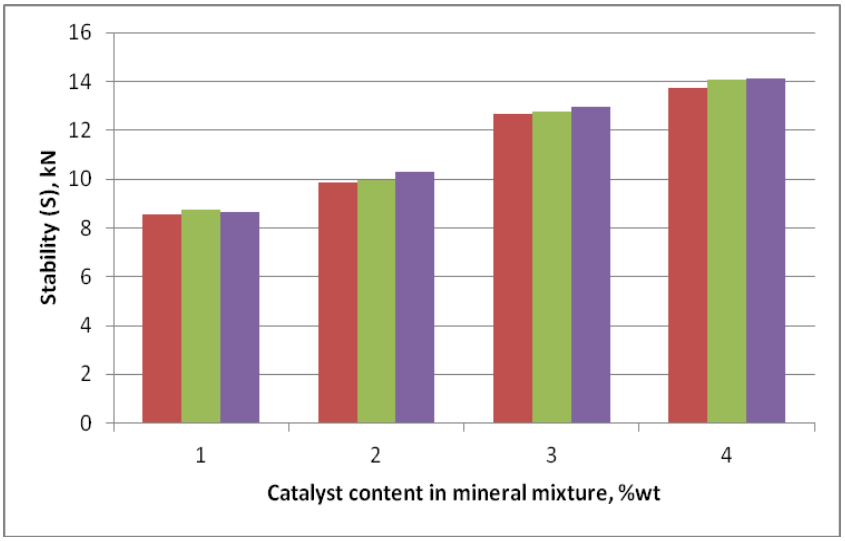

Fig.5. The influence of added FCC catalyst on the stability of the asphalt mixture.

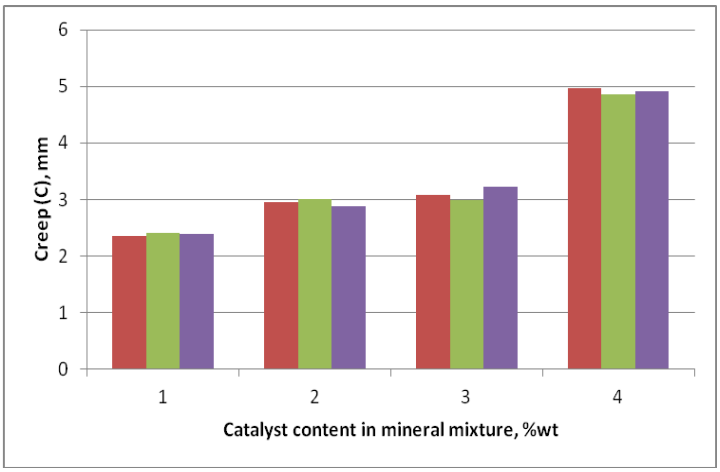

Fig.6. The influence of added FCC catalyst on the creep of the asphalt mixture.

As seen in Fig. 5 and Fig. 6, adding FCC spent catalyst increases stability and creep. Adding FCC spent catalyst up to 3% wt. is not harmful but at 4% wt., the stability and the creep are over the maximum values recommended by the standard: max. 13 kN for stability and max. 3.5 mm for creep. Since higher stability is desirable, the increased creep will affect the quality of the asphalt carpet.

Replacing the filler with FCC spent catalyst in the asphalt mixture modifies the stability-to-creep (S/C) ratio, as seen in Fig. 7, but the variation is not predictable. However, the replacement in any proportion keeps the S/C ratio between the standardized limits: 1-6.

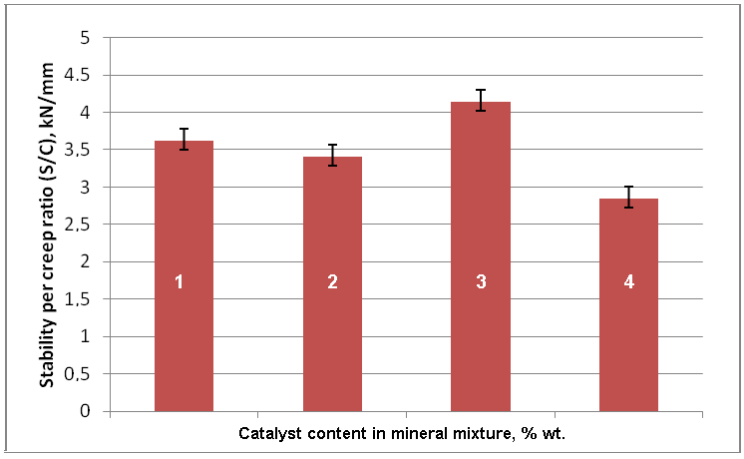

Fig.7. The influence of adding FCC catalyst to the asphalt mixture on the stability-to-creep ratio.

4. Conclusions

Use of the FCC catalyst as replacement for the filler in the mineral mixture BAD-25 for asphalt coatings is an option for the management of the spent catalysts proceeding from the crude oil refineries.

Replacing up to 75% of the filler with FCC spent catalyst will improve the apparent density of the mineral mixture and the stability of asphalt carpet, also keeping the water absorption, creep and stability-to-creep ratio in the standardized limits. This represents 3 % wt. of the mineral mixture and 2.8 % wt. of the asphalt mixture.

Total replacement of the filler with FCC spent catalyst is not recommended, because this can increase the water absorption in the mineral mixture and by consequence, in the asphalt carpet, with undesirable effect during frosty weather. Also, the total replacement of the filler with FCC spent catalyst can increase too much the creeping and by consequence, the behavior of the asphalt carpet at high traffic loads.

Further studies should enquire the use of FCC spent catalysts together with other spent catalysts in the manufacture of the asphalt mixture.

REFERENCES

[1] Marafi M., Stanislaus A., Kam E., A preliminary process design and economic assessment of a catalyst rejuvenation process for waste disposal of refinery spent catalysts, *Journal of Environmental Management*,86, (2008), 665-681.

[2] Su N., Chen Z.-H, Fang H.-Y., Reuse of spent catalyst as fine aggregate in cement mortar, *Cement and Concrete Composites*, 23(1), (2001), 111–118.

[3] Su N., Fang H.-Y., Chen Z.-H., Liu F.-Sh., Reuse of waste catalysts from petrochemical industries for cement substitution, *Cement and Concrete Research*, 30(11), (2000), 1773–1783.

[4] Al-Jabri K., Baawain M., Taha R.S, Al-Kamyani Z., Al-Shamsi K., Ishtieh A., Potential use of FCC spent catalyst as partial replacement of cement or sand in cement mortars, *Construction and Building Materials*, 39, (2013), 77–81.

[5] Payá J., Monzó J., Borrachero M.V., Fluid catalytic cracking catalyst residue (FC3R): An excellent mineral by-product for improving early-strength development of cement mixtures, *Cement and Concrete Research*, 29 (11), (1999), 1772-1779.

[6] Payá J., Monzó J., Borrachero M.V., Velasquez M., Cement equivalence factor evaluations for fluid catalytic cracking catalyst residue, *Cement & Concrete Composites*, 39, (2013), 12-17.

[7] Morozov Y., Castela A.S., Dias A.P.S., Montemor M.F., Chloride induced corrosion behaviour of reinforced steel in spent FCC catalyst modified mortars, *Cement and Concrete Research*, 47, (2013), 1-7.

[8] Meininger R.C., Effects of Aggregates and Mineral Fillers on Asphalt Mixture Performance, ASTM International Conference, STP 1147, Philadelphia, 1993.

[9] Waller H. F., Use of Waste Materials in Hot-Mix Asphalt, ASTM International Conference, STP 1193, Philadelphia, 1993, http://www.astm.org/DIGITAL_LIBRARY/STP/SOURCE_PAGES/STP1193.htm
[10] Damiean I.M., Fillers used for realizing the asphalt mixtures in Romania, Machines, Technologies, *Materials Journal, Bulgaria*, http://mech-ing.com/journal/papers/51.pdf
[11] Al-Shamsi K., Al-Jabri K., Baawain M., Taha R., Utilising waste spent catalyst in asphalt mixtures, *Procedia- Social and Behavioural Sciences, Elsevier*, 53, (2012), 326-334.
[12] *** SR EN 13108/2009 – Mixturi asfaltice. Specificatii pentru materiale (Asphalt mixtures. Materials specifications)
[13] *** AND 605/2013 – Normativ mixturi asfaltice (Standard for asphalt mixtures)

SOL-GEL SYNTHESIS OF NANOSIZED $LiMn_2O_4$ PARTICLES AND THEIR ELECTROCHEMICAL CHARACTERIZATION IN AQUEOUS ELECTROLYTE

Alexandru-Horaţiu MARINCAŞ, Firuţa GOGA*, Sorin-Aurel DORNEANU, Petru ILEA

Babeş-Bolyai University, Faculty of Chemistry and Chemical Engineering,
Department of Chemical Engineering, 11 Arany Janos, 400028 Cluj Napoca, Romania

Abstract
Lithium-ions batteries are widely used in many domains, from small dimensions gadgets to electric vehicles. For this type of batteries, an essential problem is strictly related to the achievement of an electrodic structure that will allow the reversible insertion/extraction of Li^+ ions. In this context, $LiMn_2O_4$ can be a promising material. In the present paper, nanosized $LiMn_2O_4$ particles were synthesized and physically characterized and the obtained powder was embedded in carbon-paste electrodes and electrochemical characterized by cyclic voltammetry. The obtained results prove that the synthesized powder present a spinel structure and a reversible redox activity. The best electrochemical behaviour was recorded for a mass ratio between spinel and graphite powder of 1:2.

Keywords: $LiMn_2O_4$, Spinel, Sol-gel, Cyclic voltammetry

1. Introduction

Recently, new power sources were designed and studied to be used in the last high-end devices. Lithium-ion batteries (LIB) are effective power sources for many portable devices (cell phones, laptops, digital cameras, etc.) but, in the last period of time, they were also used for electric vehicles and UPS [1, 2].
New generations of LIB match the requirements of the modern devices. Thus, LIBs exhibit better characteristics than conventional batteries: improved life cycle, higher energy density and enhanced dimensions [3].
Nowadays, most of LIBs use $LiCoO_2$ as cathode materials, but $LiMn_2O_4$ becomes as a promising material for LIBs cathodes. The $LiMn_2O_4$ exhibit numerous advantages over $LiCoO_2$ cathode material: non-toxicity, low manufacturing cost, environmental friendly, easy preparation [4, 5]. Unfortunately, $LiMn_2O_4$ presents a charge capacity fading and a poor cycle stability that can be attributed to the decomposition of the electrolyte solution during charging-discharging process [5], Jahn-Teller distortion and oxygen vacancies formation during slow dissolution of manganese in electrolyte [2]. To avoid capacity loss through Jahn-Teller distortion,

*Corresponding author: E-mail address: fgoga@chem.ubbcluj.ro (Firuta Goga)

the pure spinel can be doped with several ions such as: Cr, Fe, Zn, Cu, Ga, Co, Ni and Ti [8].
Several processes were developed to synthesize $LiMn_2O_4$. Although the main process to obtain $LiMn_2O_4$ spinel is based on the solid-state reaction [5], other methods have gained attention in the last years: sol-gel [6,7], co-precipitation [8], hydrothermal reactions [9], reverse micro-emulsion [10], Pecchini process [11], spray-drying process [12]. The sol-gel method is a promising synthesis technique to obtain nanoparticles with controlled dimensions and uniformly distributed, at relative low calcination temperatures [1].
In this paper, we describe the synthesis of $LiMn_2O_4$ nanoparticles via the sol-gel method followed by calcination at 600°C for a relative short time. The obtained spinel powder was electrochemically characterized by cyclic voltammetry in aqueous electrolyte.

2. Experimental

2.1. Reagents

The samples was prepared by the sol-gel method using solid reagents Li_2CO_3, $Mn(CH_3COO)_2 \cdot 4H_2O$, sucrose and pectin and 63% HNO_3 solution (all of analytical grade). The reagents were used without any further purification. For the electrochemical measurements, a 5M $LiNO_3$ solution was prepared using solid $LiNO_3$ of analytical grade dissolved in distillate water.

2.2. Sol-gel synthesis

The Li_2CO_3 was dissolved in HNO_3, while the manganese acetate and sucrose were dissolved in distilled water. All these three solutions were mixed and stirred under magnetic agitation, maintaining an acidic pH (~2). Further, the pectin was added and the resulting solution was stirred and heated at 65°C, until an uncoloured sol is formed. In the next step, the sol was dried for 48 h in order to eliminate all the existing water and the gel was obtained. Two gel samples, P1 and P2, were prepared using different drying temperatures: 200 and 150°C, respectively. Finally, the dry gel samples were calcinated at 600°C for 2h, in air atmosphere, resulting the $LiMn_2O_4$ spinel nanoparticles.

2.3. Working electrodes preparation

For the electrochemical measurements, several carbon-paste working electrodes were prepared. The modified carbon-paste were prepared by mixing the synthesized spinel powder from sample P1 with graphite powder, in different

mass ratio (1:1, 1:2, 1:4), and paraffin oil as binder. In order to obtain the modified carbon-paste electrode, the powders were milled with the binder and the mixture was packed into a plastic cylindrical tube, connected to a stainless steel rod. Supplementary, for reference data, a blank carbon-paste electrode was prepared using only graphite and paraffin oil.

2.4. Equipments

The calcinations processes were realized using a programmable oven of Kaloria Denkal K8/1100 type. For the thermo-gravimetric measurements, a thermo-analyser model STD Q600 was used. The X-ray spectra were obtained using a Shimadzu XRD 600 RX diffractometer. The granulometric analysis was performed using a Counter Coutler Shimadzu SALD-7101.
For the electrochemical measurements, a computer controlled multi-potentiostat model DXC-240 and LabView 8.5 applications were used. A 50 mL glass beaker was used as electrochemical cell. A Pt wire and an $Ag/AgCl/KCl_{SAT}$ electrode were used as counter-electrode and reference electrode, respectively. All the reported potentials are referred to this reference electrode.

3. Results and discussions

3.1. Thermogravimetric analysis

The thermo-gravimetric analysis (TGA) curves recorded for the sample P1 of $LiMn_2O_4$ are presented in Fig. 1. As it can be observed in Fig. 1, the TGA curve of $LiMn_2O_4$ shows an endothermic process with a small amount of mass loss (about 7%), until the temperature of 211°C. This process is characteristic for the elimination of physical absorbed water, in the precursor mixture. Between 250-456°C, are three exothermic processes, with important mass loss. The last process exhibit an important mass loss, around 50%, which is characteristic for calcination of organic compounds and liberation of gaseous compounds (especially CO_2). After 456°C, no mass changes were observed. The TGA curve is similar to others TGA curves from literature [8]. For the formation of crystalline structure, a temperature of 600°C was chosen to calcinate the dried gel.

3.2. X-ray diffraction

The XRD pattern for $LiMn_2O_4$ synthesized via sol-gel method, using different drying temperature for the obtained gel, is shown in Fig. 2. The recorded peaks for the P1 sample are higher and better defined that for the P2 sample, proving a

better crystallinity and purity of the first sample. For this reason, the P1 sample will be used for further analyses and measurements.

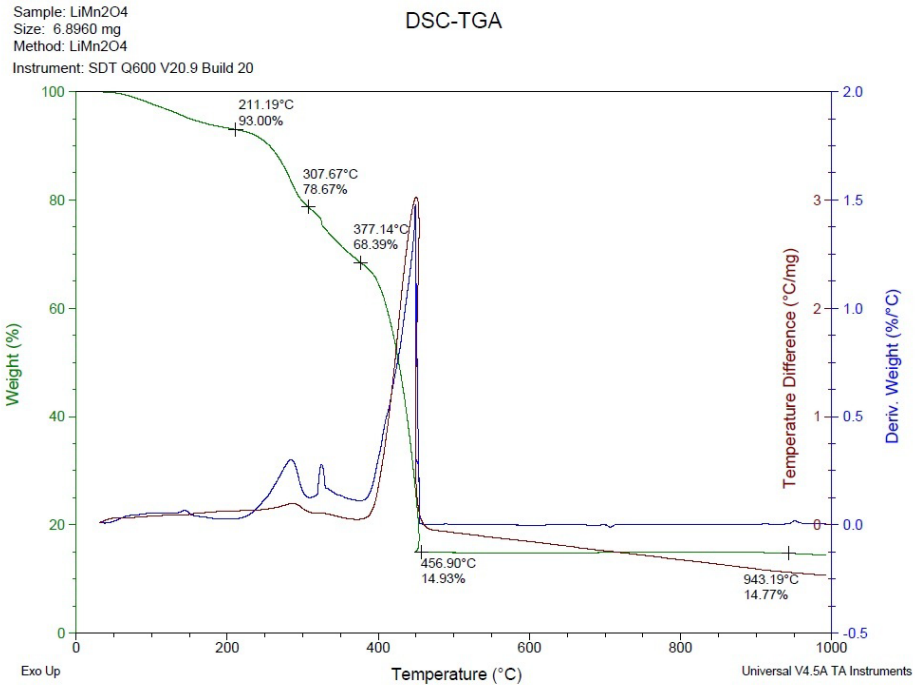

Fig. 1. The TGA curves recorded for the $LiMn_2O_4$ P1sample.

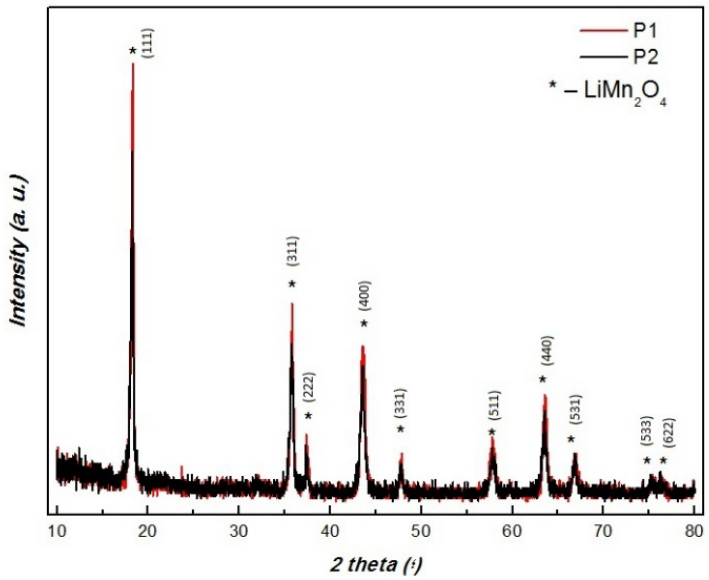

Fig. 2. XRD pattern for the two samples (P1 and P2) of synthesized spinel.

3.3. Granulometry

To determine the average diameter of the $LiMn_2O_4$ nanoparticles synthesized, the granulometric analysis was used. The size distribution of the particles is show in Fig.3. From the diagram, a uniform size distribution can be observed and most of the particles have 20 nm in size. The structural plans corresponding to the peaks 2 θ, observed in Fig. 2, can be indexed to a spinel with a cubic structure, characteristic to the 227 spatial group (*Fd3m*).

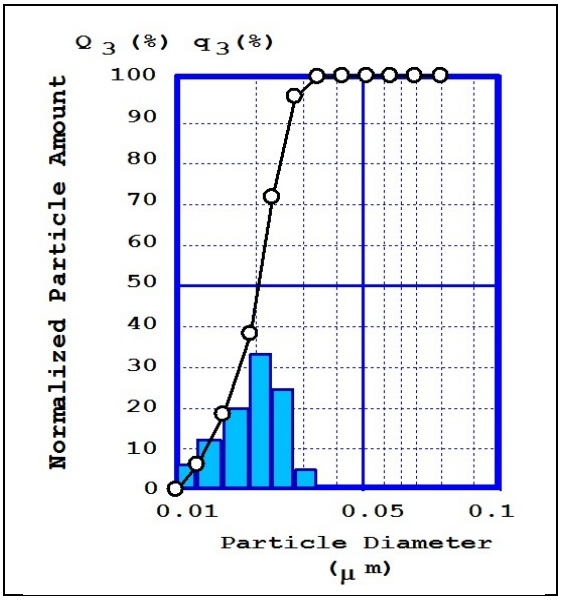

Fig. 3. Granulometric curve. The bars represent percentage size distribution and the circles represent the percentage of the analysed sample.

3.4. Electrochemical characterization by cyclic voltammetry

In order to evaluate the possibility to use synthesized spinel as active material for LIB's cathode, it was electrochemical characterized by cyclic voltammetry. According to the literature, the explored potential range was established between 0.6 and 1.4 V where $LiMn_2O_4$ exhibit redox activity. The obtained voltammograms, presented in Figure 5, where recorded in 5 M $LiNO_3$ solution using an unmodified and 3 modified carbon-paste electrodes containing different amounts of spinel powder. In order to evaluate the reversibility of the redox process, the measurements where performed at different values of the scan rate, ranged between 0.04 and 0.5 mV/s. As it can be seen from Fig. 4 A-C, for all three modified electrodes tested, two different redox couples can be observed, assigned as A1/C1 and A2/C2 (see Figure 4 D). This behaviour indicates that electrochemical process of insertion/extraction of Li^+ ions include two steps, described by the following reactions [13]**:**

$$LiMn_2O_4 \leftrightarrow (1/2)Li^+ + (1/2)e^- + Li_{0,5}Mn_2O_4\ ;$$

and

$$Li_{0,5}Mn_2O_4 \leftrightarrow (1/2)Li^+ + (1/2)e^- + 2\ \lambda - MnO_2.$$

The first reaction corresponds to A1/C1 peaks and the second reaction to A2/C2 peaks, respectively.

During the anodic scan, the Li^+ ions are extracted from two different positions of the spinel layer generating two anodic peaks (A1 and A2). Similarly, during the cathodic scan, the Li^+ ions are inserted in the same positions generating the corresponding cathodic peaks (C1 and C2).

Concerning the influence of the mass ratio between spinel and graphite powders in the carbon-paste electrodes (see Figure 4D), we concluded that the maximum redox activity was obtained for the 1:2 value. This behaviour can be attributed to the fact that, for a mass ratio of 1:4, the quantity of spinel is too small and for a value of 1:1, the electric conductivity of the electrode material decreases significantly.

From another point of view Fig. 4 A-C show that the amplitude of current peaks increase with increase of the scan rate. Moreover, as in the example presented in Fig. 5, a linear correlation can be observed between the peak currents and the scan rate.

For the example presented in Fig. 5, the values of the correlation coefficient (R) ranged between 0.9934 and 0.9993, proving a very good linear correlation between peak currents and scan rate. As described in the literature [10, 14], this behaviour is characteristics for the reversible redox species bounded to the electrode surface.

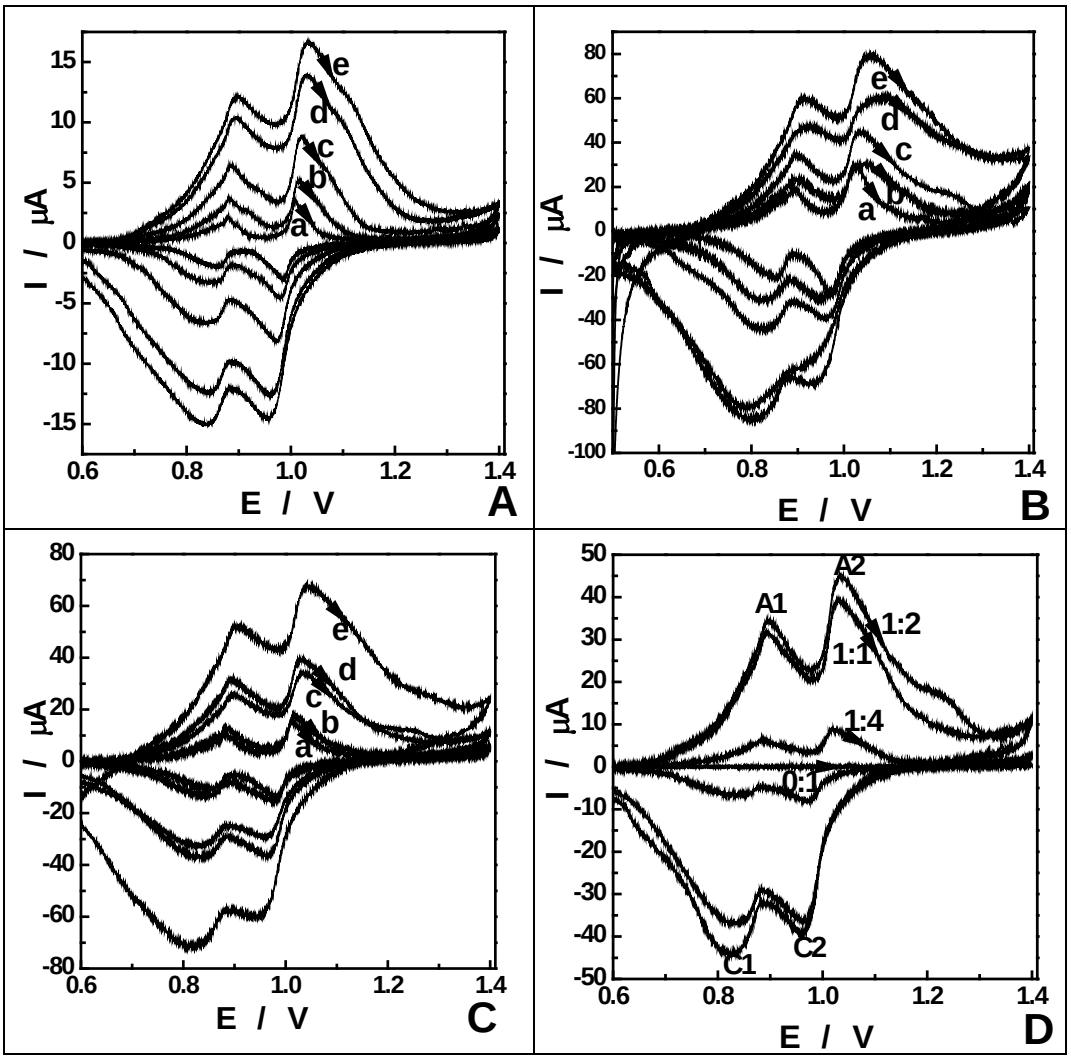

Fig. 4. Cyclic voltammograms recorded in 5 M $LiNO_3$ on modified carbon-paste electrode prepared at mass ratio between spinel and graphite of 1:4 (A), 1:2 (B) and 1:1 (C), at different scan rates of 0.04 mV/s (a), 0.1 mV/s (b), 0.2 mV/s (c), 0.4 mV/s (d) and 0.5 mV/s (e); (D) Comparison between voltammograms recorded at 0.2 mV/s for different mass ratio between spinel and graphite. The arrows indicate the scan direction.

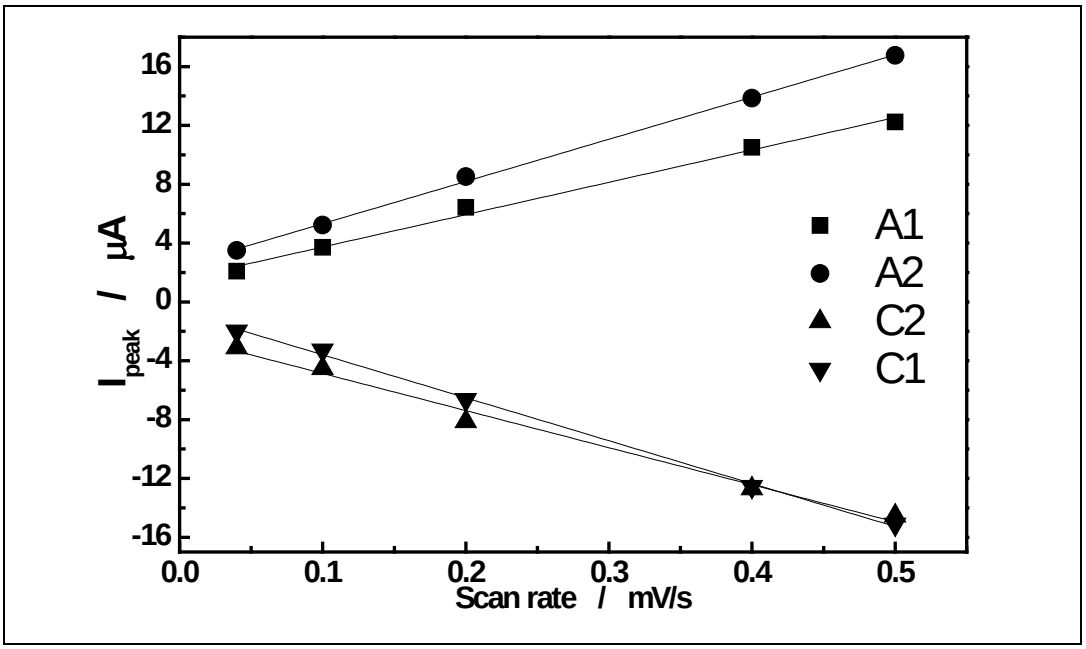

Fig. 5. Example of peak currents dependency vs. scan rate corresponding to cyclic voltammograms from Fig. 4A.

4. Conclusions

Nanosized powder of $LiMn_2O_4$ spinel was synthesized by sol-gel method followed by a relative short calcination at 600°C. The obtained material was characterized by TGA, XRD and granulometric analysis.

Based on the thermogravimetric analysis, a calcination temperature of 600°C was chosen because at this value the $LiMn_2O_4$ spinel can be obtained.

From XRD, can be observed that the spinel structure was formed in both samples, but the sample (P1 sample) dried at higher temperature (200°C) has better crystallinity than the other sample (P2 sample) dried at a lower temperature (150°C).The granulometric curve shows a uniform size distribution and most of the particles have 20 nm in size.

The electrochemical behaviour was evaluated by cyclic voltammetry performed in 5M $LiNO_3$ aqueous solution. The obtained results indicate that the synthesized material present a redox activity, characterized by two reversible redox couples and the optimal mass ratio between spinel and graphite was 1:2. This electrochemical behaviour proves that our synthesized nanosized powder of $LiMn_2O_4$ spinel is a proper material for LIBs.

REFERENCES

[1] Rajesh Y.B.R.D., Dubey R.S., Sol-Gel Synthesis and Characterization of Nanocrystalline Spinel $LiMn_2O_4$ For Battery Applications, *Nanoscience and Nanoengineering*, 1 (3), (2013), 139-141.

[2] Liu Q., Wang S., Tan H., Yang Z., Zeng J.**,** Preparation and Doping Mode of Doped $LiMn_2O_4$ for Li-Ion Batteries, *Energies* 6, (2013), 1718-1730.

[3] Scrosati B., Abraham K.M., van Schalkwijk W., Hassoun J., Lithium Batteries, *Advanced Technologies and Applications*, Wiley, 2013.

[4] Zheng C.H., Liu X., Wu Z.-F., Chen Z.-D., Fang D.L., Excellent electrochemical performance of porous nanoparticles-constructed granule $LiMn_2O_4$ derived from a highly reactive Mn_3O_4, *Electrochimica Acta*, 111, (2013), 192-199.

[5] Wang H.-E., Qiana D., Lua Z., Li Y., Synthesis and electrochemical properties of $LiMn_2O_4$ and $LiCoO_2$-coated $LiMn_2O_4$ cathode materials, *Journal of Alloys and Compounds*, 517, (2012), 186-191.

[6] Kumar V. G., Gnanaraj J. S., Ben-David S., Pickup D. M., van-Eck E. R. H., Gedanken A., Aurbach D., An aqueous reduction method to synthesize spinel-$LiMn_2O_4$ nanoparticles as a cathode material for rechargeable lithium-ion batteries, *Chemistry of Materials***,** 15, (2003), 4211-4216.

[7] Seyedahmadian M., Houshyarazar S., Amirshaghaghi A., Synthesis and characterization of nanosized of spinel $LiMn_2O_4$ via sol-gel and freeze drying methods, *Bullettin of the Korean Chemical Society*, 34 (2), (2013) 622-628.

[8] Thirunakaran R., Ravikumar R., Gopukumar S., Sivashanmugam A., Electrochemical evaluation of dual-doped $LiMn_2O_4$ spinels synthesized via co-precipitation method as cathode material for lithium rechargeable batteries, *Journal of Alloys and Compounds*, 556, (2013), 266-273.

[9] Kim D. K., Muralidharan P., Lee H.-W., Ruffo R., Yang Y., Chan C. K., Peng H., Huggins R. A., Cui Y., Spinel $LiMn_2O_4$ nanorods as lithium ion battery cathodes, *Nano Letters*, 8 (11), (2008), 3948-3952.

[10] Nikkar Sinha N., Ragupathy P., Vasan H.N., Munichandraiah N., Electrochemical characterization of submicron size particles of $LiMn_2O_4$ in Aqueous Electrolytes, *International Journal of Electrochemical Science*, 3, (2013), 691-710.

[11] Hung F.-Y., Lui T.-S., Chen L.-H., Liao H.-C., Electrochemical Characteristics of $LiMn_2O_4$ (Li/Ni) Cathode Materials, *Materials Transactions*, 47 (11), (2006), 2759-2764.

[12] Wan C., Cheng M., Wu D., Synthesis of spherical spinel $LiMn_2O_4$ with commercial manganese carbonate, *Powder Technology*, 210, (2011), 47-51.

[13] Bao S.-J., Liang Y.-Y., Li H.-L., Synthesis and electrochemical properties of $LiMn_2O_4$ by microwave-assisted sol–gel method, *Material Letters*, 59, (2005), 3761-3765.

[14] Nakayama N., Nozawa T., Iriyama Y., Abe T., Ogumi Z., Kikuchi K., Interfacial lithium-ion transfer at the $LiMn_2O_4$ thin film electrode/aqueous solution interface, *Journal of Power Sources*, 174, (2007), 695-700.

CONSIDERATIONS REGARDING A NOVEL COEFFICIENT FOR ELECTROCHEMICAL IMPEDANCE SPECTROSCOPY DATA VALIDATION

Ioana-Alina CIOBOTARU and Danut-Ionel VAIREANU*

Department of Inorganic Chemistry, Physical Chemistry and Electrochemistry,
University Politehnica of Bucharest, Faculty of Applied Chemistry and Materials,
1-3 Polizu street, Bucharest, 011061, Romania

Abstract
A novel coefficient is proposed that may be useful in deciding which pairs of data one should choose between two or more sets of correlated data, having different degrees of freedom, associated to a particular process or phenomenon. An application example is given with respect to the fitting of the electrochemical impedance spectroscopy data as Nyquist plots and their associated correlation coefficients; however, this coefficient is in no way restricted to this particular application and may be used, as well, in a large number of other applications.

Keywords: Electrochemical impedance spectroscopy, Validation coefficient, Nyquist plots, Correlation, Regression coefficient

1. Introduction

Correlation analysis has become one of the most used methods in reporting a large number of data associated to a particular process or phenomenon, but very little effort is put in including in the associated report the limitations and interpretation of such method. [1-9]. The correlation coefficient, also known as the Pearson product-moment correlation coefficient, *r*, the cornerstone of the correlation analysis, is an indicator of the dependence or correlation between two variables, an independent one and a dependent one [1-12]. The letter "*r*" is reserved for Pearson's correlation coefficient applied to a sample rather than to a population, where "ρ" is used instead of "*r*" [3-8].

Except for the experimental cases when one may clearly indicate the independent variable as well as the dependent variable or for other well defined cases, the correlation coefficient does not discriminate between the variables [4-6,8]. It can be very well calculated in cases when the places of variables are swapped, and should not be taken as an indicator of a causal link existing between the variables, but rather as an indicator of the degree of association or the measure of the strength of the relationship between the variables [4,6,8].

*Corresponding author. Email address: di_vaireanu@yahoo.co.uk (D.I. Vaireanu)

Although initially it was used to establish the linear correlation [1], it can be applied to a large range of non-linear dependencies as well (after a previous linearization, *e.g.* logarithmic, exponential, logistic curves, or without linearization, *e.g.* circular regression), yielding values between +1 and −1 inclusive [3,4,8-11]. Depending of the tendency of the dependent variable to respond to an increase in the independent variable, one may have a positive correlation, when the dependent variable increases with increasing independent variable, a negative correlation, when the dependent variable decreases with increasing independent variable or no correlation when increasing the independent variable has little or no effect (neither increasing, nor decreasing) on the dependent variable [4,6-8]. One should mention here two important features of the correlation coefficient [6-8]:

- if any or both variables are converted to a different scale, either by translation or by multiplication, the value of *r* remains the same;
- as a result of the non-causality characteristic, swapping the independent variable with the dependent one (*i.e. x* becomes *y* and *y* becomes *x*) does not affect the value of *r.*

Determination of r

One may easily calculate the value of *r* for a given experimental sample of date from the ratio of covariance of *x* and *y* to the individual variability in *x* and *y*, respectively [6-8]:

$$r = \frac{S_{xy}}{S_x S_y} \tag{1}$$

Where *r* is the correlation coefficient, S_{xy} is the covariance, S_x and S_y are the sample standard deviations for *x* and *y* variable, respectively.

Relation (1) may be further developed becoming:

$$r = \frac{\sum_{i=1}^{n}\left(x_i - \bar{x}\right)\left(y_i - \bar{y}\right)}{\sqrt{\sum_{i=1}^{n}\left(x_i - \bar{x}\right)^2}\sqrt{\sum_{i=1}^{n}\left(y_i - \bar{y}\right)^2}} \tag{2}$$

where *r* is the correlation coefficient, *n* is number of measurements, x_i, y_i the pair of points for measurement *i*, $\bar{x}$ the average value of the independent variable, $\bar{y}$ the average value of the dependent variable.

As there are a lot of computer aided procedures for carrying out regression analysis and for calculating the regression parameters, regression coefficient included, the actual method of calculating is beyond the aim of this paper, in all

practical cases, the authors made used of the associated software for calculating the regression coefficient and for the corresponding statistical tests.

When carrying out the correlations process and calculating the correlation coefficient, one should bear in mind a few common mistakes associated with this concept [6-8]:

- the correlation does not necessarily imply causality and in the absence of a preliminary experimental design it is wrong to assume that *x* causes *y* as it may well be the opposite way around;

- variables (at least one of them) should be on a normal, symmetrical distributed scale (*e.g.* having 9 measurements located around a singularity and the 10th measurement 10 times or 50 times further apart will lead to the wrong correlation and wrong conclusions);

- all the experimental points should be plotted without averaging them in cases of replicated experiments as averages tend to eliminate the individual contributions in variation of *y* and artificially increase the value of *r*;

- even though there is no linear relationship between *x* and *y*, does not necessarily mean that there is no relationship (*e.g.* a value of $r = 0$ shows a total absence of a linear relationship, but if one tries a circular regression it may well be a perfect circle with the value of *r* associated to this regression being 1);

- most often people use correlations to test the hypothesis; correlations should be used to construct hypotheses and not test them, as for this goal there are special statistical tests discussed later on below.

Correlation coefficient used in conjunction with the Electrochemical Impedance Spectroscopy

The Electrochemical Impedance Spectroscopy (EIS) presents a series of advantages over the classical electrochemical methods making it one of the most versatile and appreciated techniques employed in various electrochemical, corrosion, and surface engineering evaluations [13-19]. The main feature of this technique over the other similar ones is its ability to discriminate between the dielectric and electric properties of the investigated sample components, as well as between the individual contributions of their parts/layers, making it particularly suitable in evaluating the ionic conductivities and electronic resistivities in liquids and solids, where the classical methods often fail [13,16-19]. Being a non-destructive technique it offers valuable time-dependent information of various properties as well as information about the on-going processes occurring in a variety of fields such as batteries and fuel cells, corrosion, and other electrochemical and/or chemical processes [13-19].

The main operating principle can be resumed at superimposing a small amplitude perturbation voltage over a normal carrier signal and using it to scan a

large zone of pre-established frequencies, so that the acquired response signal is linear and may be interpreted using theories of linear transfer functions [13,14], minimizing the possible interventions in the investigated sample.

However, one of the drawbacks when conducting experiments at low frequencies is the extended duration of time (the smaller the frequency, the longer it takes). One possible solution reported in the scientific literature [17,19] is to reduce the number of measurements per decade, keeping in mind that one should still obtain enough experimental points for the regression equations in order to construct various equivalent models.

The aims of the paper were to examine whether the reduction of the number of measurements per decade during the electrochemical impedance spectroscopy measurements will adversely affect the circular regression correlation extracted from the Nyquist model representation, used as one of the standards for these types of measurements, and to propose a novel validation coefficient that may be useful, particularly in the case when two sets of data, with different degrees of freedom, are compared in order to choose one over the other.

2. Experimental

Reagents

The reagents used were of analytical grade and the solutions were prepared using the corresponding reagents distilled water. The samples for the working electrode were taken from the commercially available aluminium cans (used specifically for the food industry) and processed as specified below. The silane solution, used for coating, was prepared as an octyltrietoxysilane (OTES) 5% alcoholic solution. Silane films were deposited on the commercially available aluminium cans substrate by dip-coating for 10 minutes.

Apparatus and procedure

A standard electrochemical 50 mL thermostated three electrode cell was employed for the EIS measurements. The working electrode was an aluminium sheet of 1 cm^2, the auxiliary electrode was a Radiometer Analytical platinum electrode of 1.13 cm^2, and as reference electrode one has used a Radiometer Analytical saturated silver/silver chloride electrode (SSC) placed directly into the solution. All the relative potentials referred in this paper were measured versus this reference electrode. Before each experiment the working electrode was polished with emery paper of different grades, degreased, rinsed with distilled water, dried, and coated with the silane.

The cell was connected to a Voltalab 40 potentiostat and the corrosion behaviour of the working electrode samples immersed in 5 g/L phosphoric acid solution was investigated using EIS. The procedure consisted in applying a

sinusoidal potential perturbation of 10 mV while the frequency range was scanned between 100 kHz and 100 mHz, the number of the acquired points per decade being 5, 10 and 20 in order to investigate their influence over the validation coefficient.

Using the associated software, VoltaMaster 4.0, a circular regression procedure was applied to the acquired data and the characteristic parameters were calculated from the value of normalised impedances, taken from the intersection of regression equation with the real impedance axis of Nyquist plot in the high and low frequency zones.

3. Results and discussions

The use of Pearson's correlation coefficient at its own is subject to debate and as early as 1921 it was reported that there is a danger of relying too much on a correlation coefficient value deducted from small samples [2], and hence the need for further testing to validate this coefficient and implicitly the correlation.

The significance of r

Should the case arise when the data are subject to a normal distribution, one may calculate for a number of experimental points, *n*, and for the resulting correlation coefficient, *r*, a *t*-statistic test, using the following equation:

$$t = r\frac{\sqrt{n-2}}{\sqrt{1-r^2}} \tag{3}$$

where *t* is Student's *t* variable.

The critical correlation coefficient

As the value of *t* may be easily calculated or obtained from the statistical tables, one may calculate, for a given confidence interval, the value of the critical *r* as a function of (*n*-2) and *t*:

$$r_{critic} = \sqrt{\frac{t^2_{\alpha,(n-2)}}{t^2_{\alpha,(n-2)} + (n-2)}} \tag{4}$$

where r_{critic} is the critical correlation coefficient, *n* is number of pairs of points, *n*-2 = *df* are degrees of freedom, $t_{\alpha,(n-2)}$ Student's *t* variable, calculated for a given α (α represents the probability of being wrong/incorrect; normally α = 0.05 but it may be taken even at smaller values) and for *df* = *n*-2.

For n large enough and α = 0.05, r_{critic} may be approximated with the following formula:

$$r_{critic} = \frac{2}{\sqrt{n}} \tag{5}$$

This approximation holds for an acceptable range of pairs of points, namely from 20 to 100, the relative approximation errors being less than 2 %. This is derived from the fact that the variance of the cross-correlation coefficient, assuming the null hypothesis (zero or no correlation exists), goes to the limit to $\frac{1}{n}$ (for a large number of samples). As the coefficients are asymptotically normal (the hypothesis of a normal distribution), an approximation of the critical values for the correlation coefficient, taken at the 5% level probability of being wrong/incorrect), is $\pm\frac{2}{\sqrt{n}}$, once again, for an increased n.

A similar approximation, that holds good results for n > 50 (the relative approximation errors being less than 1 %), may be written as follows:

$$\lim_{n\to 50}(t_{\alpha=0.05,(n-2)}) \to 2 \tag{6}$$

which corroborated with relation (4) yields:

$$r_{critic} = \frac{2}{\sqrt{(n+2)}} \tag{7}$$

The critical correlation coefficient, r_{critic}, has the physical meaning of a minimum absolute value of r needed to attain the required significance for the given probability to be wrong and the corresponding degrees of freedom.

A novel validation coefficient

Once the critical value is found, for samples of the same process or phenomenon, containing different number of pairs of points, it is now possible to introduce *a novel coefficient*, called coefficient of validation, k_{VD}, its physical meaning being that of a dimensionless factor which indicates how far, in relative terms, is the modulus of the correlation coefficient, r, from its critical value, r_{critic}, the greater its value, the better the validation of the regression.

Following this reasoning, the authors propose the following formula for the calculation of this validation coefficient:

$$k_{VD} = 1 - \frac{r_{critic}}{|r|} \tag{8}$$

where $|r|$ is the correlation coefficient modulus and r_{critic} is the Pearson's critical correlation coefficient, calculated for a given number of pairs of points, *n*, and a corresponding Student's *t* variable, $t_{\alpha,(n-2)}$, calculated for a given probability of being wrong/incorrect, α (one can also use the confidence interval).

If $r_{critic} > |r|$, the null hypothesis established during the Student's *t*-test procedure, used to determine if the value of Pearson's correlation coefficient is statistically significant, is accepted, therefore the correlation is rejected and makes no sense to go further. Hence, one draws the conclusion that, in order to calculate the validation coefficient, a constrain must be put in place, namely $r_{critic} \le |r|$.

As $r_{critic} \le |r|$ and for $r_{critic} \to |r|$, it results that $k_{VD} \to 0$ and hence we have a poor validation of the correlation coefficient. For $r_{critic} \ll |r|$, it results that $k_{VD} \to 1$ and in this case we have a strong validation of the correlation coefficient. From the above demonstrations it results that:

$$0 \le k_{VD} < 1 \tag{9}$$

If $20 < n < 100$ and taken into account the approximation formula (5) for r_{critic} at large values for *n*, the validation coefficient defined by equation (8) may be written as:

$$k_{VD} = 1 - \frac{\frac{2}{\sqrt{n}}}{|r|} = 1 - \frac{2}{|r|\sqrt{n}} \tag{10}$$

$$k_{VD} = 1 - \frac{2}{\sqrt{nr^2}} \tag{11}$$

the relative approximation error being less than 2 % (see table 1).

As one may see from the table 1, the difference between the calculated and the approximated r_{critic}, using relations (4) and (5), for $20 < n < 100$ and $\alpha = 0.05$, varies between 0.003 and 0.005 units, the average being 0.004 units, so a better approximation formula, bringing the approximation error down to less than 0.5 % would be:

$$k_{VD} = 1 - \frac{2}{\sqrt{nr^2}} - 0.004 \tag{12}$$

and hence:

$$k_{VD} = 0.996 - \frac{2}{\sqrt{nr^2}} \quad (13)$$

Table 1

The relative approximation error for r_{critic}, $20 < n < 100$, $\alpha = 0.05$

n	r_{critic} calculated	r_{critic} approximated	Relative error, %
20	0.444	0.447	0.68
30	0.361	0.365	1.11
40	0.312	0.316	1.28
50	0.279	0.283	1.43
60	0.254	0.258	1.57
70	0.235	0.239	1.70
80	0.220	0.224	1.82
90	0.207	0.211	1.93
100	0.197	0.200	1.52

Relation 13 offers now a much easier way to calculate the validation coefficient, as a simple function depending on the correlation coefficient and the number of the experimental pairs of points.

Validation coefficient applied in EIS regressions

The Nyquist plots of the cumulated EIS spectra are presented in Fig. 1. This figure shows that the stability of the deposited film of OTES varies in time due to the fact that the film was not subjected to a curing treatment after the deposition. The absence of the curing procedure makes the film prone to the initiations and developments of cracks and pores which allow the solution to ingress the layer and to reach the metallic substrate and hence the decrease in the polarization resistance, and affects the diameter of the Nyquist plots. A series of circular regressions were applied to the Nyquist plots (an example is depicted in Fig. 2) and the resulting data, correlated with the number of measurements per decades, are summarised in Table 2 and Table 3.

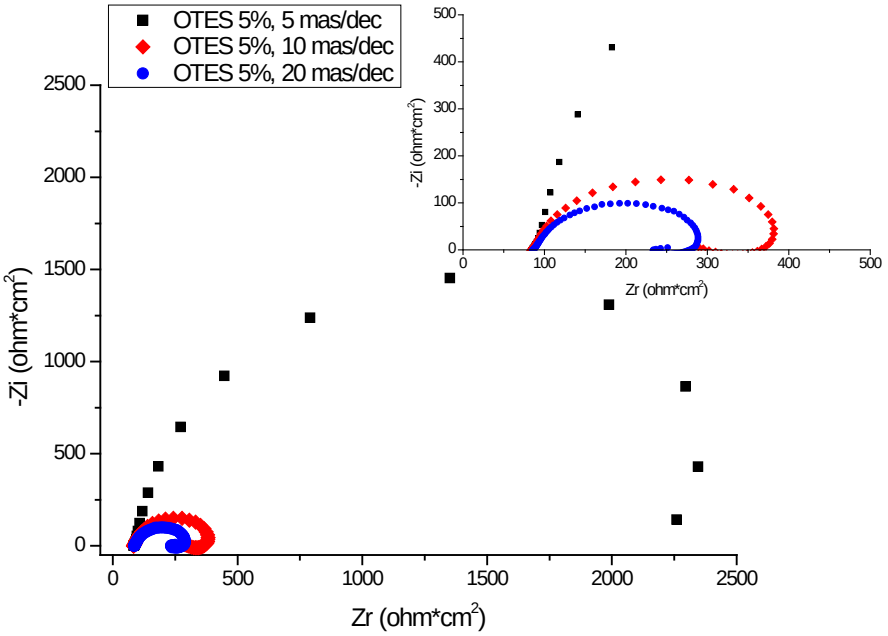

Fig. 1. Nyquist plots of OTES films deposited on aluminium samples in 5g/L phosphoric acid.

By calculating the correlation coefficient for all the experiments carried out, one may see that for 5 measurements per decade, the model does not hold, as $r < r_{critic}$. A possible solution would be to constrain the frequency domain to the lower limit of 5 Hz (see table 3), so that the perturbing process that strongly affect the model is excluded. Although the correlation coefficient for 10 measurements/decade is higher than that for 20 measurements/decade, 0.896 > 0.881, by calculating the validation coefficient, it can be seen clearly now that the circular regression model is best fitted with data acquired at 20 measurements/decade, the validation coefficient being 0.763 comparing to that for 10 measurements/decade which is 0.673.

Table 2.

Values of R1, R2, C, *r*, r_{critic}, and k_{VD} for various number of measurements per decade at 1Hz

Number of measurements per decade	Total number of points	R1, ohm·cm^2	R2, ohm·cm^2	C, µF/ cm^2	*r*	r_{critic}	k_{VD}
5	24	161.90	9538.0	3.337	0.340	0.413	Not applicable
10	48	89.35	289.8	17.350	0.896	0.288	0.673
20	95	90.70	195.7	20.320	0.881	0.203	0.763

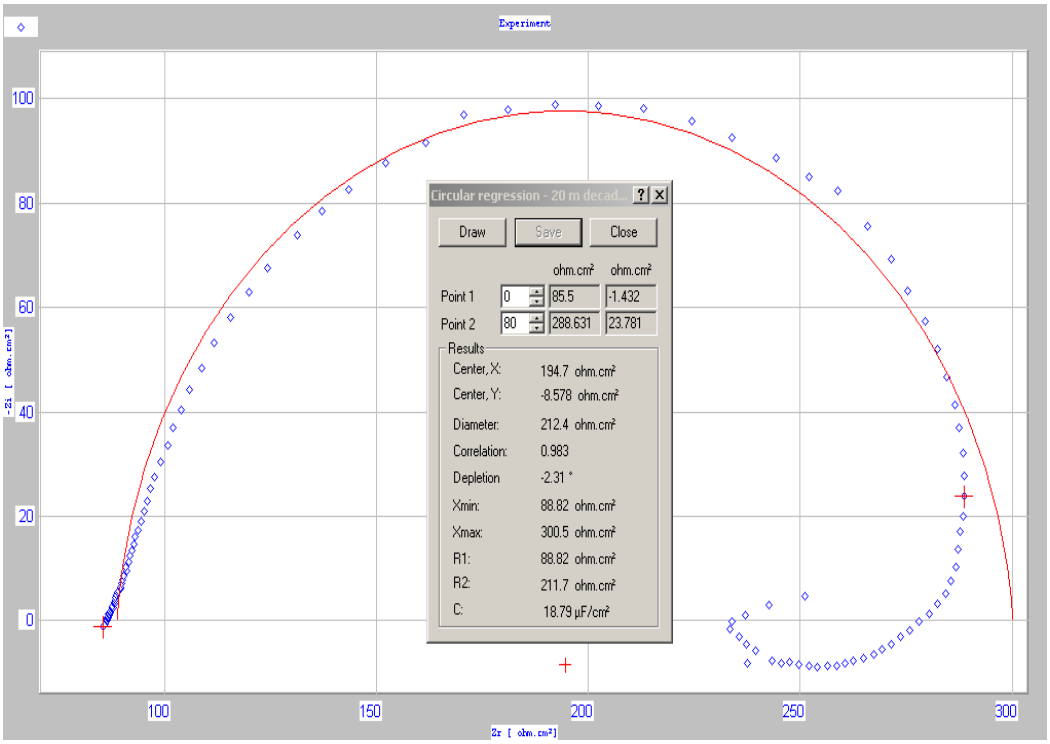

Fig. 2. Screen capture of a circular regression procedure applied to an OTES film deposited on aluminium samples in 5g/L phosphoric acid (20 measurements/decade) and the corresponding results.

This situation is also replicated even when the frequency domain is restricted to the lower limit of 5 Hz (see table 3), the correlation coefficient for 10 measurements/decade being marginally higher than that for 20 measurements/decade, 0.986 > 0.983, while the validation coefficient is lower for 10 measurements/decade comparing to 20 measurements/decade, 0.679 < 0.787.

Table 3.

Values of R1, R2, C, *r*, r_{critic}, and k_{VD} for various number of measurements per decade at 5Hz

Number of measurements per decade	Total number of points	R1, ohm·cm^2	R2, ohm·cm^2	C, µF/ cm^2	*r*	r_{critic}	k_{VD}
5	21	105.50	2530.0	5.031	0.971	0.444	0.449
10	41	86.83	313.6	16.030	0.986	0.312	0.679
20	81	88.82	211.7	18.790	0.983	0.220	0.787

6. Conclusions

Electrochemical impedance spectroscopy is a proven versatile technique that may be used in a multitude of electrochemical evaluations. There are, however, some important considerations which must be taken into account when designing or conducting the experiments. It was found that proper attention must be paid to the amplitude perturbation, the number of measurements per decade, the cell configuration, and, nevertheless, the procedure settings if one ought to have a stable electrochemical impedance spectroscopy measurement.

One may also optimise the experiment duration by reducing the frequency range, as in the case of the ionic conductivity, when the area of interest is in the zone of high frequency, maintaining an acceptable number of experimental points by increasing the number of measurements per decade.

A simplified novel validation coefficient was proposed, and also a derived relation ($k_{VD} = 0.996 - \frac{2}{\sqrt{nr^2}}$), applicable for $20 < n < 100$, which may be employed when one has to decide which set of data should choose between two or more sets of correlated data, having different degrees of freedom, associated to a particular process or phenomenon. This validation coefficient presents the following features:

- it takes into consideration the number of points/degrees of freedom as well as the correlation coefficient;
- it may be applied to any type of regression, provided that a correlation coefficient and its associated critical correlation coefficient can be calculated.

The validation coefficient clearly shows the best fitted model, even in cases when the values of the correlation coefficients are very similar (*e.g.* the correlation coefficients of 0.986 and 0.983, while the validation coefficients are 0.679 and 0.787).

REFERENCES

[1] Pearson K., Notes on regression and inheritance in the case of two parents, *Proceedings of the Royal Society of London*, 58, 240–242, 1985.
[2] Fisher, R.A., On the Probable Error of a Coefficient of Correlation Deduced from a Small Sample, *Metron* 1(4), (1921), 3–32.
[3] Taylor, R., Interpretation of the correlation coefficient: A Basic Review, *Journal of Diagnostic Medical Sonografy*, 1, 35-39, 1990.
[4] Rodgers, J. L. and Nicewander, W. A., Thirteen ways to look at the correlation coefficient. *The American Statistician*, 42(1), (1988), 59–66.

[5] Hauke, J. and Kossowski, T., Comparison of Values of Pearson's And Spearman's Correlation Coefficients on the Same Sets of Data, *Quaestiones Geographicae*, 30(2), (2011), 87-93.
[6] Edwards, A.L., The Correlation Coefficient, An Introduction to Linear Regression and Correlation, San Francisco, CA, W. H. Freeman, 33-46, 1976.
[7] Kenney, J.F. and Keeping, E.S., Linear Regression and Correlation, Mathematics of Statistics, 3rd ed. Princeton, NJ, Van Nostrand, 252-285, 1962.
[8] Snedecor, G.W. and Cochran, W.G., The Sample Correlation Coefficient r and Properties of r, Statistical Methods, 7th ed. Ames, IA, Iowa State Press, 175-178, 1980.
[9] Heckman, J.J., Schmierer D., and Urzua, S., Testing the correlated random coefficient model, *Journal of Econometrics*, 158(2), (2010), 177-203.
[10] Imbens, G.W. and Angrist, J.D., Identification and estimation of local average treatment effects, *Econometrica*, 62(2), (1994), 467-475.
[11] Fisher, N.I. and Lee, A.J., A correlation coefficient for circular data, *Biometrika*, 70, (1983), 327-32.
[12] Hopkins, W.G., Measures of reliability in sports medicine and science, *Sports Medicine*, 30, (2000), 1-15.
[13] Wagner, N., Characterization of membrane electrode assemblies in polymerelectrolyte fuel cells using a.c. impedance spectroscopy, *Journal of Applied Electrochemistry*, 32, (2002), 859-863.
[14] Parthasarathy, D., Srinivasan, A., and Martin, J., The Platinum Microelectrode / Nafion Interface: An Electrochemical Impedance Spectroscopic Analysis of Oxygen Reduction Kinetics and Nafion Characteristics, *Journal of The Electrochemical Society*, 139, (1992), 134-140.
[15] Hollaender J., Rapid assessment of food/package interactions by electrochemical impedance spectroscopy (EIS), *Food Addit. Contam*., 14, (1997), 617-626.
[16] Enache A.I. and Vaireanu, D.I., The use of electrochemical impedance spectroscopy for interactions between food and/or the food additives and the packaging materials, *Research Journal of Chemistry and Environment*, 18(1), (2014), 7-13.
[17] Vaireanu, D.I, Cojocaru, A., Maior, I., Caprarescu, S., Ionescu, A., and Radu, V., Considerations on Reducing the Experimental Duration of Electrochemical Impedance Spectroscopy Measurements used for the Evaluation of Ionic Conductivity in Polymer Electrolyte Membrane Electrolysers and Fuel Cells, *Key Engineering Materials*. 415, (2009), 61-64.
[18] Vaireanu, D.I, Maior, I., Grigore, A., and Savoiu, D., The Evaluation of Ionic Conductivity In Polymer Electrolyte Membranes, *Rev. Chimie*, 59(10), (2008), 1140-1142.
[19] Vaireanu, D.I, Cojocaru, A., Maior, I., and Caprarescu, S., Practical Considerations Regarding the Measurement of Ionic Conductivity by EIS in Conductive Polymers, *Chem. Bull. "POLITEHNICA" Univ. of Timisoara, Series Chemistry and Environmental Engineering*, 53, 67, 1-2, (2008), 258-261.